

Submitted to *Operations Research*

Two-Sided Flexibility in Platforms

(Authors' names blinded for peer review)

Authors are encouraged to submit new papers to INFORMS journals by means of a style file template, which includes the journal title. However, use of a template does not certify that the paper has been accepted for publication in the named journal. INFORMS journal templates are for the exclusive purpose of submitting to an INFORMS journal and are not intended to be a true representation of the article's final published form. Use of this template to distribute papers in print or online or to submit papers to another non-INFORM publication is prohibited.

Abstract. Flexibility is a cornerstone of operations management, crucial to hedge stochasticity in product demands, service requirements, and resource allocation. In two-sided platforms, flexibility is also two-sided and can be viewed as the compatibility of agents on one side with agents on the other side. Platform actions often influence the flexibility on either the demand or the supply side. But how should flexibility be jointly allocated across different sides? Whereas the literature has traditionally focused on only one side at a time, our work initiates the study of two-sided flexibility in matching platforms. We propose a parsimonious matching model in random graphs and identify the flexibility allocation that optimizes the expected size of a maximum matching. Our findings reveal that flexibility allocation is a first-order issue: for a given flexibility budget, the resulting matching size can vary greatly depending on how the budget is allocated. Moreover, even in the simple and symmetric settings we study, the quest for the optimal allocation is complicated. In particular, easy and costly mistakes can be made if the flexibility decisions on the demand and supply side are optimized independently (e.g., by two different teams in the company), rather than jointly. To guide the search for optimal flexibility allocation, we uncover two effects, flexibility cannibalization, and flexibility abundance, that govern when the optimal design places the flexibility budget only on one side or equally on both sides. In doing so we identify the study of two-sided flexibility as a significant aspect of platform efficiency.

Key words: Flexibility, Two-sided Platforms, Bipartite Matching, Incentive Designs

1. Introduction

Flexibility is arguably one of the fundamental topics in operations research and computer systems. As an operational concept, it classically applies to a range of settings including for example (1) the ability of a plant to process multiple types of products in a manufacturing system (Fine and Freund 1990), (2) the ability of servers, due to cross-training, to handle multiple types of requests (Wallace and Whitt 2005), or (3) the pooling of resources in a network of newsvendors (Bassamboo et al. 2010). All of these classical applications target the supply side of an operating system. More recently, flexibility has also been used for the

demand side: its value has been demonstrated in opaque selling for retail inventory management (Elmachtoub and Hamilton 2021), in online grocery shopping delivery (Zhou 2021), and in car-sharing (Ströhle et al. 2019). In both the traditional, supply-focused, and the more recent, demand-focused, applications, the literature identifies the necessary investment in one lever of flexibility to gain operational value.

However, contemporary markets feature flexibility on both sides. In online retail markets, for instance, Amazon provides a spectrum of delivery time options, ranging from a few hours to several weeks. Price differentiation across these options exploits different levels of flexibility among the customers, which leads to lower (higher) revenue from more (less) flexible customers. On the supply side, Amazon operates both local storage hubs and larger regional warehouses to fulfill demand. Storage at local hubs is more expensive but yields the necessary inventory flexibility to fulfill customer demand with short delivery windows. Two-sided flexibility is also prevalent in platforms that connect buyers and service providers. In Table 1 we provide examples that illustrate how flexibility levers, on both sides of a platform, increase the likelihood of connections between demand and supply being feasible. Despite the significant role that flexibility plays on both the demand and the supply side, due to their organizational structure, firms usually optimize flexibility independently on each side. Moreover, we also know of no prior work that examines how different kinds of flexibility on two market sides interact with each other.

Industry	Platform(s)	Demand side lever	Supply side lever
Retail	Amazon	Wider delivery windows	Heterogeneous inventory storage
Hospitality	Airbnb	Flexible duration/location of stay	Superhost Ambassadors
Trucking	Uber Freight	Flexible load types (e.g., LTL)	Powerloop network
Ride-hailing	Lyft	Wait and save	Car seat mode

Table 1 Examples of two-sided platforms with flexibility incentives on both the supply and the demand sides. These levers typically encourage flexibility on the demand side on how/when the service is fulfilled and increase compatibility on the supply side to cater to diverse customer needs.

Motivated by this gap in the literature, we study how a given budget of flexibility should be allocated across the two sides of a platform. This allocation question differs from traditional studies of flexibility in that it examines the interplay between different flexibility levers. Since most of our examples in Table 1 (i.e., trucking, hospitality, ride-hailing) originate in different types of matching platforms, we consider a parsimonious matching model to identify a platform's optimal flexibility investment on both market sides. Our matching problem is modeled as a bipartite random graph, where flexibility is captured through *flexible nodes* (on either side) with an increased probability of forming edges with the other side of the graph. We optimize over the fraction of flexible nodes on each market side to maximize the matching probability, i.e., the expected fraction of nodes that are part of a maximum matching.

Our results show that the choice of flexibility allocation has a significant impact on the performance of a two-sided matching platform. Even with a constant flexibility budget, the matching probability (and

consequently the profit of a matching platform) can vary significantly depending on how the budget is allocated between the two sides of the platform. As illustrated in Fig. 4, the profit gap between different allocations of the same flexibility budget for every model we consider can be as large as 20%. Moreover, we find that optimality occurs at one of two natural flexibility allocation strategies: (1) the one-sided allocation, which places flexibility only on one side, and (2) the balanced allocation, which evenly distributes half of the flexibility budget to both sides. As shown in Fig. 3, either of these allocations can improve the matching size by more than 8% compared to the other. Hence, matching platforms with flexibility levers on both sides may pay a high price if they only optimize their flexibility budget but not its allocation.

Despite the impact of the flexibility allocation, optimizing it poses nontrivial difficulties. Even in a simple and symmetric matching model, our analysis of the geometry of the matching size (as a function of the flexibility allocation) reveals saddle points in which a platform might get stuck. In particular, the current practice of many platforms, wherein separate teams optimize separate flexibility levers on different market sides, might converge to such saddle points. Near these saddle points, both teams mistakenly perceive themselves to be at an optimum, as flexibility should neither be increased nor decreased on either market side; however, the platform would benefit from jointly reducing flexibility on one side while increasing it on the other. These structural insights are unique to our study of two-sided flexibility, and our numerical results show that they generalize beyond our particular models. We show that these geometries and the dominance of different flexibility allocations are driven by an interplay of two opposing effects: *flexibility cannibalization* and *flexibility abundance*. These effects lend strength to the one-sided and the balanced allocations respectively, and they allow us to outline the parameter regimes where each effect and the corresponding flexibility allocation dominate. In identifying these different behaviors, and their first-order impact on performance, our results underscore the need to understand the interactions of different flexibility levers to enable more efficient market designs.

1.1. Contributions

Our work initiates the study of two-sided flexibility. It characterizes the interactions between different flexibility levers through a parsimonious matching model and allows us to study different questions regarding the optimal allocation of flexibility.

Flexibility structures and their driving effects. We examine three graph models within the framework of Section 2: the 2×2 model, the local model, and the global model. The 2×2 model is a small setting that can be fully characterized, and the local model is an asymptotic generalization that shares the same local edge structure and leads to similar results. A surprising result is that the one-sided allocation of flexibility is optimal, whereas following the usual guidance to add just a little flexibility incrementally¹ likely leads

¹A little flexibility is all you need, see Jordan and Graves (1995), Bassamboo et al. (2012)

to a suboptimal saddle point. In particular, we show that the matching probability is concave with respect to flexibility on either the demand or supply side but is jointly convex as one moves between the one-sided allocation on the supply side and that on the demand side. In other words, our setting reveals that it may be better to focus a lot of flexibility on one side instead of a little flexibility on each side. We present these results in Section 3 and highlight the need for joint experimentation to avoid the suboptimal saddle points.

The global model does not have a local edge structure, introducing new complex effects. In particular, we show that the one-sided allocation can be suboptimal. In Section 4 we present the *flexibility cannibalization* effect, which results from the fact that flexible nodes have a higher expected degree in the balanced allocation. Since each node can only be matched through one edge, the balanced allocation cannibalizes many of the edges incident to high-degree nodes, which degrades its performance. We show that this cannibalization drives the dominance of the one-sided allocation in particularly sparse graphs (roughly, average degree less than e). When flexible nodes have a much higher average degree, and there is an abundant number of incident edges, we highlight a countering effect, which we term *flexibility abundance*. In Section 5 we show that flexibility cannibalization becomes a second-order effect in that regime and the balanced allocation becomes optimal. Section 7 demonstrates the robustness of these effects in various numerical extensions of our model.

Analyses of sparse bipartite random graphs. Our main technical contributions aim to characterize and compare the matching probability in bipartite random graphs with heterogeneous node types, a task that is especially challenging for the global model. In comparing different flexibility designs for that model, we develop three very different techniques. In Section 4 we design a careful coupling between realizations under the balanced and the one-sided flexibility allocations and show, for certain parameters, that flexibility cannibalization leads to a smaller matching size for the balanced allocation. Then, in Section 5 we apply concentration bounds for parameters where flexible nodes have high average degree. In such settings, both allocations match almost all flexible nodes, but the balanced allocation is better at matching non-flexible ones. Finally, in Section 6 we analyze the Karp-Sipser (KS) algorithm (Karp and Sipser 1981) to explicitly characterize the asymptotic matching probability in the so-called subcritical regime (see Section 3). Our KS-style analysis innovates upon prior works in that we (i) analyze a graph with heterogeneous node types, and (ii) explicitly compute the asymptotic matching probability with a provable level of precision, which allows us to compare different flexibility allocations in computer-aided proofs.

1.2. Related Work

Flexibility in operations. Flexibility has a long history in operations with early works, dating back to Buzacott and Yao (1986) and Fine and Freund (1990), focusing on the ability of a manufacturing system to produce multiple types of products. Most early works in this literature have focused on determining the optimal amount of flexible manufacturing capacity (Fine and Freund 1990, Van Mieghem 1998, Netessine

et al. 2002, Chod and Rudi 2005), thus optimizing over a single dimension on the supply side. In contrast, our decision also involves the demand side. More importantly, we identify not just the optimal flexibility investment, but also structural properties that arise from the interplay of flexibility on both sides and can cause potential pitfalls in practice.

In our focus on structural insights, our study relates more closely to those works in process flexibility that aim to identify the optimal flexibility design rather than the optimal amount of flexibility. The seminal work of (Jordan and Graves 1995) first introduced the “long chain”, which enables a small amount of flexibility ($2n$ carefully placed edges in a manufacturing system with n plants and n types of products) to yield almost all the benefits of a perfectly flexible system (one with all n^2 edges). Since then, a vast literature has studied process flexible designs and the value thereof for manufacturing and service systems (Iravani et al. 2005, Akşin and Karaesmen 2007, Chou et al. 2011, Simchi-Levi and Wei 2012, Chen et al. 2015, Désir et al. 2016). Effective flexibility designs have also been investigated in staffing (Wallace and Whitt 2005) and queuing (Tsitsiklis and Xu 2017), among other settings.

A key distinction between our work and this stream of work lies in the structure of our flexibility levers: as most contemporary matching platforms involve stochastically formed edges that connect the supply and demand sides, we cannot model flexibility as a fixed compatibility design. Instead, platforms use various incentive levers to increase the likelihood of compatibility between the supply and demand sides of the market. As such, our approach optimizes over the fraction of flexible nodes on each side, rather than optimizing over specific edges, and requires a fundamentally different toolkit.

Our work also relates to papers that study flexibility on online marketplaces, though they focus on flexibility on a single side. In ride-hailing services, prior works study supply-side levers such as driver repositioning incentives (Ong et al. 2021) or a priority mode (Krishnan et al. 2022), and demand-side levers such as waiting mechanisms (Freund and van Ryzin 2021) or subscriptions Berger et al. (2023). More explicitly focused on demand-side flexibility, some works study opaque selling Elmachtoub et al. (2019) and flexible time windows (Zhou 2021) in online retail. Our work differs from all of these in that we focus on the interplay of two different flexibility levers.

In-organization Incentives. A reasonable interpretation of our structural results is that modern platforms are unlikely to find the optimal flexibility allocation if they optimize over two sides independently. Nonetheless, given the organizational structure of many platforms, with separate verticals working on the supply and the demand side, jointly experimenting and thus optimizing over levers on different market sides is uncommon. This misalignment relates to a stream of literature that identifies conflicting organizational incentives, e.g., the so-called marketing-operations alignment. There, organizations may face inefficiencies due to two departments (marketing and operations) having opposing incentives (Shapiro 1977). Solutions for marketing-operations conflicts focus on aligning incentives, including through internal integration of

different functional teams within an organization (Weir et al. 2000), increasing the interface between manufacturing and marketing management (Hausman et al. 2002), and achieving a strategic alignment between external positioning and internal arrangement (Henderson and Venkatraman 1999). In our work, the separate verticals do not have misaligned incentives. Instead, the inefficiency arises from a lack of visibility, i.e., without joint experimentation, both teams lack visibility over the interplay between the two flexibility decisions.

Random graphs. The core technical component of our work relies on an asymptotic analysis of random graphs. Classical related works include characterizations of the asymptotic threshold for connectivity (Erdős et al. 1960) or the existence of perfect matchings (Erdős and Rényi 1966, Walkup 1980). As we focus on sparse random graphs, where the asymptotic probability that a node is matched is strictly between 0 and 1, our work falls into an area in which the Karp-Sipser (KS) algorithm is commonly applied (Karp and Sipser 1981). This algorithm is asymptotically optimal for the canonical maximum matching problem in a sparse random graph with n nodes and a uniform edge probability c/n between any two nodes (for constant c as $n \rightarrow \infty$). Karp and Sipser prove this by characterizing the asymptotic matching probability as a solution to a system of nonlinear equations, using convergence results (Kurtz 1970). Some of our results (Theorems 3 and 7) resemble a class of papers that adapt the KS algorithm (Aronson et al. 1998, Bohman and Frieze 2011, Zdeborová and Mézard 2006) to different classes of random graphs. Most closely related is the work of Balister and Gerke (2015), who proved that the KS algorithm yields the asymptotically optimal matching probability in a class of bipartite random graphs based on a “configuration model.” Though similar, their model does not capture our setting with flexible and non-flexible nodes.² Nonetheless, we extend a similar analysis to our setting. Finally, a significant distinction between our work and the above is that we leverage our KS-style derivation in computer-aided proofs. Despite computer-aided proofs having a proud tradition in combinatorics, including proofs of the four-color theorem (Appel and Haken 1977, Robertson et al. 1996), we know of no other papers with provable comparisons of the limiting behavior of different random graphs that combine a KS-style analysis, continuity arguments, and a computer-aided grid search. In that regard, Gamarnik et al. (2006) may be closest to our approach, though they only compute a single explicit solution to a nonlinear equation (to compute the size of a largest independent set), whereas our grid search requires us to solve, within provable tolerance, approximately $\approx 6 \times 10^6$ systems of nonlinear equations.

2. Model

Our two-sided platform flexibility models all share the same structure: maximum matching in a random bipartite graph. We first present this framework before introducing each specific model.

²E.g., our model, but not theirs, allows two nodes with positive expected degree to have 0 probability of being adjacent.

Random Graph Formation. We consider a bipartite graph G containing $n \in \mathbb{N}^+$ nodes on each side³. The set of nodes on the left-hand side and right-hand side of G are denoted by V_l and V_r , respectively, and $V = V_l \cup V_r$ is the set of all nodes. Nodes are indexed from $1, \dots, n$ on each side, so that $V_l = \{v_1^l, \dots, v_n^l\}$ and $V_r = \{v_1^r, \dots, v_n^r\}$. We denote the set $\{1, \dots, n\}$ by $[n]$.

The sole decision variable in our model is $\mathbf{b} = (b_l, b_r) \in [0, 1]^2$, where b_l and b_r respectively specify probabilities that a node on the left-hand side and right-hand side is *flexible*. For each node in V_k , $k \in \{l, r\}$, we independently sample Bernoulli random variables $F_i^k \sim \text{Bernoulli}(b_k)$, $\forall i \in [n]$. Then, a node $v_i^k \in V_k$ is *flexible* if $F_i^k = 1$; otherwise, it is *non-flexible*. The flexibility decision (b_l, b_r) incurs a linear cost of $c \cdot (b_l + b_r)$ for some constant $c > 0$.

The decision \mathbf{b} impacts the edge probabilities in our random bipartite graph. The presence of each edge is controlled by a Bernoulli random variable R_{ij} , $\forall i, j \in [n]$. The edge that connects node v_i^l and v_j^r realizes if and only if $R_{ij} = 1$. If a node is flexible, we assume that the probability of any potential incident edges increases in a stochastic dominance sense:

$$\begin{aligned} \forall i, j \in [n] : \mathbb{P} \left[R_{ij} = 1 | F_i^l = 1, F_j^r = 1 \right] &\geq \mathbb{P} \left[R_{ij} = 1 | F_i^l = 1, F_j^r = 0 \right] = \mathbb{P} \left[R_{ij} = 1 | F_i^l = 0, F_j^r = 1 \right] \\ &\geq \mathbb{P} \left[R_{ij} = 1 | F_i^l = 0, F_j^r = 0 \right]. \end{aligned}$$

This implicitly assumes that we are in a symmetric setting where flexibility on either side contributes equally to the formation of an edge. In Section 2.1-2.3, we explore three models that correspond to specific edge distributions. In all of them, R_{ij} is sampled independently (but not necessarily identically) conditional on F_i^l and F_j^r .

Maximum Matching. In the resulting $n \times n$ random bipartite graph G , we use the random variable $\mathcal{M}_n(b_l, b_r)$ to denote the size of a *maximum matching*—that is, a matching that contains the largest possible number of edges. We define the *matching probability* $\mu_n(b_l, b_r)$ as the expected fraction of nodes that are part of a maximum matching, i.e., $\mu_n(b_l, b_r) = \mathbb{E} [\mathcal{M}_n(b_l, b_r)/n]$. We drop the dependency on n whenever it is clear from context.

Objective. We choose the flexibility parameters (b_l, b_r) to maximize the matching probability while accounting for the cost of flexibility. That is, we focus on the optimization problem

$$\max_{\mathbf{b} \in [0, 1]^2} \mu(b_l, b_r) - c \cdot (b_l + b_r) \tag{1}$$

We will use the notation $g(b_l, b_r) := \mu(b_l, b_r) - c \cdot (b_l + b_r)$ to refer to this objective function. The optimization problem in (1) can be decomposed into two stages:

- (i) For a given budget $B \geq 0$, we optimize the allocation (b_l, b_r) subject to $b_l + b_r = B$.

³While we focus on balanced bipartite graphs in the main body of the paper, we also conduct simulations to explore imbalanced markets in Section 7.

(ii) Knowing the optimal allocation for every given budget $B \geq 0$, we find B that maximizes (1).

Stage (ii) represents the trade-off between the benefit and the cost of flexibility, and the optimal flexibility budget B depends on the exogenous cost parameter c . Stage (i), the main focus of our work, optimizes the flexibility allocation (b_l, b_r) given a budget B . For instance, if (b_l^*, b_r^*) is an optimal solution to Eq. (1), does setting $b_l^* = B$ and $b_r^* = 0$ maximize $\mu(b_l, b_r)$ for fixed B ? If so, then this suggests that two-sided marketplaces should only invest in flexibility on one side of their market; on the other hand, if $b_l^* = b_r^*$, then teams responsible for flexibility levers on different market sides should jointly identify the optimal level of flexibility to invest in. To characterize this optimal solution structure, we aim to understand the geometric properties of $\mu(b_l, b_r)$.

We explore three versions of the matching model that capture different aspects of matching applications. In our simplest model with non-trivial effects, the 2×2 model, there are only two nodes on each side. Then, we move on to a *local* model that takes the number of nodes to infinity, but nodes can only be matched if they are physically or spatially close to each other. This assumption holds true in ride-hailing dispatch systems, for instance. Finally, we consider the most complex model, the *global* model, which also takes the number of nodes to infinity but allows edges to form between any two nodes on both sides of the market (with equal probability conditioned on whether neither, one, or both of the nodes are flexible). We formally define these three models in the remainder of this section and state our results in Section 3. In the formalism we defined above, our results are of the following flavor: we show that $\mu(B, 0) > \mu(b_l, B - b_l)$ for any $B \in (0, 1]$, $b_l \in [0, B]$ for the 2×2 and the local model, whereas for the global model, depending on the value of B and the probability of edges occurring, we can have either $\mu(B, 0) > \mu(B/2, B/2)$ or $\mu(B, 0) < \mu(B/2, B/2)$. We define the three models in such a way that the expected number of edges that arises under a given budget B is invariant of the specific choice of \mathbf{b} . This allows us to focus on intricate matching dynamics arising from the distribution of edges within a graph rather than the number of edges.

2.1. The 2×2 Model

Our 2×2 model helps illustrate the set-up. We introduce two exogenous parameters p^f, p , and take

$$\mathbb{P} \left[R_{ij} = 1 | F_i^l, F_j^r \right] = 2p + (F_i^l + F_j^r) \cdot (p^f - p), \forall i, j \in [2].$$

As illustrated in Fig. 1, this means that for every pair of nodes v_i^l and v_j^r , having a flexible node increases the probability of incident edges realizing by $p^f - p$. This additive edge probability ensures that the expected number of edges is affine in $B = b_l + b_r$, and in particular that it is invariant to (b_l, b_r) for fixed B . To ensure that flexibility increases the probability of edges forming and that the edge probability remains in $[0, 1]$, we make the following assumption:

ASSUMPTION 1. $0 \leq p < p^f \leq 1/2$.

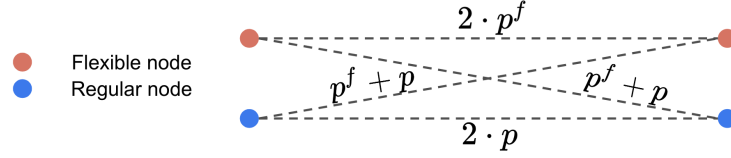


Figure 1 Illustration of the edge probability in the 2×2 model, for a given realization of the node types.

In line with notations defined in the general model, we denote the size of a maximum matching in the 2×2 model by $\mathcal{M}_2^{2 \times 2}(b_l, b_r)$ and the matching probability by $\mu_2^{2 \times 2}(b_l, b_r) = \mathbb{E} \left[\frac{\mathcal{M}_2^{2 \times 2}(b_l, b_r)}{2} \right]$. Then, $g_2^{2 \times 2}(b_l, b_r) := \mu_2^{2 \times 2}(b_l, b_r) - c \cdot (b_l + b_r)$. Our goal is to characterize the optimal solution to

$$\max_{\mathbf{b} \in [0,1]^2} g_2^{2 \times 2}(b_l, b_r) = \max_{\mathbf{b} \in [0,1]^2} \mu_2^{2 \times 2}(b_l, b_r) - c \cdot (b_l + b_r).$$

We omit the super- and subscripts for the 2×2 model whenever it is clear from the context.

An advantage of the 2×2 model is that we can fully characterize the $\mu(b_l, b_r)$ as a polynomial function with respect to b_l, b_r, p^f and p . The 2×2 model has two features that will inspire our more complex models. First, each node only connects to a limited number of nodes. Second, conditioned on whether the nodes are flexible/non-flexible, all edges in the 2×2 model have the same distribution. When scaling to larger networks, the *local* model maintains the first property, whereas the *global* model maintains the second, as illustrated in Fig. 2.

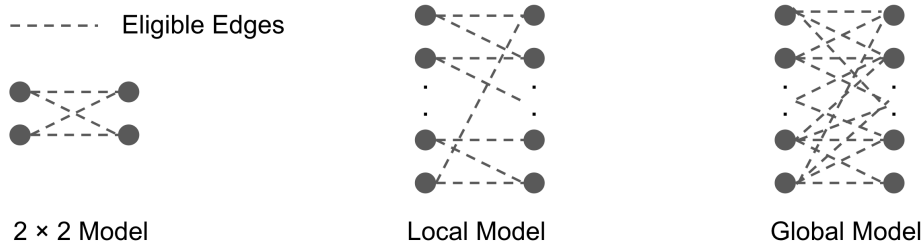


Figure 2 Illustration of the graph models.

2.2. The Local Model

In the local model, for any $i < n$, $v_i^l \in V_l$ is only eligible to connect to v_i^r and v_{i+1}^r in V_r , and $v_n^l \in V_l$ is only eligible to connect to v_n^r and v_1^r . Therefore, $v_j^r \in V_r$ can only connect to its previous two neighbors in V_l . As with the 2×2 model, we take exogenous parameters p^f and p subject to Assumption 1. Edges then realize with the following conditional probabilities:

$$\mathbb{P} \left[R_{ij} = 1 \mid F_i^l, F_j^r \right] = \begin{cases} 2p + (F_i^l + F_j^r) \cdot (p^f - p) & \text{if } ((j-i) \bmod n) \leq 1 \\ 0 & \text{otherwise} \end{cases}$$

Notice that these conditional probabilities follow the same additive properties as in the 2×2 model.

In line with notations for the general model, for the local model the size of a maximum matching is denoted by $\mathcal{M}_n^{loc}(b_l, b_r)$ and the matching probability by $\mu_n^{loc}(b_l, b_r) := \mathbb{E} \left[\frac{\mathcal{M}_n^{loc}(b_l, b_r)}{n} \right]$. We are interested in the asymptotic behavior of $\mu_n^{loc}(b_l, b_r)$ with respect to (b_l, b_r) as $n \rightarrow \infty$, a conventional scale of interest in the study of random graphs. We denote this asymptotic quantity⁴ by $\mu^{loc}(b_l, b_r)$, and with $g^{loc}(b_l, b_r) := \mu^{loc}(b_l, b_r) - c \cdot (b_l + b_r)$, our goal will be to characterize the optimum of

$$\max_{\mathbf{b} \in [0,1]^2} g^{loc}(b_l, b_r) = \max_{\mathbf{b} \in [0,1]^2} \mu^{loc}(b_l, b_r) - c \cdot (b_l + b_r) = \max_{\mathbf{b} \in [0,1]^2} \lim_{n \rightarrow \infty} \mu_n^{loc}(b_l, b_r) - c \cdot (b_l + b_r).$$

We omit the superscript for the local model whenever it is clear from the context.

2.3. The Global Model

An orthogonal extension of the 2×2 model scales the number of nodes on each side to n and allows nodes to connect with any node on the opposite side of the graph. This gives rise to our global model, illustrated in Fig. 2. We focus on the *sparse* random graph regime, where the expected degree of each node remains constant as the size of the graph n scales large.⁵ Specifically, we take constants α^f and α such that $0 \leq \alpha < \alpha^f$ and define $p_n^f = \alpha^f/n$, $p_n = \alpha/n$, respectively. Then,

$$\mathbb{P} \left[R_{ij} = 1 | F_i^l, F_j^r \right] = 2p_n + (F_i^l + F_j^r) \cdot (p_n^f - p_n), \forall i, j \in [n].$$

As in the 2×2 model, the conditional probabilities are additive and independent of i and j .

In the global model, we denote the size of a maximum matching realization by $\mathcal{M}_n^{glb}(b_l, b_r)$ and the matching probability by $\mu_n^{glb}(b_l, b_r) := \mathbb{E} \left[\frac{\mathcal{M}_n^{glb}(b_l, b_r)}{n} \right]$. As in the local model, we are interested in the asymptotic matching probability $\mu^{glb}(b_l, b_r) := \limsup_{n \rightarrow \infty} \mu_n^{glb}(b_l, b_r)$, which is equal to $\lim_{n \rightarrow \infty} \mu_n^{glb}(b_l, b_r)$ when the latter exists. Then, with $g^{glb}(b_l, b_r) = \mu^{glb}(b_l, b_r) - c \cdot (b_l + b_r)$, our goal is to characterize $\arg \max_{\mathbf{b} \in [0,1]^2} g^{glb}(b_l, b_r)$. We drop the superscript when clear from context.

Due to the difficulties of analyzing this model, we complement our theoretical results for a subset of instances with numerical results. Specifically, we resort to simulations to compute the empirical mean for given (b_l, b_r) . Provided with s random graph samples yielding maximum matching sizes $\mathcal{M}_n^1(b_l, b_r), \mathcal{M}_n^2(b_l, b_r), \dots, \mathcal{M}_n^s(b_l, b_r)$, the empirical mean is computed as

$$\mu_{n,s}^{\text{EMP}}(b_l, b_r) := \frac{\sum_{s'} \mathcal{M}_n^{s'}(b_l, b_r)}{s \cdot n}.$$

⁴We prove the existence of the limit in Theorem 2.

⁵Erdős and Rényi (1966) proved for $c > 1$ that a random graph with n nodes and i.i.d. edge probability $c \cdot \log(n)/n$ almost surely possesses a perfect matching as $n \rightarrow \infty$. Thus, subsequent studies (Karp and Sipser 1981, Balister and Gerke 2015) often focus on the case where the edge probability is in $\mathcal{O}(1/n)$ and each node's expected degree is $\mathcal{O}(1)$.

Since the samples are independently and identically distributed (i.i.d.), the Law of Large Numbers (LLN) implies that $\mu_{n,s}^{\text{EMP}}(b_l, b_r) \rightarrow \mu_n(b_l, b_r)$ almost surely as $s \rightarrow \infty$. In our experiments, unless stated otherwise, we use $s = 1000$ and omit the dependency of $\mu_{n,s}^{\text{EMP}}(b_l, b_r)$ on s for brevity.

Plans for the subsequent sections. Recall that our main interest lies in the second stage described after Eq. (1), i.e., identifying the optimal allocation (b_l, b_r) given budget $B \geq 0$. For all our models, B determines the expected number of edges; thus, differences in the maximum matching size are due to the distribution of edges within the graph rather than their expected quantity. In the next section, we aim to characterize the geometry of $\mu(b_l, b_r)$ by answering the following questions:

- I. For given budget B , what does the optimal flexibility allocation look like in these models?
- II. More broadly, does the surface of $g(b_l, b_r)$ exhibit convexity, concavity, both or neither?

Then, in Section 4 and 5, we characterize intuitive effects driving the results in the global model.

3. Main Results

This section presents the main results to address questions I and II for each of our models.

3.1. Comparison of Different Flexibility Allocations

We start by defining two intuitive flexibility allocation strategies: one-sided and balanced.

DEFINITION 1. For given budget $B \in (0, 1]$, the flexibility allocation $\mathbf{b} = (B, 0)$ or $\mathbf{b} = (0, B)$ is called the *one-sided allocation*, whereas $\mathbf{b} = (B/2, B/2)$ is called the *balanced allocation*.

We have strong evidence that in all three models, given fixed $B \in (0, 1]$, either the one-sided allocation⁶ $(B, 0)$ or the balanced allocation $(B/2, B/2)$ is optimal for $\mu(b_l, b_r)$: in the 2×2 model, we find that $(B, 0)$ is the optimal flexibility profile for any given $B > 0$. In the local model, we prove that $(1, 0)$ dominates any other flexibility design when $b_l + b_r = B = 1$, and our simulations indicate that the same holds true for $B < 1$. In the global model, numerical evidence strongly suggests that optimality occurs at either $(B, 0)$ or $(B/2, B/2)$ for any given $B > 0$.⁷

Motivated by these findings, we compare the performance of the one-sided and the balanced allocation. Table 2 summarizes the results: in the 2×2 and the local model, the one-sided allocation consistently dominates. However, in the global model either one can dominate, depending on the edge density and the budget. In our model $\alpha^f + \alpha$ measures the edge density, and for a range of sparse random graphs e , the Euler's number, is known as a critical value that demarcates a transition from tree-like graph analyses to

⁶We omit allocation $(0, B)$ in the subsequent discussions since it is trivially equivalent to $(B, 0)$ by symmetry.

⁷The finding in the global model is supported by a combination of simulation results and a grid search over $\mu^{\text{KS}}(b_l, b_r)$, an analytical expression adapted from the literature (Section 6). Whereas we prove $\mu(b_l, b_r) = \mu^{\text{KS}}(b_l, b_r)$ for some parameters, simulations suggest that the two quantities are always close.

more complex structures (Karp and Sipser 1981, Aronson et al. 1998). In our analysis as well, the *subcritical*, where $\alpha^f + \alpha < e$, and the *supercritical* regime, where $\alpha^f + \alpha \geq e$, show stark differences. In the subcritical regime, or when $B = 1$, we recover the result from the other models that the one-sided flexibility allocation performs best. However, when $B < 1$, balanced allocation may be a better flexibility design in the supercritical regime. We formalize these in the following theorems.

Model	Quantity	Comparison
2×2 model	$\mu^{2 \times 2}(b_l, b_r)$	$\forall B \in (0, 1] : \mu^{2 \times 2}(B, 0) > \mu^{2 \times 2}(B/2, B/2)$
Local model	$\mu^{loc}(b_l, b_r)$	$\forall B \in (0, 1] : \mu^{loc}(B, 0) > \mu^{loc}(B/2, B/2)$
Global model (most of subcritical regime, and whenever $\alpha = 0$)	$\mu^{glb}(b_l, b_r)$	$\mu^{glb}(1, 0) \geq \mu^{glb}(1/2, 1/2)$
Global model (subset of supercritical regime)	$\mu^{glb}(b_l, b_r)$	$\forall B \in [0.4, 0.8] : \mu^{glb}(B, 0) < \mu^{glb}(B/2, B/2)$

Table 2 Comparison of the one-sided and the balanced allocations. We prove the results for the subcritical regime for $10^{-4} < \alpha < 0.77\alpha^f - 0.16$, and those for the supercritical regime for $\alpha^f \geq 22, \alpha \in [0.01, 0.05]$.

THEOREM 1. $\mu^{2 \times 2}(B, 0) > \mu^{2 \times 2}(B/2, B/2)$ for any $B \in (0, 1]$.

In the 2×2 model we derive a closed-form solution to the matching probabilities by computing the probability of each subset of the 4 edges realizing (see proof in Appendix B.1). A similar analysis yields the same result for the local model (Appendix C.1).

THEOREM 2. $\mu^{loc}(B, 0) > \mu^{loc}(B/2, B/2)$ for any $B \in (0, 1]$.

These properties also hold, for parameters as specified in Theorem 3, in the global model. We prove Theorem 3 (i) through a careful coupling technique (Section 4); in the proof of Theorem 3 (ii) we use the KS algorithm to exactly characterize the matching probability (see Section 6).

THEOREM 3. $\mu^{glb}(1, 0) \geq \mu^{glb}(1/2, 1/2)$ if either (i) $\alpha = 0$, or (ii) $10^{-4} < \alpha < 0.77\alpha^f - 0.16$ and $\alpha^f + \alpha < e$.⁸

However, in the global model the balanced allocation may be better than the one-sided one. The next result states that this occurs in a parameter regime with large α^f , small positive α and $B < 1$.

THEOREM 4. For any $B \in [0, 4, 0.8]$, $\alpha \in [0.01, 0.05]$, and $\alpha^f \geq 22$, $\mu^{glb}(B/2, B/2) > \mu^{glb}(B, 0)$.

⁸This boundary arises from the ability for a computer-aided proof to verify the inequality within a reasonable runtime: for $\delta > 0$, we construct and compute a lower bound the value of $\mu(1, 0) - \mu(1/2, 1/2)$ within each set of $[\alpha^f, \alpha^f + \delta] \times [\alpha, \alpha + \delta]$ within the subcritical regime. Taking $\delta = 0.001$ yields the boundary in Theorem 3 (ii) and runs in approximately 20 hours.

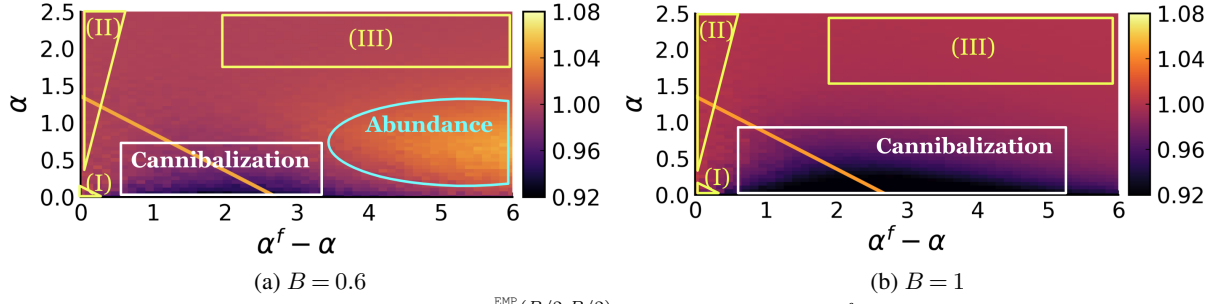


Figure 3 The plots present heat-map values of $\frac{\mu_n^{\text{EMP}}(B/2, B/2)}{\mu_n^{\text{EMP}}(B, 0)}$ across varying α and $\alpha^f - \alpha$ values when $n = 100$. The orange line highlights the boundary of the subcritical and supercritical regimes.

In Section 4 and 5 we describe two key effects –*flexibility cannibalization* and *flexibility abundance* – that drive the diverging behaviors in Theorem 3 and 4. Intuitively, flexibility cannibalization is a problem of the balanced allocation, where flexible nodes can make edges with flexible nodes. This increases the degree of flexible nodes, which already have the highest degree, and may lead to wasted edges as each flexible node can only be matched once: the flexible edges cannibalize each other. Flexibility abundance arises when α^f is so large that such cannibalization becomes insignificant; instead, the primary driver of the matching probability shifts towards matching the regular nodes among themselves, a task that is more effectively achieved by the balanced allocation.

Our theoretical results suggest that flexibility cannibalization is most prominent for moderate values of α^f and α , whereas flexibility abundance arises when α^f is large, α is small and $B < 1$. Fig. 3 displays simulation results for $\mu_n^{\text{EMP}}(b_l, b_r)$ when $n = 100$, and confirms that insight. It also displays that both allocations perform equally well in the regions labeled I-III. In region (I), $\alpha^f + \alpha$ is extremely small, creating a very sparse graph in which almost all edges appear in a maximum matching. When the number of matches approximates the number of edges, we know that $\mu(B/2, B/2) \approx \mu(B, 0)$ as both flexibility allocations yield the same number of edges in expectation. In region (II) flexibility does not notably increase the edge probability as $((\alpha^f - \alpha)/\alpha) \approx 0$; thus, it matters little how flexibility is allocated. Finally, in region (III), with large α^f and α , almost all nodes are matched irrespective of the flexibility allocation. In contrast to these patterns, which are easily understood, Section 4 and 5 characterize where flexibility cannibalization and abundance arise.

3.2. Geometric Properties of $g(b_l, b_r)$

Beyond characterizing the optimal flexibility allocation, we also identify other geometric properties of $g(b_l, b_r)$. In particular, we explore the existence of local optima or saddle points. Such points provide insights for the experimental design of a platform that applies different flexibility levers, e.g., they may indicate that one should run experiments in which b_l and b_r are varied jointly. To derive such results for $g(b_l, b_r)$, we first define directional concavity and convexity.

DEFINITION 2 (DIRECTIONAL CONCAVITY AND CONVEXITY). Consider a function $g : [0, 1]^2 \mapsto \mathbb{R}$ and a vector $\mathbf{d} = (d_l, d_r) \in \mathbb{R}^2$. The directional derivative of g at (b_l, b_r) in the direction (d_l, d_r) is, provided this limit exists, $\nabla_{\mathbf{d}} g(b_l, b_r) = \lim_{h \rightarrow 0} \frac{g(b_l + h \cdot d_l, b_r + h \cdot d_r) - g(b_l, b_r)}{h}$. Similarly, the second directional derivative of g at (b_l, b_r) in the direction (d_l, d_r) is, provided this limit exists,

$$\nabla_{\mathbf{d}}^2 g(b_l, b_r) = \lim_{h \rightarrow 0} \frac{g(b_l + h \cdot d_l, b_r + h \cdot d_r) - 2g(b_l, b_r) + g(b_l - h \cdot d_l, b_r - h \cdot d_r)}{h^2}.$$

Then, g is concave (resp. convex) in the direction of (d_l, d_r) at (b_l, b_r) if $\nabla_{\mathbf{d}}^2 g(b_l, b_r) \leq 0$ (resp. ≥ 0). The convexity or concavity is strict if the corresponding inequality is strict.

We investigate the concavity and convexity properties of the function $g(b_l, b_r)$ (or, equivalently, the function $\mu(b_l, b_r)$) in the directions $(1, 0), (0, 1)$ and $(1, -1)$. Fig. 4 illustrates our results: in the 2×2 model we establish that $g(b_l, b_r)$ is concave in the directions $(1, 0), (0, 1)$ and convex in the direction $(1, -1)$ for any $(b_l, b_r) \in (0, 1)^2$. In the local model, we obtain the same results, but only along specific axes of interest. As we do not, in general, have a closed form solution for the global model, we resort to a surrogate function $\mu^{KS}(b_l, b_r)$, later explained in Section 6 and Appendix A.3, which is provably equal to $\mu^{KS}(b_l, b_r)$ at $(b_l, b_r) = (1/2, 1/2)$ and numerically indistinguishable otherwise. We prove for most of the subcritical regime that $\mu^{KS}(b_l, b_r)$ exhibits local convexity and concavity at $(1/2, 1/2)$. We formalize these results in the statements below.⁹

THEOREM 5. At any $\mathbf{b} \in (0, 1)^2$, $\mu^{2 \times 2}(b_l, b_r)$ is (i) strictly concave in the directions $(0, 1), (1, 0)$ and $(1, 1)$, and (ii) strictly convex in the direction $(1, -1)$.

The proof of this result can be found in Appendix B.2. For the local model we find similar geometric properties along three specific diagonals (see proof in Appendix C.2).

THEOREM 6. $\mu^{loc}(b_l, b_r)$ is strictly concave in the direction $(0, 1)$ when $b_l \in \{0, \frac{1}{2}\}$ and in the direction $(1, 0)$ when $b_r \in \{0, \frac{1}{2}\}$. $\mu^{loc}(b_l, b_r)$ is strictly convex in the direction $(1, -1)$ when $b_l + b_r = 1$.

In most of the subcritical regime, the surrogate function $\mu^{KS}(1/2, 1/2)$ for the global model exhibits similar geometric properties (see Appendix A.3.4).

THEOREM 7. When $10^{-4} < \alpha < 0.64\alpha^f - 0.03$ and $0.62\alpha^f + \alpha < 1.68$, $\mu^{KS}(1/2, 1/2)$ is (i) strictly concave in the directions $(0, 1)$ and $(1, 0)$, and (ii) strictly convex in the direction $(1, -1)$.

Beyond the subcritical regime, the geometries of the global model can be more nuanced, and Fig. 5 shows that μ^{KS} is not necessarily convex in the direction $(1, -1)$.

⁹Since the cost of flexibility is linear, the structural properties of $\mu(b_l, b_r)$ extend directly to the function $g(b_l, b_r)$.

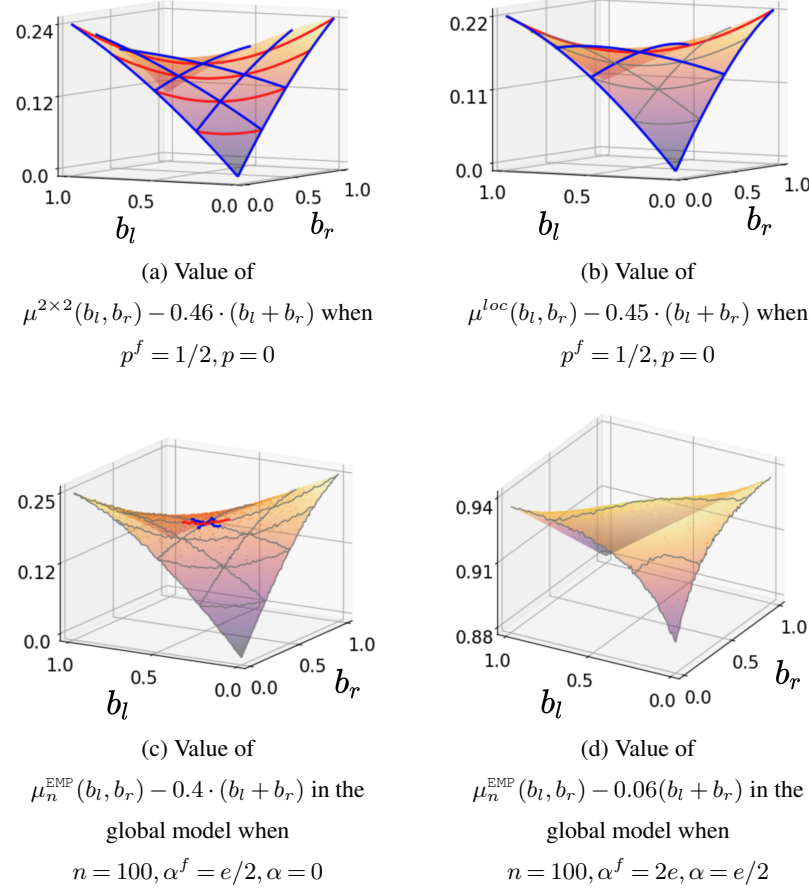


Figure 4 In instances (a) and (b) we highlight provable concavity in blue and provable convexity in red; in instance (c) we show local convexity and concavity for $\mu^{KS}(b_l, b_r)$ at $(1/2, 1/2)$; in instance (d) we illustrate that convexity can break down in the supercritical regime of the global model.

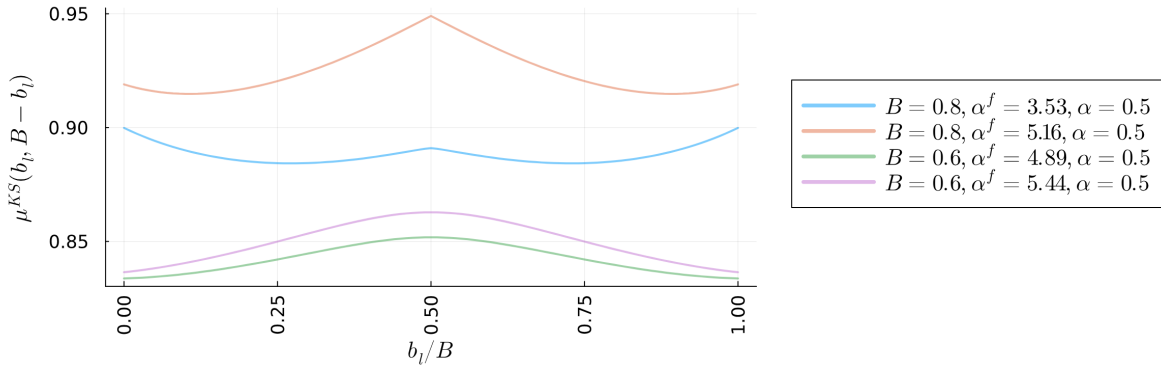


Figure 5 Illustration of $\mu^{KS}(b_l, B - b_l)$ with respect to b_l/B for varying values of B, α^f and α .

REMARK 1. The concavity results in the directions $(1, 0)$ and $(0, 1)$ reflect the decreasing marginal returns of flexibility that are commonly observed (e.g., Fine and Freund (1990), Bassamboo et al. (2012)). In contrast, convexity in the direction $(1, -1)$ uncovers a novel and surprising interplay between two flexibility

levers. This interplay has serious practical ramifications: first, balanced allocation can be a saddle point. Moreover, treating the flexibility optimization along two axes as a game between two verticals within an organization (see Section 1.2), we show that this suboptimal solution can emerge as a local Nash Equilibrium. We formalize these interpretations of our results in Appendix D.

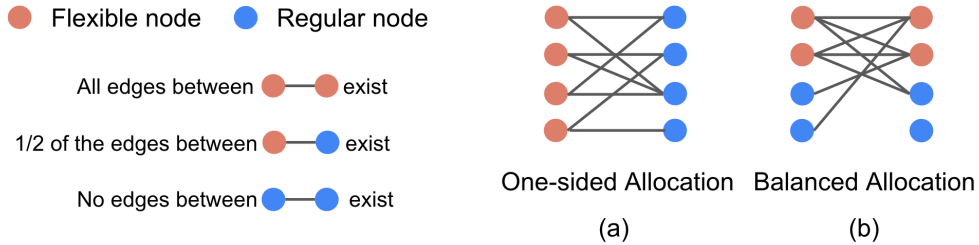


Figure 6 Illustration of flexibility cannibalization. Plot (a) and (b) present comparable node and edge realizations of one-sided and balanced allocations. To highlight the effect, half of the nodes are flexible and the edges are chosen with the simple, almost deterministic rule described in the figure. Both plots contain the same number of edges, but plot (b) has fewer matches due to a concentration of edges on the top subgraph.

4. Flexibility Cannibalization

The intuition behind the flexibility cannibalization effect in the global model comes from the simple insight that a feasible matching includes at most one of the edges incident to any given node. As such, flexibility designs should strive to avoid having many edges incident to the same node, as many of these end up wasted. In a balanced allocation, each flexible node has an expected degree of $\alpha^f(1 + B/2) + \alpha(1 - B/2)$. This is greater than the expected degree of any node in the one-sided flexibility design, which can be at most $\alpha^f + \alpha$. This higher expected degree of flexible nodes in the balanced allocation is mostly due to the possibility of creating flexible-to-flexible edges, which is why we name the effect “flexibility cannibalization”. Fig. 6 provides an example to illustrate how flexible nodes tend to have higher average degrees in balanced allocations; moreover, it shows that edges end up being cannibalized in the concentrated subgraph of flexible nodes, which leaves more regular nodes unmatched than in the one-sided allocation. In this section, we leverage flexibility cannibalization in the proof of Theorem 3 (i).

Proof of Theorem 3 (i). We prove that the one-sided allocation dominates the balanced one when $B = 1$ and $\alpha = 0$. Below, we state two lemmas and prove they imply the theorem, deferring the proofs and constructions for the lemmas to Section 4.1-4.2 and the corresponding appendices.

We first introduce a new bipartite random graph distribution, denoted G_n^b . This distribution is easier to analyze than the balanced allocation random graph (denoted $G_n(1/2, 1/2)$) but has the same asymptotic matching probability. In G_n^b , exactly $n/2$ nodes are flexible on each side (see Fig. 7). Each flexible node generates directed edges to the nodes on the other side (flexible or not), independently and with a probability p_n^f for each edge. This means that an edge between two flexible nodes can be generated in both

directions. When computing a maximum matching in G_n^b we ignore the directionality of the edges and treat such double edges between nodes as just a single edge. We introduce G_n^b as its realizations can be more easily coupled with the random graph of the one-sided allocation. Denoting the size of a realized maximum matching in G_n^b by the random variable \mathcal{M}_n^b and that of $G_n(1/2, 1/2)$ by $\mathcal{M}_n(1/2, 1/2)$, we show nodes in G_n^b and $G_n(1/2, 1/2)$ have the same asymptotic matching probability.

LEMMA 1. *With the above construction, $\limsup_{n \rightarrow \infty} \mathbb{E} [\mathcal{M}_n(1/2, 1/2) - \mathcal{M}_n^b] / n = 0$.*

Now, we compare G_n^b to the random graph with one-sided allocation. We denote the latter by G_n^o and its maximum matching size by $\mathcal{M}_n(1, 0)$. The next lemma compares \mathcal{M}_n^b and $\mathcal{M}_n(1, 0)$ in a non-asymptotic way. This is the key step of this proof, relying on an intricate coupling of interest in its own right.

LEMMA 2. *With the above construction, $\mathbb{E} [\mathcal{M}_n^b] \leq \mathbb{E} [\mathcal{M}_n(1, 0)] \forall n$.*

In the following derivation, Lemma 1 gives us the second equality and Lemma 2 the inequality:

$$\mu(1/2, 1/2) = \limsup_{n \rightarrow \infty} \mathbb{E} \left[\frac{\mathcal{M}_n(1/2, 1/2)}{n} \right] = \limsup_{n \rightarrow \infty} \mathbb{E} \left[\frac{\mathcal{M}_n^b}{n} \right] \leq \limsup_{n \rightarrow \infty} \mathbb{E} \left[\frac{\mathcal{M}_n(1, 0)}{n} \right] = \mu(1, 0),$$

which completes the proof of Theorem 3 (i). \square

4.1. Proof sketch of Lemma 1

As illustrated in Fig. 7, the graph G_n^b is a directed random graph that contains edges generated from left to right (denoted R_{ij}^l) and edges generated from right to left (R_{ij}^r). The edge probabilities are given by:

$$\mathbb{P} [R_{ij}^l = 1] = p_n^f, \forall i \in [n/2], j \in [n] \text{ and } \mathbb{P} [R_{ij}^r = 1] = p_n^f, \forall j \in [n/2], i \in [n]. \quad (2)$$

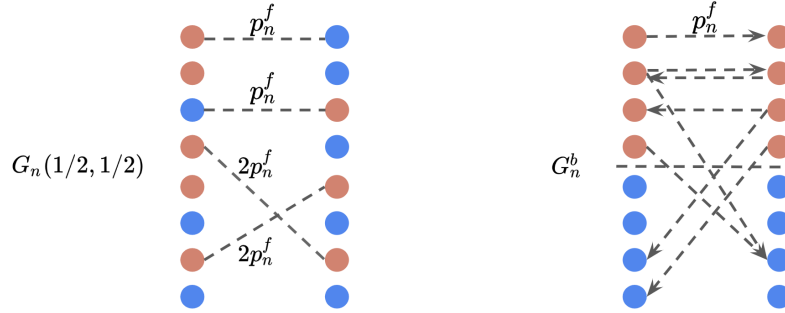


Figure 7 Illustration of $G_n(1/2, 1/2)$ and G_n^b . In G_n^b we assume that the top $n/2$ nodes on each side are “flexible” nodes that generate a directed edge towards any node on the opposite side with probability p_n^f .

G_n^b differs from $G_n(1/2, 1/2)$ in two ways: (i) G_n^b contains $n/2$ flexible nodes on each side of the bipartite graph, whereas every node in $G_n(1/2, 1/2)$ is flexible with probability $1/2$; (ii) in G_n^b an edge between v_i^l and $v_j^r, i, j \in [n/2]$, is generated from each side with probability p_n^f , instead of being generated only

once with probability $2p_n^f$. It is intuitive that neither (i) or (ii) significantly change the asymptotic matching size: standard concentration bounds guarantee that (i) affects $o(n)$ nodes, and (ii) affects $\sum_{i,j \in [n/2]} (p_n^f)^2 = \sum_{i,j \in [n/2]} (\alpha^f/n)^2 \in \mathcal{O}(1)$ possible edges in expectation. In Appendix A.1.1, we formalize this intuition.

4.2. Proof sketch of Lemma 2

In our proof, we construct a coupling between *pairs* of realizations of G_n^b and of G_n^o to compare the maximum matching sizes therein. First, we show that this coupling is valid in the sense that the coupled realizations occur with the same probability in their respective graphs. Second, we show that the average maximum matching size in the pair of realizations in G_n^b is smaller-equal to that in G_n^o . We present the key steps of our proof here and defer the complete proof to Appendix A.1.2.

Coupling the Realizations of Graphs. We partition the directed edges in a realization of G_n^b into sets X_1, X_2, X_3 and X_4 , depending on whether they are from left/right to top/bottom (see Fig. 8 (A)).

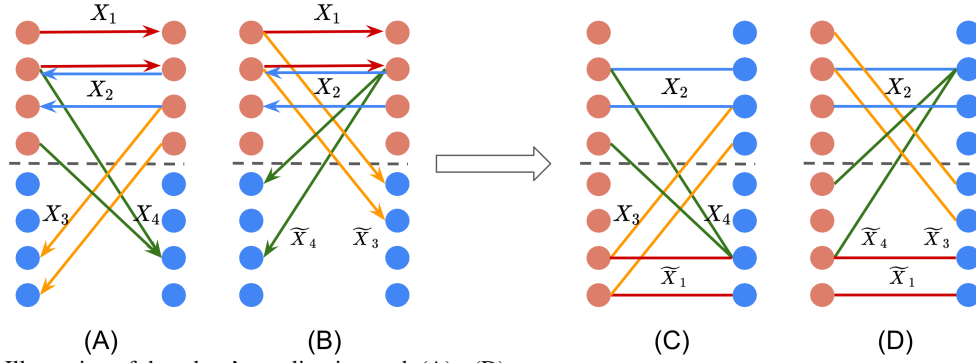


Figure 8 Illustration of the edges' coupling in graph (A) - (D)

We couple each realization of edges, i.e., of sets X_1, X_2, X_3 and X_4 , with a second realization (B), also from G_n^b , that occurs with the same probability (Fig. 8 (B)). Essentially, we “flip” the edges in X_3 and X_4 across the vertical axis to obtain the sets \tilde{X}_3 and \tilde{X}_4 . Then, we couple (A) and (B) with two realizations, (C) and (D) (see Fig. 8 (C) and (D)), of G_n^o . There, we “flip” the edges in X_1 from the upper sub-graph in (A) and (B) to the lower sub-graph in (C) and (D). Denoting by M_A, M_B, M_C, M_D the maximum matching sizes in the respective graphs, we then show that $M_A + M_B \leq M_C + M_D$ holding for all X_1, X_2, X_3 , and X_4 guarantees that $\mathbb{E} [\mathcal{M}_n^b] \leq \mathbb{E} [\mathcal{M}_n(1, 0)]$. We include the formal coupling and proof in Appendix A.1.2.

Proving the Dominance of One-sided Allocation. Our proof concludes by showing that the required property $M_A + M_B \leq M_C + M_D$ indeed holds for arbitrary X_1, X_2, X_3 and X_4 . As illustrated in Fig. 9, in (A) we denote by sets $Y_i \subset X_i$ the edges that are part of a given maximum matching; in (B), we denote by sets $Y'_i \subset X_1, Y'_2 \subset X_2, \tilde{Y}_3 \subset \tilde{X}_3$ and $\tilde{Y}_4 \subset \tilde{X}_4$ the edges that join a maximum matching. We then injectively map all edges of M_A and M_B (i.e., those in $Y_1 - Y_4, Y'_1, Y'_2, \tilde{Y}_3$ and \tilde{Y}_4) into existing edges of (C) and (D)

that also form a matching, which immediately proves $M_A + M_B \leq M_C + M_D$. The construction consists of two steps.

Step 1: mapping Y_1, Y_2, Y'_1 and Y'_2 . We start by directly copying the matched edges from Y_1, Y_2, Y'_1 and Y'_2 into (C) and (D), following the coupling rules. This corresponds to the red, blue, pink, and navy edges in Fig. 9.

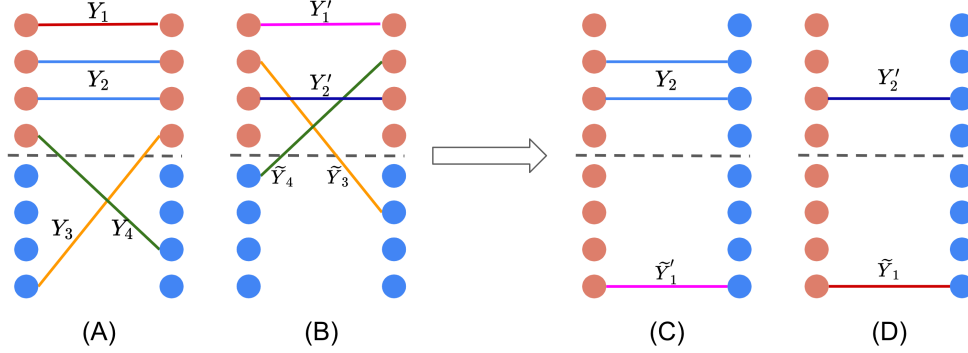


Figure 9 Illustration of the matches in (A) and (B), and the position they are copied into in (C) and (D).

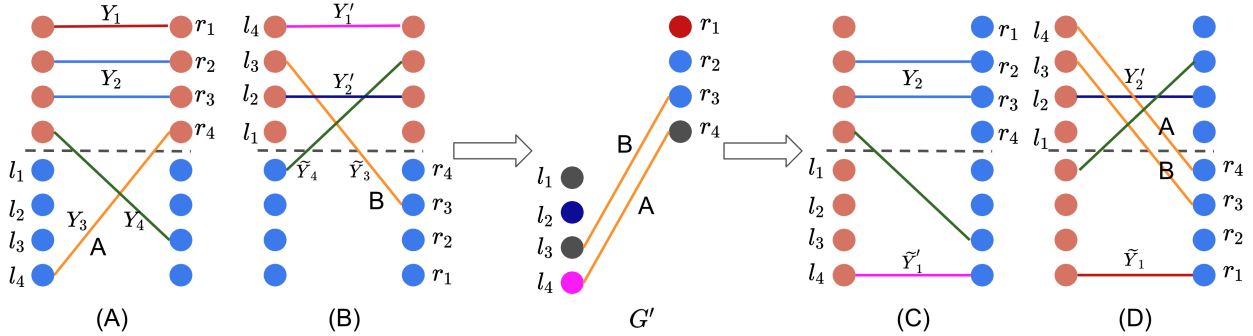


Figure 10 The plot illustrates the mapping of edges in Y_3 and \tilde{Y}_3 (the yellow edges) to (C) and (D) through the constructed graph G' . The labels indicate the correspondence between nodes/edges in G' and those in graphs (A)-(D). A second graph G'' can be constructed to map the edges in Y_4 and \tilde{Y}_4 (the green edges) into the indicated positions in (C) and (D).

Step 2: mapping Y_3, Y_4, \tilde{Y}_3 and \tilde{Y}_4 . The rest of the matched edges (the yellow and green edges) can also be mapped into (C) and (D), but this mapping is not static and depends on the matches that are already copied into the graphs. As the nodes in (C) and (D) that are matched through these copied edges can no longer be matched to any other node in the graphs, we denote the remaining nodes in (C) and (D) by \bar{C} and \bar{D} and the set of edges among these nodes by $E(\bar{C})$ and $E(\bar{D})$. Then, it suffices to show that we can injectively map all other matches (that we have not copied already) in (A) and (B) to $M(\bar{C}) \cup M(\bar{D})$, where $M(\bar{C})$ and $M(\bar{D})$ are respectively matchings that we construct in $E(\bar{C})$ and $E(\bar{D})$. We construct such a

mapping for edges in Y_3 and \tilde{Y}_3 based on a $\frac{n}{2} \times \frac{n}{2}$ colored bipartite multigraph G' (see Fig. 10). G' includes all edges from Y_3 and \tilde{Y}_3 that occur in graph (A) and (B); we label edges in G' that come from Y_3 as type A edges and edges from \tilde{Y}_3 as type B edges (there can be two edges, one of type A and one of type B, between a pair of nodes in G'). We color the nodes in G' based on whether the corresponding nodes in (A) and (B) are incident to Y_1, Y_2, Y'_1 and Y'_2 . Analogous to G' , we create a second graph G'' that contains all the edges from X_4 that are part of maximum matchings in (A) and (B). We show that edges in G', G'' can be mapped into graphs (C) and/or (D) based on their types and the colors of their incident nodes so that, together with the already copied edges, they produce feasible matchings in (C) and (D). As a result, each edge from M_A and M_B can be found in a matching in either (C) or (D), implying that $M_A + M_B \leq M_C + M_D$. Thus, $\mathbb{E} [\mathcal{M}_n^b] \leq \mathbb{E} [\mathcal{M}_n(1,0)] , \forall n$ when $\alpha = 0$. We formalize these constructions in Appendix A.1.2.

REMARK 2. Flexibility cannibalization arises in G_B^n due to an over-concentration of edges in the upper subgraph (see Fig. 8 (A) and (B)). Our coupling method shows that this yields fewer matches than would be possible when some edges are moved to the lower subgraph (see (C) and (D)).

5. Flexibility Abundance

Flexibility cannibalization is not a primary concern when α^f is very large, as flexible nodes have many incident edges and, in particular, to non-flexible nodes. However, in this situation where flexibility is *abundant*, another effect favors balanced allocations.

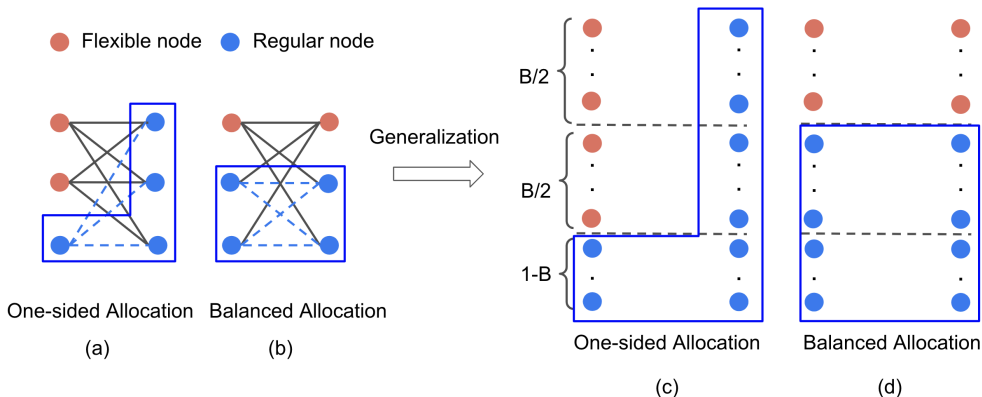


Figure 11 Intuition for flexibility abundance. Plot (a) and (b) assume that each flexible node is connected to all nodes on the other side of the graph. We find that a perfect matching in plot (a) requires the realization of one of the three dashed edges, whereas one in plot (b) requires the realization of one of the four dashed edges.

To gain intuition, suppose flexibility is so abundant that each flexible node is adjacent to every node on the other side of the graph (see Fig. 11 (a) and (b)). In this case, an optimal matching procedure is to proceed in two stages. First, identify a maximum matching among the regular nodes, and second, add as many matches as possible using the flexible nodes. In the second stage, it is preferable to match flexible

nodes with regular nodes to avoid wasteful flexible-flexible matches. Intuitively, this is possible when α is small enough that enough regular nodes are not matched in the first stage. In that case, the matching size is determined by the first stage, as the second stage always adds exactly one match per flexible node. And it turns out that the balanced allocation is more effective in the first stage. Though both allocations have about $(2 - B)n$ regular nodes in the entire graph, the balanced allocation has an equal number of regular nodes on both sides, whereas the one-sided allocation contains a subgraph of regular nodes with $(1 - B)n$ nodes on one side and n on the other (see Fig. 11 (c) and (d)). As a result, the expected number of edges in the subgraph of regular nodes is $(1 - B/2)^2/(1 - B) > 1$ times greater for the balanced allocation than for the one-sided allocation. Since the size of a maximum matching is close to the number of edges when α is small, the balanced allocation is thus more conducive to matching the regular nodes among themselves. This same intuition presents itself at a smaller scale in Fig. 11 (a) and (b) where having all flexible nodes on one side means that a perfect matching requires the realization of one of *three* potential blue edges among the regular nodes, whereas an even distribution of flexible nodes means that a perfect matching requires the realization of one of *four* potential blue edges among the regular nodes.

As we have observed in Fig. 3 (a), flexibility abundance arises for a wide range of parameters. Intuitively, it requires three ingredients: a high value of α^f to ensure that flexible nodes have abundant incident edges (and that wasting such edges is not a primary concern), (ii) $B < 1$ to ensure that one-sided flexibility cannot just match all flexible nodes to all regular nodes, and (iii) small (but positive) α to ensure that there exists a non-trivial matching among the regular nodes while avoiding an outcome that is so dense that all nodes can trivially be matched.¹⁰ Theorem 4 exemplifies such a regime, requiring $B \in [0, 4, 0.8]$, $\alpha \in [0.01, 0.05]$ and $\alpha^f \geq 22$ to assert that $\mu(B/2, B/2) > \mu(B, 0)$.

Proof sketch of Theorem 4. We now provide a proof sketch for Theorem 4 that generalizes the insights from Fig. 11 (a) and (b). Our proof first derives an upper bound on the number of matched nodes under one-sided flexibility, and a lower bound on the number of matched nodes under balanced flexibility. We then prove the theorem by verifying that the upper bound is dominated by the lower bound in the specified parameter regime.

Upper bound on the number of matched nodes for one-sided flexibility. For one-sided flexibility, we rely on the number of isolated (regular) nodes on the side on which we have flexibility. As there are about $(1 - B)n$ regular nodes on this side, out of which about $(1 - B)n e^{-2\alpha}$ are isolated, at most $(1 - B)(1 - e^{-2\alpha})n$ of these regular nodes can be matched.

Lower bound on the number of matched nodes for balanced flexibility. For balanced flexibility, we analyze what happens when we first match the regular nodes among themselves (stage 1), and then show that sufficiently many flexible nodes can be matched afterwards (stage 2). For stage 1, we prove (Appendix

¹⁰Recalling the example in Fig. 11, it should be significantly more likely for one of four edges to realize than for one of three edges to realize: with large α , the latter is too likely for this to be the case, when $\alpha = 0$, both are impossible.

A.2.1) the following bound on the maximum matching size in a $(1 - B/2)n \times (1 - B/2)n$ graph of regular nodes,¹¹ denoted by random variable m_1 :

LEMMA 3. $\mathbb{E}[m_1] \geq 2 \cdot (1 - B/2) n [1 - (1 - B/2)\alpha - e^{-2\alpha(1-B/2)}]$ as $n \rightarrow \infty$.

Intuitively, for small α the expected maximum matching size should be close to the expected number of edges because very few nodes have degree more than 1. Our proof explicitly characterizes this, and lower bounds m_1 by subtracting the number of “redundant edges” (those incident to nodes with degree > 1) from the total number of edges. This allows us to derive the lower bound for $\mathbb{E}[m_1]$ in Lemma 3.

Assuming that all flexible nodes are matched to an unmatched regular node in stage 2, it suffices to compare the number of matches between regular nodes. By verifying that

$$(1 - B)(1 - e^{-2\alpha})n < 2 \cdot (1 - B/2) n [1 - (1 - B/2)\alpha - e^{-2\alpha(1-B/2)}]$$

for $\alpha \in [0.01, 0.05]$ and $B \in [0.4, 0.8]$, we confirm that the balanced allocation creates more matches in the sub-graph of regular nodes. In the proof of Theorem 4 (Appendix A.2.2) we show that the gap in the above inequality is sufficiently large to account for the fact that, in the balanced allocation, some flexible nodes may not be matched in stage 2.

REMARK 3. The flexibility cannibalization in the 2×2 and the local model can be described similarly to the effect presented in Section 4. However, we do not find an effect equivalent to flexibility abundance in these two models. This is because flexibility abundance only arises when flexible nodes have sufficiently high degrees, making the waste of edges between them (due to flexibility cannibalization) a second-order effect. In the 2×2 and the local model, nodes have a maximum-degree of 2, which prevents the occurrence of the flexibility abundance effect.

6. Analyses Based on the Karp-Sipser Algorithm

In this section, we devise a less intuitive but more powerful tool to analyze the properties of $\mu(b_l, b_r)$ in the global model. In particular, this will allow us to overcome a limitation of the intuitive coupling proof presented in Section 4 for Theorem 3 (i), which is that the method is specific to $\alpha = 0$. To some extent, this is unavoidable: the proof applies to arbitrarily large α^f and, as we saw in the previous section, with large α^f , $B < 1$ and $\alpha > 0$, the one-sided allocation does not yield a larger matching. In contrast, in this section, we predominantly target the subcritical regime. A classical approach to analyzing the maximum matching size in sparse random graphs is the Karp-Sipser (KS) algorithm, which is known to be asymptotically optimal for a range of sparse random graphs (Karp and Sipser 1981, Balister and Gerke 2015). As formalized in Algorithm 1 in Appendix A.3, the KS algorithm iteratively matches and prunes nodes with degree 1 until no

¹¹While the number of regular nodes on each side of the graph is not deterministically $(1 - B/2)n$, it concentrates around this value as n scales large and we assume this deterministic number for the purpose of this proof sketch.

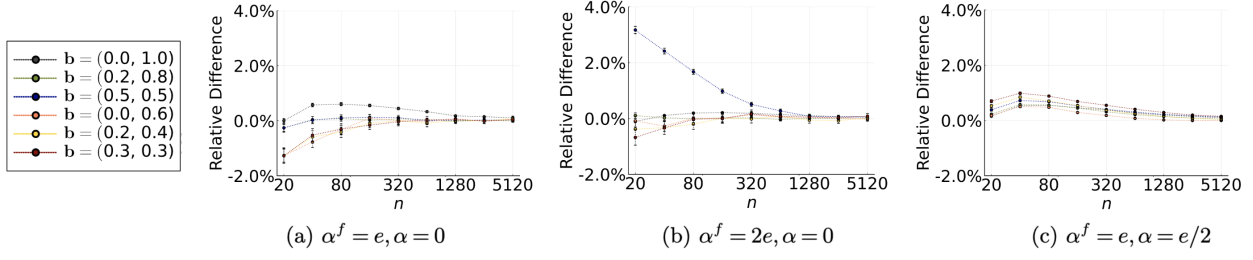


Figure 12 The plots present $(\mu^{\text{KS}}(b_l, b_r) - \mu_n^{\text{EMP}}(b_l, b_r)) / \mu_n^{\text{EMP}}(b_l, b_r)$ across varying (b_l, b_r) as n scales large.

such nodes remain; thereafter, it randomly selects edges to match. In this section, we generalize the known analyses of the KS algorithm to the bipartite random graphs in our model.

Our analysis is based on the quantity $\mu^{\text{KS}}(b_l, b_r)$, which is constructed from a set of 8 nonlinear equations provided in (11) and Theorem 9 in the appendix. Theorem 8 below demonstrates the equivalence of $\mu(b_l, b_r)$ and $\mu^{\text{KS}}(b_l, b_r)$ for the one-sided and balanced allocations in almost all of the subcritical regime. These equations arise from the KS-based analysis that characterizes the fraction of nodes that are “target” or “loser” (Karp and Sipser 1981); in our case, 8 such equations are required to determine the probability for flexible or regular nodes on either side to be either target or loser.

THEOREM 8. *When $10^{-4} < \alpha < \alpha^f, \alpha^f + \alpha < e$, and $\mathbf{b} = (1, 0)$ or $(1/2, 1/2)$, $\mu(b_l, b_r) = \mu^{\text{KS}}(b_l, b_r)$.*

Though Theorem 8 characterizes regions where $\mu(\cdot, \cdot) = \mu^{\text{KS}}(\cdot, \cdot)$, this in itself is not sufficient to make formal comparisons between $\mu(1, 0)$ and $\mu(1/2, 1/2)$; since there are no closed-form solutions to these nonlinear equations, we need to use a computer-aided proof and show that we can solve the nonlinear equations that $\mu^{\text{KS}}(b_l, b_r)$ depends on to provable numerical precision in these regions (see (25) in Appendix A.3.3). This then allows us to compare $\mu(1, 0)$ and $\mu(1/2, 1/2)$ for these α^f and α values. Moreover, by deriving a continuity property of μ^{KS} in α^f and α , we can construct local lower bounds for $\mu(1, 0) - \mu(1/2, 1/2)$ (see (23) and (24)), and conclude by verifying in a computer-aided proof that this lower bound exceeds 0 across the parameters specified by Theorem 3 (ii).¹²

Though Theorem 8 only applies to particular parameters, our numerical results (Fig. 12) suggest that $\mu_n^{\text{EMP}}(b_l, b_r)$ approaches $\mu^{\text{KS}}(b_l, b_r)$ as n for any parameters. We therefore use $\mu^{\text{KS}}(b_l, b_r)$ to evaluate different flexibility allocations, not just the balanced and one-sided one, across a wider range of parameters. Specifically, we conduct a grid search over $B, \alpha^f, \alpha, b_l, b_r$ with the set of parameters denoted S (details in Appendix A.3.6); we trust this to give a better estimate of the true asymptotic matching probability while also being computationally more efficient. We highlight the following observations:

Either the one-sided or the balanced allocation is optimal. Our numerical results support our focus on a comparison between the one-sided and the balanced allocations (see Fig. 5). Intuitively, one-sided

¹²The geometric properties stated in Theorem 7 follows from a similar computer-aided proof. For concavity, we construct local upper bounds to show that the second-order derivative (SOD) of $\mu^{\text{KS}}(1/2, 1/2)$ is negative in the direction $(0, 1)$; for convexity, we use local lower bounds to show that the SOD is positive in the direction $(1, -1)$.

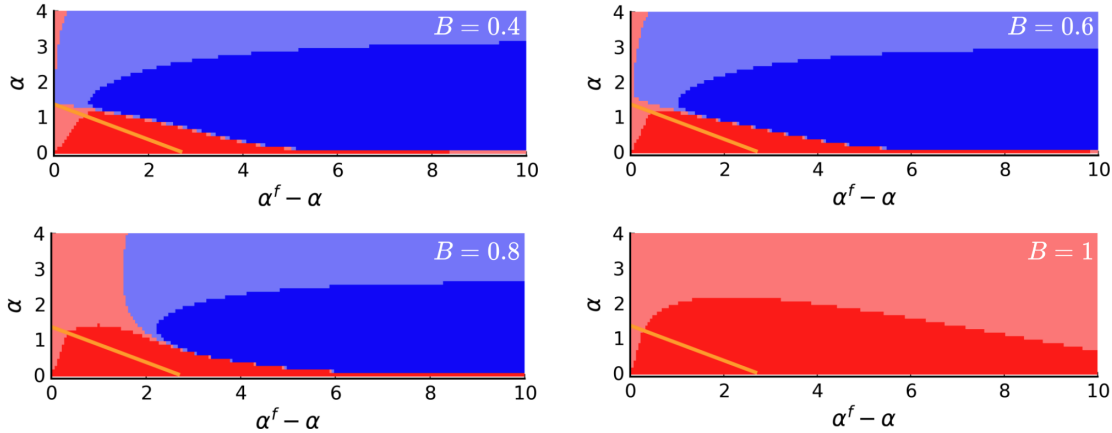


Figure 13 The plots present the values of $\frac{\mu^{\text{KS}}(B/2, B/2)}{\mu^{\text{KS}}(B, 0)}$ across varying α^f and $\alpha - \alpha^f$: the ratio is smaller than 1 in the red region (light red if between 0.999 and 1) and greater than 1 in blue region (light blue if between 1 and 1.001). The orange line highlights the boundary of the subcritical and supercritical regimes.

flexibility (i) minimizes the cannibalization effect (no flexible node can be a neighbor of another) and (ii) maximizes the abundance effect (least number of potential edges between the regular nodes). For the balanced allocation, these two are exactly reversed. Our numerical findings suggest that one always wants to minimize either one of the two effects to have an optimal allocation. If we could quantify the contribution of each effect, this leads us to believe that it would be concave in the fraction of flexibility allocated to one side (as the optimum always occurs at one of the two endpoints rather than at any point in between).

In the subcritical regime, the one-sided allocation is better. In Theorem 3 (ii) we proved this result for most of the sub-critical regime when $B = 1$. For $B < 1$ we do not know how to prove Theorem 8, and as a result we cannot provably generalize our computer-aided proof to this regime. However, we still find numerically that the one-sided allocation is better within the sub-critical regime for all tested values of B (see Fig. 13). This also matches our theoretical findings in that α^f cannot be too large in the subcritical regime, and thus the impact of flexibility abundance is also limited.

When $B = 1$ or $\alpha = 0$ the one-sided allocation is better. We find that $B = 1$ and $\alpha = 0$ are the special cases where the one-sided allocation always dominates,¹³ regardless of the value of α^f . Comparing this with our reasoning in Section 5, we find that these are exactly the cases where the flexibility abundance effect dissipates. This also explains why the coupling technique presented in Section 4 is specific to $B = 1$ and $\alpha = 0$: for large α^f Fig. 13 shows that the dominance of the one-sided allocation breaks down very close to the regime where $B = 1$ and $\alpha = 0$.

Finally, the numerical results based on $\mu^{\text{KS}}(b_l, b_r)$ confirm the characterization of Fig. 3 that we gave in Section 3.1: when α^f and α are very small (region (I) of Fig. 3), when $\alpha^f/\alpha \approx 1$ (region (II)), and when α^f and α are very large (region (III)), the performances of the one-sided and the balanced allocations are

¹³For $\alpha = 0$, though hard to see in the plots, there is always a thin red line just above the x-axis.

comparable. In the remaining regions, it is either flexibility abundance or flexibility cannibalization that drives the optimality of a particular flexibility design.

7. Simulation Results for Extended Models

Due to the complexity of analyzing maximum matching in random graphs, this paper focuses on idealized matching settings. However, the intuition behind the main flexibility allocation effects we uncover, the cannibalization and abundance effects, should generalize to more realistic or complex settings. To illustrate this, we first consider a spatial model where matches are feasible when nodes are spatially closer, as in ride-hailing matching problems. We also explore unbalanced markets, using an uneven number of supply and demand nodes in the spatial matching model.

We evaluate these models numerically by computing the empirical average matching probability. With a slight abuse of notation, we denote this quantity $\mu_{n,s}^{\text{EMP}}(b_l, b_r)$, the same notation that we used for our original model.¹⁴ We set $n = 100, s = 1000$ and drop the dependency of $\mu_{n,s}^{\text{EMP}}(b_l, b_r)$ on these two parameters. Our simulations reveal that even when we relax some of the assumptions behind the 2×2 , the local and the global model (e.g., conditional independence in edge generation, the expected edge count only depending on B but not on \mathbf{b} , and the symmetry of the two sides), flexibility cannibalization and abundance continue to make an appearance in the respective parameter regimes of interest. However, we also find that the additional complexities introduce new effects compared to before.

7.1. Spatial Matching

In the spatial matching model, we consider a two-dimensional grid $[0, 1]^2$ containing n drivers and n riders, uniformly distributed. Driver locations are denoted by vectors $\mathbf{d}_1, \mathbf{d}_2, \dots, \mathbf{d}_n$, and rider locations by $\mathbf{r}_1, \mathbf{r}_2, \dots, \mathbf{r}_n$. For a given flexibility allocation $\mathbf{b} = (b_l, b_r)$, driver i is flexible if random variable $F_i^l \sim \text{Bernoulli}(b_l)$ takes the value of 1, otherwise the driver is regular. Similarly, each rider j is associated with $F_j^r \sim \text{Bernoulli}(b_r)$, and the rider is flexible if and only if $F_j^r = 1$. We take constants α^f and α such that $0 \leq \alpha < \alpha^f$ and define $p_n^f = \alpha^f / \sqrt{n}, p_n = \alpha / \sqrt{n}$, respectively. We assume that an edge exists between a driver i and a rider j if their distance is within a threshold decided by their respective flexibility types:

$$\mathbb{P}[R_{ij} = 1 | F_i^l, F_j^r] = \begin{cases} 1 & \text{if } \|\mathbf{d}_i - \mathbf{r}_j\|_2 \leq 2p_n + (F_i^l + F_j^r) \cdot (p_n^f - p_n) \\ 0 & \text{otherwise} \end{cases}$$

In other words, \mathbf{r}_j has an edge with \mathbf{d}_i if their distance is within $2p_n + (F_i^l + F_j^r) \cdot (p_n^f - p_n)$. The asymptotic set-up $p_n^f, p_n \in \Theta(1/\sqrt{n})$ ensures that the expected number of edges in the spatial graph is in $\Theta(1)$, same as the asymptotic regime studied in the global model.

¹⁴For the imbalanced market model, n is the number of agents on the surplus side and we parameterize the number of agents on the other side by $\lambda \cdot n$, where $\lambda \in (0, 1]$.

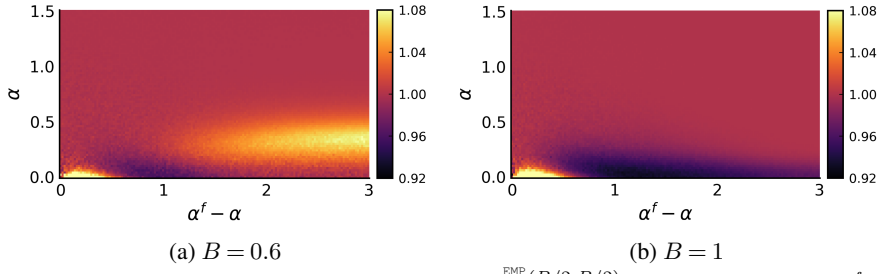


Figure 14 The plots present heat-map values of $\frac{\mu^{\text{EMP}}(B/2, B/2)}{\mu^{\text{EMP}}(B, 0)}$ across varying α and $\alpha^f - \alpha$.

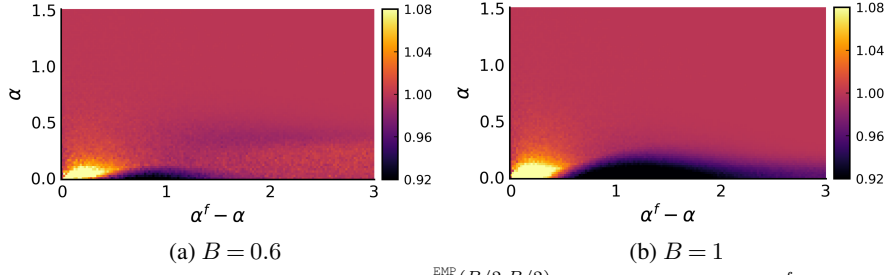


Figure 15 The plots present heat-map values of $\frac{\mu^{\text{EMP}}(B/2, B/2)}{\mu^{\text{EMP}}(B, 0)}$ across varying α and $\alpha^f - \alpha$ when $\lambda = 0.8$.

The spatial model relaxes two assumptions that are common to the 2×2 , the local and the global model: (1) the conditional independence assumption on edge realization R_{ij} with respect to indices i and j , and (2) the equivalence of different flexibility allocations in expected edge counts. In particular, in the one-sided allocation the expected number of riders that connects to a random driver is¹⁵ $(B(p_n^f + p_n)^2 + (1 - B)(2p_n)^2) \cdot \pi \cdot n$. This is smaller than the expected number of riders that connects to a random driver in balanced allocation, which equals

$$\left((B/2)^2 (2p_n^f)^2 + 2 \cdot B/2(1 - B/2) (p_n^f + p_n)^2 + (1 - B/2)^2 (2p_n)^2 \right) \cdot \pi \cdot n.$$

As such, we expect the balanced allocation to have an advantage over the one-sided allocation in the spatial setting. Indeed, in Fig. 14 we find that in a parameter regime with small α^f and α , the balanced allocation now outperforms the one-sided allocation. This follows because the maximum matching size is close to the number of edges in this very sparse regime, and the later is higher in expectation in the balanced allocation. In other parts of the heatmap we find consistency with results in the global model: one-sided allocation can be over 8% better than the balanced allocation when $B = 1$ or when α^f is moderate; moreover, it can be over 8% worse than the balanced allocation when α^f is very large, α is a positive small number, and $B < 1$.

7.2. Imbalanced Market

In our theoretical analysis we focused on fully symmetric markets to identify structural insights. In this subsection we explore flexibility allocations in imbalanced spatial matching markets and highlight the associated complexities. Specifically, we extend the spatial model in the previous subsection by allowing $\lambda \cdot n$

¹⁵We assume for simplicity that the driver is at least $2p_n$ away from the boundary of the $[0, 1]^2$ grid, an event that occurs with probability 1 as $n \rightarrow \infty$.

rather than n riders, where $\lambda \in (0, 1]$ (we ignore for symmetry the setting where the market has more demand than supply). We assume that, for a given flexibility allocation (b_l, b_r) , each driver is flexible with probability $b_l \cdot \lambda$ and each rider is flexible with probability b_r . This ensures that the cost of incentivizing an equal number of riders and drivers remains the same. We remark that the one-sided flexibility allocation $(B, 0)$ is no longer equivalent to $(0, B)$, as the latter generates more edges in expectation and thereby yields better solutions in this regime. In Fig. 15 (a) and (b) we show that the resulting advantage for the one-sided allocation mostly counteracts the flexibility abundance effect we previously observed for $B < 1$. Nonetheless, the regions where flexibility cannibalization dominates align with our findings in the global and the symmetric spatial matching model.

8. Managerial Insights and Conclusion

We conclude with the managerial implications of the results presented in Section 3, illustrating a potential pitfall of current platform experimentation designs. Many platforms today operate with separate teams dedicated to controlling flexibility incentives on the demand and supply sides. Through frequent experimentation, including continuous local improvement of algorithmic parameters, these teams aim to optimize the flexibility investment on each respective side of the market. For illustrative purposes, suppose the supply and demand teams iteratively vary the flexibility investment on their own side (b_l and b_r) by γ if doing so improves the objective. The teams settle at a point at which neither team has an incentive to further change its flexibility investment. We build upon the numerical results in Section 7.1 to illustrate the results of such experiments. As shown in Fig. 16 (a), when the balanced allocation is akin to a saddle point on the surface of $\mu^{\text{EMP}}(b_l, b_r) - c \cdot (b_l + b_r)$, the platform may get stuck at a sub-optimal balanced flexibility design. In contrast, Fig. 16 (b) shows that the platform may also be trapped at a sub-optimal one-sided allocation: when one team already operates with more flexibility than is jointly optimal, the other team has no incentive to further increase its flexibility. Thus, regardless of the dominance of the one-sided or balanced allocation, it is necessary for teams to experiment jointly in order to identify the optimal flexibility allocation; this finding also applies to the graph models considered in Section 2.

In summary, our work initiates the study of two-sided flexibility. In Section 3 we characterize the outcomes of different flexibility allocations, which result from the interplay of flexibility levers on different sides. We identify two effects in Sections 4 and 5, flexibility cannibalization and flexibility abundance, that respectively lend strength to the one-sided and balanced allocations. Doing so is a theoretical challenge, and we leverage a coupling construction, employ concentration bounds, and generalize KS algorithm-based analyses. Nonetheless, our work leaves many questions open. Firstly, our model intentionally focuses on a particular type of edge probability distribution, which keeps the expected number of edges invariant for a given budget B . However, different constructions (e.g., based on random geometric graphs) may be of practical interest. Secondly, though our effects seem to be robust under some such different constructions

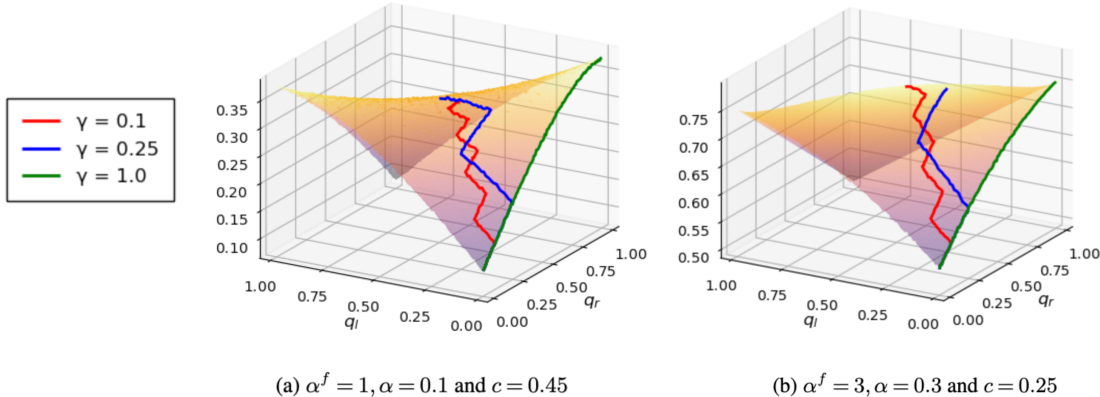


Figure 16 The colored lines illustrate the trajectory of experimentation on the surface of $\mu^{\text{EMP}}(b_l, b_r) - c \cdot (b_l + b_r)$ given different choices of λ . Due to the lack of joint experimentation, the search terminates around a sub-optimal balanced allocation in (a) when λ is too small, and around a sub-optimal one-sided allocation in (b) when λ is too large.

(see Section 7), all of our results are based on a central decision maker maximizing an unweighted matching, whereas many platforms in practice involve choice among agents on both sides; we know of no results in this direction and believe it to likely yield interesting findings. Finally, our work focuses on a matching model, but two-sided flexibility may also appear in queueing and manufacturing settings. All of these directions may be fruitful and, together, potentially reveal a general theory of two-sided flexibility.

References

- O Zeynep Akşin and Fikri Karaesmen. Characterizing the performance of process flexibility structures. *Operations Research Letters*, 35(4):477–484, 2007.

Kenneth Appel and Wolfgang Haken. The solution of the four-color-map problem. *Scientific American*, 237(4):108–121, 1977.

Jonathan Aronson, Alan Frieze, and Boris G Pittel. Maximum matchings in sparse random graphs: Karp–sipser revisited. *Random Structures & Algorithms*, 12(2):111–177, 1998.

Paul N Balister and Stefanie Gerke. Controllability and matchings in random bipartite graphs. *Surveys in combinatorics*, 424:119, 2015.

Achal Bassamboo, Ramandeep S Randhawa, and Jan A Van Mieghem. Optimal flexibility configurations in newsvendor networks: Going beyond chaining and pairing. *Management Science*, 56(8):1285–1303, 2010.

Achal Bassamboo, Ramandeep S Randhawa, and Jan A Van Mieghem. A little flexibility is all you need: on the asymptotic value of flexible capacity in parallel queuing systems. *Operations Research*, 60(6):1423–1435, 2012.

Ben Berger, Hongyao Ma, David Parkes, and Shreyas Sekar. Optimal subscription pricing design for ridesharing platforms. 2023.

Tom Bohman and Alan Frieze. Karp–sipser on random graphs with a fixed degree sequence. *Combinatorics, Probability and Computing*, 20(5):721–741, 2011.

- John A Buzacott and David D Yao. Flexible manufacturing systems: a review of analytical models. *Management science*, 32(7):890–905, 1986.
- Xi Chen, Jiawei Zhang, and Yuan Zhou. Optimal sparse designs for process flexibility via probabilistic expanders. *Operations Research*, 63(5):1159–1176, 2015.
- Jiri Chod and Nils Rudi. Resource flexibility with responsive pricing. *Operations Research*, 53(3):532–548, 2005.
- Mabel C Chou, Geoffrey A Chua, Chung-Piaw Teo, and Huan Zheng. Process flexibility revisited: The graph expander and its applications. *Operations research*, 59(5):1090–1105, 2011.
- Antoine Désir, Vineet Goyal, Yehua Wei, and Jiawei Zhang. Sparse process flexibility designs: Is the long chain really optimal? *Operations Research*, 64(2):416–431, 2016.
- Adam N Elmachtoub and Michael L Hamilton. The power of opaque products in pricing. *Management Science*, 67(8):4686–4702, 2021.
- Adam N Elmachtoub, David Yao, and Yeqing Zhou. The value of flexibility from opaque selling. *Available at SSRN* 3483872, 2019.
- Pál Erdős and Alfréd Rényi. On the existence of a factor of degree one of a connected random graph. *Acta Math. Acad. Sci. Hungar.*, 17:359–368, 1966.
- Paul Erdős, Alfréd Rényi, et al. On the evolution of random graphs. *Publ. math. inst. hung. acad. sci.*, 5(1):17–60, 1960.
- Charles H Fine and Robert M Freund. Optimal investment in product-flexible manufacturing capacity. *Management science*, 36(4):449–466, 1990.
- Daniel Freund and Garrett van Ryzin. Pricing fast and slow: Limitations of dynamic pricing mechanisms in ride-hailing. *Available at SSRN* 3931844, 2021.
- David Gamarnik, Tomasz Nowicki, and Grzegorz Swirszczy. Maximum weight independent sets and matchings in sparse random graphs. exact results using the local weak convergence method. *Random Structures & Algorithms*, 28(1):76–106, 2006.
- Warren H Hausman, David B Montgomery, and Aleda V Roth. Why should marketing and manufacturing work together?: Some exploratory empirical results. *Journal of operations management*, 20(3):241–257, 2002.
- John C Henderson and Harihara Venkatraman. Strategic alignment: Leveraging information technology for transforming organizations. *IBM systems journal*, 38(2.3):472–484, 1999.
- Seyed M Iravani, Mark P Van Oyen, and Katharine T Sims. Structural flexibility: A new perspective on the design of manufacturing and service operations. *Management Science*, 51(2):151–166, 2005.
- William C Jordan and Stephen C Graves. Principles on the benefits of manufacturing process flexibility. *Management science*, 41(4):577–594, 1995.
- Richard M Karp and Michael Sipser. Maximum matching in sparse random graphs. In *22nd Annual Symposium on Foundations of Computer Science (sfcs 1981)*, pages 364–375. IEEE, 1981.

- Varun Krishnan, Ramon Iglesias, Sebastien Martin, Su Wang, Varun Patabhiraman, and Garrett Van Ryzin. Solving the ride-sharing productivity paradox: Priority dispatch and optimal priority sets. *INFORMS Journal on Applied Analytics*, 52(5):433–445, 2022.
- Thomas G Kurtz. Solutions of ordinary differential equations as limits of pure jump markov processes. *Journal of applied Probability*, 7(1):49–58, 1970.
- Serguei Netessine, Gregory Dobson, and Robert A Shumsky. Flexible service capacity: Optimal investment and the impact of demand correlation. *Operations Research*, 50(2):375–388, 2002.
- NLsolve. NLsolve.jl: A Julia package for solving nonlinear equations. <https://github.com/JuliaNLsolvers/NLsolve.jl>, 2017. Version v4.5.1, MIT License.
- Hao Yi Ong, Daniel Freund, and Davide Crapis. Driver positioning and incentive budgeting with an escrow mechanism for ride-sharing platforms. *INFORMS Journal on Applied Analytics*, 51(5):373–390, 2021.
- Neil Robertson, Daniel Sanders, Paul Seymour, and Robin Thomas. A new proof of the four-colour theorem. *Electronic research announcements of the American Mathematical Society*, 2(1):17–25, 1996.
- Benson P Shapiro. Can marketing and manufacturing co-exist. *Harvard Business Review*, 55(5):104, 1977.
- David Simchi-Levi and Yehua Wei. Understanding the performance of the long chain and sparse designs in process flexibility. *Operations research*, 60(5):1125–1141, 2012.
- Philipp Ströhle, Christoph M Flath, and Johannes Gärttner. Leveraging customer flexibility for car-sharing fleet optimization. *Transportation Science*, 53(1):42–61, 2019.
- John N Tsitsiklis and Kuang Xu. Flexible queueing architectures. *Operations Research*, 65(5):1398–1413, 2017.
- Jan A Van Mieghem. Investment strategies for flexible resources. *Management Science*, 44(8):1071–1078, 1998.
- David W Walkup. Matchings in random regular bipartite digraphs. *Discrete mathematics*, 31(1):59–64, 1980.
- Rodney B Wallace and Ward Whitt. A staffing algorithm for call centers with skill-based routing. *Manufacturing & Service Operations Management*, 7(4):276–294, 2005.
- KA Weir, AK Kochhar, SA LeBeau, and DG Edgeley. An empirical study of the alignment between manufacturing and marketing strategies. *Long Range Planning*, 33(6):831–848, 2000.
- Douglas Brent West et al. *Introduction to graph theory*, volume 2. Prentice hall Upper Saddle River, 2001.
- Lenka Zdeborová and Marc Mézard. The number of matchings in random graphs. *Journal of Statistical Mechanics: Theory and Experiment*, 2006(05):P05003, 2006.
- Yeqing Zhou. *Supply Chain and Service Operations with Demand-Side Flexibility*. Columbia University, 2021.

Appendix A: Proofs of the Global Model

A.1. Proofs of the Global Model through the Coupling Argument

In this section, we prove Lemma 1 and Lemma 2, which are the key auxiliary results for Theorem 3 (i).

A.1.1. Proof of Lemma 1

Proof. Recall that we have constructed a random graph G_n^b in (2) that decomposes the $2p_n^f$ edges as two groups of directed edges, in each of which an edge exists with probability p_n^f . Notice that when constructing a maximum matching in G_n^b , we do not differentiate between edges of different directions. However, we maintain the requirement that no two edges (of either direction) can share a node in the matching. In the rest of the proof we show that neither difference (i) nor (ii) identified in Section 4.1 changes the asymptotic matching size.

We assume without loss of generality that n is an even number (else, we can ignore nodes v_n^l and v_n^r without changing the asymptotic matching probability). We start by applying standard concentration bounds to show that assuming $n/2$ flexible nodes on each side leads to $o(n)$ error in the asymptotic matching size. Specifically, we define the event that in $G_n(1/2, 1/2)$

$$E_1 := \left\{ \left| \sum_i F_i^l - n/2 \right| \leq n^{5/8} \text{ and } \left| \sum_j F_j^r - n/2 \right| \leq n^{5/8} \right\}.$$

Specifically, letting E_1^c be the complement of event E_1 , we have

$$\begin{aligned} \mathbb{E} [\mathcal{M}_n(1/2, 1/2) - \mathcal{M}_n^b] &= \mathbb{E} [\mathcal{M}_n(1/2, 1/2) | E_1^c] \mathbb{P}[E_1^c] + \mathbb{E} [\mathcal{M}_n(1/2, 1/2) | E_1] \mathbb{P}[E_1] - \mathbb{E} [\mathcal{M}_n^b] \\ &\leq n \cdot e^{-\Omega(n^{1/4})} + \mathbb{E} [\mathcal{M}_n(1/2, 1/2) | E_1] - \mathbb{E} [\mathcal{M}_n^b] \\ &\leq \mathbb{E} [\mathcal{M}_n(1/2, 1/2) | E_1] - \mathbb{E} [\mathcal{M}_n^b] + \mathcal{O}(1) \\ &\leq \mathbb{E} [\mathcal{M}_n(1/2, 1/2) \left| \sum_i F_i^l = \sum_j F_j^r = n/2 \right.] + o(n) - \mathbb{E} [\mathcal{M}_n^b] + \mathcal{O}(1) \\ &= \mathbb{E} [\mathcal{M}_n(1/2, 1/2) - \mathcal{M}_n^b \left| \sum_i F_i^l = \sum_j F_j^r = n/2 \right.] + o(n). \end{aligned}$$

Notice that the first inequality above is a concentration result that follows from the Chernoff bound, and the third inequality above follows from the fact that having $n^{5/8}$ additional flexible nodes on each side of $G_n(1/2, 1/2)$ creates at most $o(n)$ additional matches.

We next show that drawing two edges, each with probability p_n^f , is close to drawing a single edge with probability $2p_n^f$ in the asymptotic regime we study. With $\sum_i F_i^l = \sum_j F_j^r = n/2$, we reorder the nodes such that the first $n/2$ nodes on each side of $G_n(1/2, 1/2)$ are flexible. We then couple the edges in the two graphs (G_n^b and a balanced graph with $\sum_i F_i^l = \sum_j F_j^r = n/2$) by drawing a random variable $\omega_{ij} \sim U(0, 1)$

for every $i, j \in [n]$ and using ω_{ij} to generate the edge between i and j . Specifically, we set $R_{ij} = 1$ if and only if $\omega_{ij} \leq \mathbb{P}[R_{ij} = 1]$ in the respective graph.¹⁶ In the balanced graph, in which the first $n/2$ nodes are flexible on each side, we obtain $\mathbb{P}[R_{ij} = 1] = 2p_n^f, \forall i, j \in [n/2]$ and in G_n^b we get

$$\mathbb{P}[R_{ij} = 1] = \mathbb{P}\left[R_{ij}^l + R_{ij}^r \geq 1\right] = 2p_n^f - \left(p_n^f\right)^2, \forall i, j \in [n/2].$$

The probabilities for all other edges are the same in both graphs. This characterization of the probability of $R_{ij} = 1$ in each graph implies for a given realization of ω that

$$\mathbb{E}\left[\mathcal{M}_n(1/2, 1/2) - \mathcal{M}_n^b \middle| \omega, \sum_i F_i^l = \sum_j F_j^r = n/2\right] \leq \sum_{i,j \in [n/2]} \mathbb{1}_{\omega_{ij} \in \left[2p_n^f - \left(p_n^f\right)^2, 2p_n^f\right]}$$

because the number of additional matches in $\mathcal{M}_n(1/2, 1/2)$ is upper bounded by the number of additional edges in the graph. Taking expectation over ω , we find that

$$\mathbb{E}\left[\mathcal{M}_n(1/2, 1/2) - \mathcal{M}_n^b \middle| \sum_i F_i^l = \sum_j F_j^r = n/2\right] \leq \sum_{i,j \in [n/2]} \mathbb{P}\left[\omega_{ij} \in \left[2p_n^f - \left(p_n^f\right)^2, 2p_n^f\right]\right] = \sum_{i,j \in [n/2]} \left(p_n^f\right)^2 = O(1)$$

This implies that

$$\mathbb{E}\left[\mathcal{M}_n(1/2, 1/2) - \mathcal{M}_n^b\right] \leq \mathbb{E}\left[\mathcal{M}_n(1/2, 1/2) - \mathcal{M}_n^b \middle| \sum_i F_i^l = \sum_j F_j^r = n/2\right] + o(n) = o(n).$$

Thus, when $\alpha = 0$ we have $\limsup_{n \rightarrow \infty} \mathbb{E}[\mathcal{M}_n(1/2, 1/2) - \mathcal{M}_n^b] / n = 0$. \square

A.1.2. Proof of Lemma 2

Proof. Recall from Section 4.2 that we start by constructing a valid coupling of realizations of G_n^b and G_n^o , and then compare the matching sizes among the coupled graphs. In G_n^b , we denote an edge from v_i^l to v_j^r by (v_i^l, v_j^r) and an edge from v_j^r to v_i^l by (v_j^r, v_i^l) . Then, we partition the realized edges in G_n^b into four groups:

$$\begin{aligned} X_1 &:= \left\{(v_i^l, v_j^r) \mid i, j \in [n/2], R_{ij}^l = 1\right\}, \quad X_2 := \left\{(v_j^r, v_i^l) \mid i, j \in [n/2], R_{ij}^r = 1\right\}, \\ X_3 &:= \left\{(v_j^r, v_i^l) \mid j \in [n/2], i \in \{n/2+1, \dots, n\}, R_{ij}^r = 1\right\}, \quad X_4 := \left\{(v_i^l, v_j^r) \mid i \in [n/2], j \in \{n/2+1, \dots, n\}, R_{ij}^l = 1\right\}. \end{aligned}$$

In Fig. 8 (A) we illustrate the edges in X_1, X_2, X_3, X_4 as red, blue, yellow, and green, respectively.

Fix a realization of X_1, X_2, X_3 and X_4 . We start by flipping X_1, X_3 and X_4 vertically around the middle of the bipartite graph and swapping the directions accordingly, defining

$$\begin{aligned} \widetilde{X}_1 &:= \left\{(v_{n+1-i}^l, v_{n+1-j}^r) \text{ for each } (v_i^l, v_j^r) \in X_1\right\}, \quad \widetilde{X}_3 := \left\{(v_{n+1-i}^l, v_{n+1-j}^r) \text{ for each } (v_j^r, v_i^l) \in X_3\right\}, \\ \text{and } \widetilde{X}_4 &:= \left\{(v_{n+1-j}^r, v_{n+1-i}^l) \text{ for each } (v_i^l, v_j^r) \in X_4\right\}. \end{aligned}$$

¹⁶In G_n^b , $R_{ij} = 1$ if and only if $R_{ij}^l + R_{ij}^r \geq 1$.

Then, we construct the following graphs: graph (A) contains edges in X_1, X_2, X_3 and X_4 ; graph (B) contains edges in X_1, X_2, \tilde{X}_3 and \tilde{X}_4 ; graph (C) contains edges in $\tilde{X}_1, X_2, X_3, X_4$, (and drop their directions); and graph (D) contains edges in $\tilde{X}_1, X_2, \tilde{X}_3, \tilde{X}_4$, (and drop their directions). Fig. 8 provides an illustration of the different graphs. As before, the edges in X_1, X_2, X_3, X_4 are colored in red, blue, yellow, and green, respectively, and the coloring is maintained for their (flipped) copies in graphs (B)-(D). Essentially, we flip X_3 and X_4 to construct graph (B), and then we flip X_1 in (A) and (B) to construct (C) and (D). Our goal is to couple the realizations of G_n^b as (A) or (B) with the realizations of G_n^o as (C) or (D), so that it suffices to compare the combined size of the matchings in graph (A) and (B) with that of (C) and (D). This means that our proof builds on a coupling between two pairs of graphs rather than just one pair; we explain below how this allows us to find for each edge in a matching of either (A) or (B) a corresponding edge that can be part of a matching in (C) or (D).

We denote the sizes of a maximum matching in the four graphs, (A)-(D), by M_A, M_B, M_C , and M_D . Notice that this is a slight abuse of notation because we omitted the dependency of these quantities on X_1, X_2, X_3 and X_4 for notational convenience. We now argue that graph (A) and (B) are possible realizations of G_n^b , while graph (C) and (D) are possible realizations of G_n^o , all of which occur with the same probability in the respective random graphs. With $p_n = \alpha/n = 0$, in G_n^o (as $\alpha = 0$), we have $\mathbb{P}[R_{ij} = 1] = p_n^f, \forall i, j \in [n]$. Combined with (2), we thus know that, given X_1, X_2, X_3 and X_4 ,

$$\begin{aligned} \mathbb{P}\left[G_n^b \text{ realizes as (A)}\right] &= \mathbb{P}\left[G_n^b \text{ realizes as (B)}\right] = \mathbb{P}[G_n^o \text{ realizes as (C)}] = \mathbb{P}[G_n^o \text{ realizes as (D)}] \\ &= \left(p_n^f\right)^{|X_1|+|X_2|+|X_3|+|X_4|} \left(1-p_n^f\right)^{n^2-(|X_1|+|X_2|+|X_3|+|X_4|)}. \end{aligned}$$

We now prove the coupling based on X_1, X_2, X_3 and X_4 is valid. When $X_3 = \tilde{X}_3$ and $X_4 = \tilde{X}_4$,¹⁷ i.e., (A) and (B) are identical, we trivially have $M_A = M_B$, and the maximum matching size in (A) can be written as $(M_A + M_B)/2$. On the other hand, when $X_3 \neq \tilde{X}_3$ or $X_4 \neq \tilde{X}_4$, since G_n^b realize as (A) and (B) with the same probability the weighted average maximum matching size in (A) and (B) is also $(M_A + M_B)/2$. Thus, for any n ,

$$\mathbb{E}\left[\mathcal{M}_n^b\right] = \sum_{\substack{\text{all realizations of} \\ X_1, X_2, X_3, X_4}} \left(p_n^f\right)^{|X_1|+|X_2|+|X_3|+|X_4|} \left(1-p_n^f\right)^{n^2-(|X_1|+|X_2|+|X_3|+|X_4|)} \cdot \frac{M_A + M_B}{2}.$$

Similarly, we find that

$$\mathbb{E}\left[\mathcal{M}_n(1, 0)\right] = \sum_{\substack{\text{all realizations of} \\ X_1, X_2, \tilde{X}_3, \tilde{X}_4}} \left(p_n^f\right)^{|X_1|+|X_2|+|X_3|+|X_4|} \left(1-p_n^f\right)^{n^2-(|X_1|+|X_2|+|X_3|+|X_4|)} \cdot \frac{M_C + M_D}{2}.$$

¹⁷This may occur when all edges in X_3 and X_4 are symmetric around the middle of the bipartite graph, i.e., they “flip” to themselves.

Thus, as long as we can show that,

$$\forall X_1, X_2, X_3 \text{ and } X_4 : M_A + M_B \leq M_C + M_D, \quad (3)$$

we can conclude that $\mathbb{E} [\mathcal{M}_n^b] \leq \mathbb{E} [\mathcal{M}_n(1, 0)] \ \forall n$ when $\alpha = 0$.

In the rest of the proof, we verify (3). We pick an arbitrary matching in (A) and denote the edges in X_1, X_2, X_3 and X_4 that are involved in the maximum matching by Y_1, Y_2, Y_3 and Y_4 . Similarly, we pick any matching in (B) and denote the edges in X_1, X_2, \tilde{X}_3 and \tilde{X}_4 that are involved in the maximum matching by Y'_1, Y'_2, \tilde{Y}'_3 and \tilde{Y}'_4 .¹⁸ Our proof proceeds by constructing feasible matchings in (C) and (D) that have a combined size that is greater-equal to the combined size of the matchings in (A) and (B). We drop the direction of the edges as (v_i^l, v_j^r) and (v_j^r, v_i^l) cannot appear in the same matching, and with a slight abuse of notation, we denote an undirected edge between v_i^l and v_j^r by (v_i^l, v_j^r) . Fig. 9 (A) and (B) illustrate Y_1, Y'_1, Y_2, Y'_2 as red, pink, blue, and navy; moreover, the plots illustrate Y_3 and \tilde{Y}'_3 as yellow, and Y_4 and \tilde{Y}'_4 as green.

To construct matchings in (C) and (D), we flip Y_1, Y'_1 vertically and define

$$\tilde{Y}_1 := \left\{ (v_{n+1-i}^l, v_{n+1-j}^r) \text{ for each } (v_i^l, v_j^r) \in Y_1 \right\} \quad \text{and} \quad \tilde{Y}'_1 := \left\{ (v_{n+1-i}^l, v_{n+1-j}^r) \text{ for each } (v_i^l, v_j^r) \in Y'_1 \right\}.$$

Since graph (C) contains all edges in \tilde{X}_1 and X_2 , \tilde{Y}'_1 and Y_2 are part of a feasible matching in (C). Similarly, since graph (D) also contains all edges in \tilde{X}_1 and X_2 , Y'_2 and \tilde{Y}'_1 are part of a feasible matching in (D). As illustrated in Fig. 9 (C) and (D), we copy \tilde{Y}'_1 and Y_2 into the construction of a matching in (C), and copy Y'_2 and \tilde{Y}'_1 into a matching in (D) (as before, the figure maintains consistent coloring for the flipped edges in different subgraphs).

Then, it suffices to show that all edges in Y_3, \tilde{Y}_3, Y_4 and \tilde{Y}_4 can also be mapped into (C) and (D). We denote by \bar{C} and \bar{D} the remaining nodes in (C) and (D) that are not incident to the already copied matches, and by $E(\bar{C})$ and $E(\bar{D})$ the available edges among \bar{C} and \bar{D} . Below we construct a mapping that injectively maps all edges in Y_3, \tilde{Y}_3, Y_4 and \tilde{Y}_4 to two matchings $M(\bar{C})$ in (C) and $M(\bar{D})$ in (D), where $M(\bar{C}) \subseteq E(\bar{C})$ and $M(\bar{D}) \subseteq E(\bar{D})$. This then immediately implies that $M_A + M_B \leq M_C + M_D$.

Since the edges in X_3 (\tilde{X}_3) are not incident to those in X_4 (\tilde{X}_4), the resulting matches Y_3, \tilde{Y}_3 and Y_4, \tilde{Y}_4 can be analyzed separately. We next show that the matches in Y_3 and \tilde{Y}_3 can be injectively mapped to $(M(\bar{C}) \cap X_3) \cup (M(\bar{D}) \cap \tilde{X}_3)$ in graph (C) and (D) by constructing a multigraph G' . The injective mapping from Y_4 and \tilde{Y}_4 to $(M(\bar{C}) \cap X_4) \cup (M(\bar{D}) \cap \tilde{X}_4)$ follows from symmetry through a similarly constructed graph G'' , and thus our focus is on G' for the rest of this proof. Specifically, we construct G' as a

¹⁸Notice that the distinction between Y_1, Y_2 and Y'_1, Y'_2 arises from the fact that the edges in X_1 and X_2 that are involved in a maximum matching for (A) may be different from those for (B).

bipartite graph with $n/2$ nodes on each side, indexing nodes on the left as v_1^l through $v_{n/2}^l$ and on the right as v_1^r through $v_{n/2}^r$. The edge set of G' consists of¹⁹

$$\left\{ (v_{i-n/2}^l, v_j^r) \text{ for each } (v_i^l, v_j^r) \in Y_3 \right\} \cup \left\{ (v_{n/2+1-i}^l, v_{n+1-j}^r) \text{ for each } (v_i^l, v_j^r) \in \tilde{Y}_3 \right\}.$$

We refer to the former set as type A edges (as they come from Y_3 in graph (A)) and the later set as type B edges. Finally, we color the nodes in G' :²⁰

- We color v_j^r in G' by red (blue) if in graph (A) v_j^r is matched by an edge in Y_1 (Y_2);
- We color v_i^l in G' by pink (navy) if in graph (B) $v_{n/2+1-i}^l$ is matched by an edge in Y'_1 (Y'_2).

Fig. 10 provides an illustration of G' that is constructed based on Fig. 9 (A) and (B). Notice that a node on the left of G' cannot be colored twice because it is matched by at most one edge in $Y_1 \cup Y_2$, and similarly those on the right cannot be colored twice because they are matched by at most one edge in $Y'_1 \cup Y'_2$.

We begin by analyzing the degree of nodes in G' . Recall that every edge in G' comes from either Y_3 or \tilde{Y}_3 . Thus, each node in G' has degree at most 2, as otherwise at least two incident edges would come from either Y_3 or \tilde{Y}_3 , contradicting that Y_3 and \tilde{Y}_3 are subsets of matchings in (A) and (B), respectively. Indeed, colored nodes in G' have a degree of at most 1 because, if the colored node is already matched by an edge in graph (A), then it cannot connect to any type A edges; if it is matched by an edge in graph (B), then it cannot connect to any type B edges. Thus, in G' each colored node can connect to at most one edge from either type A or type B.

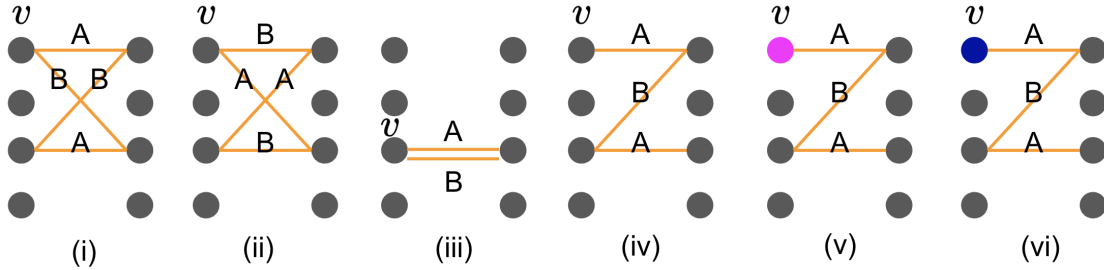


Figure 17 Illustrations of possible connected components in G' .

Since nodes in G' have a degree of at most 2, any connected component in G' is either a path or a cycle (page 109 of West et al. (2001)). Fig. 17 illustrates examples of connected components in G' .²¹ We next construct the matchings $M(\bar{C})$ and $M(\bar{D})$ based on the structure of paths and cycles in G' through two mappings that respectively map the edges in G' to $M(\bar{C})$ and $M(\bar{D})$. The mappings ensure that all

¹⁹As G' is a multigraph, this union may contain two copies of the same edge.

²⁰Notice that the coloring is based on the edges, rather than the colors of the flexible/regular nodes that we used for illustrations in (A)-(D).

²¹The result in West et al. (2001) applies only to simple graphs; as nodes in G' have degree at most 2, whenever there are multiple edges between 2 nodes, this means that these 2 nodes have no other edges incident to them (see Figure 17 (iii)). Therefore, such a pair of nodes also forms a cycle.

edges in G' of either type A or B are mapped to either $M(\bar{C}) \cap X_3$ or $M(\bar{D}) \cap \tilde{X}_3$. This then immediately completes the proof. Specifically, we use the following bijective mappings from edges in G' to $M(\bar{C}) \cap X_3$ and $M(\bar{D}) \cap \tilde{X}_3$, which we denote by f_C and f_D , respectively:

$$f_C : (v_i^l, v_j^r) \rightarrow (v_{i+n/2}^l, v_j^r), f_D : (v_i^l, v_j^r) \rightarrow (v_{n/2+1-i}^l, v_{n+1-j}^r), \forall i, j \in [n/2]. \quad (4)$$

In the rest of the proof, we show that every edge in G' is mapped by either f_C or f_D to its respective image in either $M(\bar{C}) \cap X_3$ or $M(\bar{D}) \cap \tilde{X}_3$, i.e., the edge is mapped to part of a feasible matching solution.

We begin by considering the case of cycles in G' . Since all nodes in a cycle have a degree of 2, no node in the cycle can be colored. Moreover, in a bipartite graph, all cycles are of even length. Since no two type A edges or two type B edges may share the same node, the edges in the cycle must be alternating in type A and B. As illustrated in Fig. 17 (i) and (ii), as one traverses through the cycle starting from node v on the top left and moves to the top right, the edges must either be of (1) type A, B, A, B, ..., or (2) type B, A, B, A, ... To create feasible matchings in (C) and (D), we need to ensure that the edges that are incident to the same node in G' are not both mapped by f_C (resp. f_D), since they would otherwise share a node in graph (C) (resp. (D)). Thus, for structure (1), we choose for each type A edge e the edge $f_C(e)$ to become part of the matching in (C) and for each type B edge e the edge $f_D(e)$ to become part of the matching in graph (D).²² These choices always lead to a feasible matching because the allocated edges are not incident to any colored nodes, and thus not incident to any matches already copied from Y_1, Y_2, Y'_1 , and Y'_2 . The construction based on structure (2) is symmetric. We remark that the structure in Fig. 17 (iii), with two edges between a pair of nodes, is a special case of a cycle in G' .

Now, we consider the case of paths. Since all but the endpoints of a path have a degree of 2, only the two endpoints of a path may be colored. Thus, it suffices to consider the following three sub-cases: (1) the two endpoints of the path are both uncolored, (2) one of the endpoints is colored, and (3) both of the endpoints of the path are colored.

- In sub-case (1), as illustrated in Fig. 17 (iv), the path must alternate between edges of type A and B. Thus, we can iteratively include all edges in the path in $M(\bar{C})$ or $M(\bar{D})$, as we did in the case of cycles.
- In sub-case (2), if an end-point v is colored pink, as illustrated in Fig. 17 (v), then the edge that connects to the endpoint must be of type A. Any subsequent edge to v must then alternate between type B, A, B, To avoid the first edge sharing a node with \tilde{Y}'_1 in graph (C), we include all type A edges by using f_D to map them into $E(\bar{D})$, and all type B edges by using f_C to map them into $E(\bar{C})$. In contrast, if an end-point v is navy, as illustrated in Fig. 17 (vi), then the edge that connects to the endpoint must be of type A. Thus, the subsequent edges follow type B,A,B, To avoid the first edge sharing a node with

²²An alternative option is to map all type A edges using f_D and type B edges using f_C .

Y'_2 in graph (D), we then include for each type A edge its image in $E(\bar{C})$ under f_C and for each type B edge its image under f_D in $E(\bar{D})$. All subsequent edges in the path are incident to uncolored nodes and thus their images under f_C and f_D are not incident to any edges already copied from Y_1, Y_2, Y'_1 , and Y'_2 . The cases with one of the endpoints being red or blue are symmetric. Fig. 10 shows how type A and type B edges are mapped to graph (C) and (D) based on colors in G' .

- Finally, we observe that it is not possible for both endpoints of a path to be colored. If the path is of odd length, the two endpoints must be on different sides of the bipartite graph. Thus, one of the endpoints is colored pink/navy and the other is colored red/blue. Since the edges, starting from the endpoint colored pink/navy, must alternate between type A and B, with an odd number of edges the last edge must be of type A. This contradicts the feasibility of the matching in graph (A) because the colored node is already occupied by Y_1 or Y_2 in graph (A). On the other hand, if the path is of even length, both of the endpoints must be on the same side of the bipartite graph. Assume without loss of generality that both endpoints are colored pink/navy (the other case is exactly symmetric). Then, starting from one of the endpoints, the path must alternate between edges of type A and B and end with an edge of type B. This contradicts the feasibility of the matching in graph (B) because the colored node is already occupied by Y'_1 or Y'_2 in graph (B). Thus, sub-case (3) is not possible.

Therefore, in all possible sub-cases the matches in Y_3 and \tilde{Y}_3 can be injectively mapped to $(M(\bar{C}) \cap X_3) \cup (M(\bar{D}) \cap \tilde{X}_3)$ in graph (C) and (D). This shows that $M_A + M_B \leq M_C + M_D$ for any X_1, X_2, X_3 and X_4 , and thus $\mathbb{E} [\mathcal{M}_n^b] \leq \mathbb{E} [\mathcal{M}_n(1, 0)] \forall n$ when $\alpha = 0$. \square

A.2. Proofs of the Global Model through Probability Bounds

A.2.1. Proof of Lemma 3

Proof. Denote the number of nodes in V_l and V_r that have a degree of d by random variables q_d^l and q_d^r , respectively. We start by showing that, in any realization of the $(1 - B/2)n \times (1 - B/2)n$ bipartite graph,

$$m_1 \geq \sum_d q_d^l \cdot d - \sum_{d=2}^{(1-B/2)n} q_d^l \cdot (d-1) - \sum_{d=2}^{(1-B/2)n} q_d^r \cdot (d-1). \quad (5)$$

Notice that $\sum_d q_d^l \cdot d = \sum_d q_d^r \cdot d$ is the number of edges in the graph, and the second and third term in (5) respectively capture the extra edges, i.e., those incident to nodes with degree > 1 , on the left and right-hand side of the graph. This lower bound holds because, after deleting $d-1$ edges from all nodes with degree $d > 1$ in V_l and V_r , all remaining edges in the graph would have degree 1 on both ends. In other words, the remaining edges are not incident to each other and thus trivially form a (not necessarily maximum) matching.

Notice that the probability for a node v on the left or right-hand side of the graph to have degree d is the same in this symmetric bipartite graph. Taking expectations over the lower bound in (5), we find that

$$\begin{aligned}
 \mathbb{E}[m_1] &\geq (1 - B/2)n \sum_{d=1}^{(1-B/2)n} \mathbb{P}[\deg(v) = d] \cdot d - 2(1 - B/2)n \sum_{d=2}^{(1-B/2)n} \mathbb{P}[\deg(v) = d] \cdot (d - 1) \\
 &= (1 - B/2)n \mathbb{E}[\deg(v)] - 2(1 - B/2)n \sum_{d=2}^{(1-B/2)n} \mathbb{P}[\deg(v) = d] \cdot (d - 1) \\
 &= (1 - B/2)^2 n 2\alpha - 2(1 - B/2)n \sum_{d=2}^{(1-B/2)n} \mathbb{P}[\deg(v) = d] \cdot (d - 1).
 \end{aligned} \tag{6}$$

We simplify the second term by substituting $t = (1 - B/2)n$ and observing that

$$\begin{aligned}
 \lim_{n \rightarrow \infty} \sum_{d=2}^{(1-B/2)n} \mathbb{P}[\deg(v) = d] \cdot (d - 1) &= \lim_{n \rightarrow \infty} \sum_{d=2}^{(1-B/2)n} \binom{(1-B/2)n}{d} (2\alpha/n)^d \cdot (1 - 2\alpha/n)^{(1-B/2)n-d} \cdot (d - 1) \\
 &= \lim_{t \rightarrow \infty} \sum_{d=2}^t \binom{t}{d} (2\alpha(1 - B/2)/t)^d \cdot (1 - 2\alpha(1 - B/2)/t)^{t-d} \cdot (d - 1) \\
 &= \lim_{t \rightarrow \infty} \sum_{d=1}^t \binom{t}{d} (2\alpha(1 - B/2)/t)^d \cdot (1 - 2\alpha(1 - B/2)/t)^{t-d} \cdot (d - 1) \\
 &= 2\alpha(1 - B/2) - \lim_{t \rightarrow \infty} \sum_{d=1}^t \binom{t}{d} (2\alpha(1 - B/2)/t)^d \cdot (1 - 2\alpha(1 - B/2)/t)^{t-d} \\
 &= 2\alpha(1 - B/2) + e^{-2\alpha(1 - B/2)} - 1.
 \end{aligned}$$

Plugging this into (6), we find that

$$\begin{aligned}
 \mathbb{E}[m_1] &\geq (1 - B/2)^2 n 2\alpha - 2(1 - B/2)n \left(2\alpha(1 - B/2) + e^{-2\alpha(1 - B/2)} - 1 \right) \\
 &= 2 \cdot (1 - B/2) n \left[1 - (1 - B/2)\alpha - e^{-2\alpha(1 - B/2)} \right] \text{ as } n \rightarrow \infty.
 \end{aligned}$$

□

A.2.2. Proof of Theorem 4

Proof. We first provide an upper bound on $\mu(B, 0)$ and then derive a lower bound on $\mu(B/2, B/2)$. When $\mathbf{b} = (B, 0)$, a node $v \in V_l$ is regular with probability $1 - B$ and all nodes in V_r are regular nodes. Thus, a regular node v forms an edge with a node $u \in V_r$ with probability $2\alpha/n$. Then,

$$\begin{aligned}
 \mu(B, 0) &\leq 1 - \lim_{n \rightarrow \infty} \mathbb{P}[v \in V_l \text{ is regular and has degree 0}] \\
 &= 1 - \lim_{n \rightarrow \infty} (1 - B) (1 - 2\alpha/n)^n = 1 - (1 - B) \cdot e^{-2\alpha}.
 \end{aligned} \tag{7}$$

Then, to lower bound $\mu(B/2, B/2)$, we adopt a greedy matching scheme: in the first stage we only match the regular nodes in V_l with the regular nodes in V_r , and in the second stage we greedily match the rest of

the flexible nodes. Denote the number of matches formed in stage 1 and 2 by n_1 and n_2 , respectively. Since each node $v \in V_l$ is regular with probability $1 - B/2$, we can use a Chernoff bound to find that the event

$$E_1 := \left\{ \left| \sum_i F_i^l - B/2 \cdot n \right| \leq n^{5/8} \text{ and } \left| \sum_j F_j^r - B/2 \cdot n \right| \leq n^{5/8} \right\}$$

occurs with a probability of at least $1 - e^{-\Omega(n^{1/4})}$. By Lemma 3, a graph of $(1 - B/2)n$ regular nodes on each side has a maximum matching among its nodes of size at least $2 \cdot (1 - B/2) n [1 - (1 - B/2)\alpha - e^{-2\alpha(1-B/2)}] - o(n)$. Correspondingly, a subgraph of $(1 - B/2)n - n^{5/8}$ regular nodes on each side has the same asymptotic maximum matching size (up to $o(n)$ nodes that are removed). Conditioning on E_1 Lemma 3 thus implies that as $n \rightarrow \infty$

$$\begin{aligned} \mathbb{E}[n_1] &= \mathbb{E}[n_1|E_1]\mathbb{P}[E_1] + \mathbb{E}[n_1|E_1^c]\mathbb{P}[E_1^c] \geq (\mathbb{E}[m_1] - o(n)) \cdot \left(1 - e^{-\Omega(n^{1/4})}\right) - n^{5/8} \cdot e^{-\Omega(n^{1/4})} \\ &\geq 2 \cdot (1 - B/2) n \left[1 - (1 - B/2)\alpha - e^{-2\alpha(1-B/2)}\right] - o(n). \end{aligned}$$

Through a similar conditioning we find that, for any $\alpha \leq 0.05$ and $B \geq 0.4$,

$$\begin{aligned} &\lim_{n \rightarrow \infty} \mathbb{P}[\text{regular node } v \in V_l \text{ not connected to any regular node in } V_r] \\ &\geq \lim_{n \rightarrow \infty} (1 - 2\alpha/n)^{(1-B/2)n+n^{5/8}} \cdot \left(1 - e^{-\Omega(n^{1/4})}\right) + 0 \cdot e^{-\Omega(n^{1/4})} \\ &\geq \lim_{n \rightarrow \infty} (1 - 0.1/n)^{(1-B/2)n+n^{5/8}} = e^{-0.1(1-B/2)}. \end{aligned}$$

Thus, as $n \rightarrow \infty$ we can also upper bound

$$\begin{aligned} \mathbb{E}[n_1] &= \mathbb{E}[n_1|E_1]\mathbb{P}[E_1] + \mathbb{E}[n_1|E_1^c]\mathbb{P}[E_1^c] \\ &\leq \left(1 - e^{-0.1(1-B/2)}\right) ((1 - B/2)n + n^{5/8}) \cdot \left(1 - e^{-\Omega(n^{1/4})}\right) + n \cdot e^{-\Omega(n^{1/4})} \\ &< \left(1 - e^{-0.1(1-B/2)}\right) \cdot (1 - B/2) \cdot n + o(n). \end{aligned}$$

Now we examine the flexible nodes and argue that, even if we greedily match the flexible nodes to any unmatched regular nodes on the opposite side, almost all of the flexible nodes will be matched in the second stage. Given n' unmatched regular nodes in V_r , the number of edges between a flexible node $v \in V_l$ and these n' nodes is governed by $\text{Binom}\left(n', \frac{\alpha^f + \alpha}{n}\right)$. For any $n' \in \Theta(n)$, by the Poisson Limit Theorem we find that $\text{Binom}\left(n', \frac{\alpha^f + \alpha}{n}\right)$ converges in distribution to $\text{Poisson}\left(\frac{n'}{n} (\alpha^f + \alpha)\right)$ as $n \rightarrow \infty$. Thus, as $n \rightarrow \infty$

$$\mathbb{P}[v \text{ not connected to any unmatched regular node in } V_r | n'] = e^{-\frac{n'}{n} (\alpha^f + \alpha)}.$$

We now apply this bound to the flexible nodes in V_l . Observe that the event

$$E_2 := E_1 \cap \left\{ n_1 \leq \left(1 - e^{-0.1(1-B/2)}\right) (1 - B/2)n + 2n^{5/8} \right\}$$

occurs with a probability of at least $1 - e^{-\Omega(n^{1/4})}$ by Chernoff bound.²³ Under E_2 , we greedily match each flexible node to any unmatched regular node in V_r . In particular, for the i th flexible node under consideration, even if all previous $i - 1$ flexible nodes are already matched to regular nodes in V_r , there will still be at least

$$(1 - B/2) \cdot n - (1 - e^{-0.1(1-B/2)}) (1 - B/2)n - i - 3 \cdot n^{5/8}$$

unmatched regular nodes in V_r . This allows us to bound:

$$\begin{aligned} & \mathbb{P}[i\text{th flexible node not connected to any unmatched regular node in } V_r | E_2] \\ & \leq e^{-\frac{(1-B/2)\cdot n - (1-e^{-0.1(1-B/2)})(1-B/2)n - i - 3 \cdot n^{5/8}}{n}(\alpha^f + \alpha)} \leq e^{-\left((1-B/2) - (1-e^{-0.1(1-B/2)})(1-B/2) - i/n\right)\alpha^f} \text{ as } n \rightarrow \infty. \end{aligned}$$

Thus, as $n \rightarrow \infty$, through the greedy algorithm that iteratively matches each flexible to any unmatched regular node, the i th flexible node ends up matched with probability at least

$$1 - e^{-\left((1-B/2) - (1-e^{-0.1(1-B/2)})(1-B/2) - i/n\right)\alpha^f} = 1 - e^{-\left(-i/n + e^{-0.1(1-B/2)}(1-B/2)\right)\alpha^f}.$$

This is a lower bound on the matching probability for any $i \in \{1, 2, \dots, B/2 \cdot n - n^{5/8}\}$. In particular, with $B \in [0.4, 0.8]$ the expression $-i/n + e^{-0.1(1-B/2)}(1-B/2)$ is strictly positive, and thus the above probability is monotonically increasing in α^f . The argument for matching flexible nodes in V_r with regular nodes in V_l is symmetric, and we find that when $\alpha \in [0.01, 0.05]$,

$$\begin{aligned} \lim_{n \rightarrow \infty} \mathbb{E} \left[\frac{n_2}{n} | E_2 \right] & \geq 2 \cdot \lim_{n \rightarrow \infty} \left[\sum_{i=1}^{B/2 \cdot n - n^{5/8}} \left(1 - e^{-\left(-i/n + e^{-0.1(1-B/2)}(1-B/2)\right)\alpha^f} \right) / n \right] \\ & = 2 \cdot B/2 - 2 \cdot \lim_{n \rightarrow \infty} \left[\sum_{i=1}^{B/2 \cdot n} e^{-\left(-i/n + e^{-0.1(1-B/2)}(1-B/2)\right)\alpha^f} \right] / n \\ & = B - 2 \cdot \lim_{n \rightarrow \infty} \frac{e^{\alpha^f(1/n - (1-B/2)e^{-0.1(1-B/2)})} (e^{\alpha^f B/2} - 1)}{n (e^{\alpha^f/n} - 1)} \\ & = B - 2 \cdot \frac{\lim_{n \rightarrow \infty} e^{\alpha^f(1/n - (1-B/2)e^{-0.1(1-B/2)})} (e^{\alpha^f B/2} - 1)}{\lim_{n \rightarrow \infty} n (e^{\alpha^f/n} - 1)} \\ & = B - 2 \cdot \frac{e^{-\alpha^f(1-B/2)e^{-0.1(1-B/2)}} (e^{\alpha^f B/2} - 1)}{\lim_{n \rightarrow \infty} n (e^{\alpha^f/n} - 1)} \\ & = B - \frac{2}{\alpha^f} \left[\left(e^{\alpha^f \cdot B/2} - 1 \right) e^{-\alpha^f(1-B/2)e^{-0.1(1-B/2)}} \right], \end{aligned} \tag{8}$$

²³With high probability there are at most $(1 - B/2)n + n^{5/8}$ regular nodes on both sides; each such node is isolated with probability $e^{-0.1(1-B/2)}$, so we expect to match at most $((1 - B/2)n + n^{5/8})(1 - e^{-0.1(1-B/2)})$ of them in the first stage.

where the second equality comes from the sum of a geometric sequence, the third from the quotient rule, and the fifth from an application of the L'Hôpital's rule on $\lim_{n \rightarrow \infty} (e^{\alpha^f/n} - 1) / (1/n)$. Moreover, from the monotonicity result for $1 - e^{(-i/n + e^{-0.1(1-B/2)}(1-B/2))\alpha^f}$ with respect to α^f we know that (8) is also monotonically increasing in α^f .

Thus, when $\alpha \in [0.01, 0.05]$,

$$\begin{aligned} \mu(B/2, B/2) &\geq \lim_{n \rightarrow \infty} \mathbb{E} \left[\frac{n_1 + n_2}{n} \right] \\ &\geq \lim_{n \rightarrow \infty} \mathbb{E} \left[\frac{n_1}{n} \right] + \lim_{n \rightarrow \infty} \left(\mathbb{E} \left[\frac{n_2}{n} | E_2 \right] \cdot \mathbb{P}[E_2] \right) + 0 \cdot \lim_{n \rightarrow \infty} (1 - \mathbb{P}[E_2]) \\ &\geq 2 \cdot (1 - B/2) \left[1 - (1 - B/2)\alpha - e^{-2\alpha(1-B/2)} \right] \\ &\quad + B - \frac{2}{\alpha^f} \left[\left(e^{\alpha^f \cdot B/2} - 1 \right) e^{-\alpha^f(1-B/2)e^{-0.1(1-B/2)}} \right]. \end{aligned} \quad (9)$$

Due to the non-linearity of the bounds in (7) and (9), it is difficult compare $\mu(B, 0)$ and $\mu(B/2, B/2)$ analytically for a wide range of B, α^f and α values. Instead, we fix $\alpha^f = 22$,²⁴ and construct local upper and lower bounds for $\mu(B, 0)$ and $\mu(B/2, B/2)$ within a small interval of B and α values to show that $\mu(B, 0) < \mu(B/2, B/2)$ within this small interval. Then, we adopt a computer-aided proof to verify the inequality over all such intervals. Specifically, given $\delta > 0$, for any $(B', \alpha') \in [B - \delta, B] \times [\alpha - \delta, \alpha] \subseteq [0.4, 0.8] \times [0.01, 0.05]$, we can upper bound

$$\mu(B', 0) \leq 1 - (1 - B') \cdot e^{-2\alpha'} \leq 1 - (1 - B) \cdot e^{-2\alpha}$$

and lower bound

$$\begin{aligned} \mu(B'/2, B'/2) &\geq 2 \cdot (1 - B'/2) \left[1 - (1 - B'/2)\alpha' - e^{-2\alpha'(1-B'/2)} \right] \\ &\quad + B' - \frac{2}{\alpha^f} \left[\left(e^{\alpha^f \cdot B'/2} - 1 \right) e^{-\alpha^f(1-B'/2)e^{-0.1(1-B'/2)}} \right] \\ &\geq 2 \cdot (1 - B/2) \left[1 - (1 - (B - \delta)/2)\alpha - e^{-2(\alpha - \delta)(1-B/2)} \right] \\ &\quad + (B - \delta) - \frac{2}{\alpha^f} \left[\left(e^{\alpha^f \cdot B/2} - 1 \right) e^{-\alpha^f(1-B/2)e^{-0.1(1-(B-\delta)/2)}} \right]. \end{aligned}$$

Thus, it suffices to show

$$\begin{aligned} 1 - (1 - B) \cdot e^{-2\alpha} &\leq 2 \cdot (1 - B/2) \left[1 - (1 - (B - \delta)/2)\alpha - e^{-2(\alpha - \delta)(1-B/2)} \right] \\ &\quad + (B - \delta) - \frac{2}{\alpha^f} \left[\left(e^{\alpha^f \cdot B/2} - 1 \right) e^{-\alpha^f(1-B/2)e^{-0.1(1-(B-\delta)/2)}} \right] \end{aligned} \quad (10)$$

to verify that $\mu(B', 0) < \mu(B'/2, B'/2)$ for any $(B', \alpha') \in [B - \delta, B] \times [\alpha - \delta, \alpha]$.

²⁴The result for $\alpha^f > 22$ follows from the monotonicity of (8) with respect to α^f .

To obtain Theorem 4, we partition the parameter regime $B \in [0.4, 0.8]$ and $\alpha \in [0.01, 0.05]$ into a grid in which all cells are of the form $[B - \delta, B] \times [\alpha - \delta, \alpha]$, and then verify inequality (10) in each such cell. In `Theorem4.ipynb`,²⁵ we take $\delta = 0.0001$ and verify (10) for all for $B \in \{0.4000, 0.4001, \dots, 0.7999, 0.8000\}$ and $\alpha \in \{0.0100, 0.0101, \dots, 0.0499, 0.0500\}$. Thus, $\mu(B/2, B/2) > \mu(B, 0)$ for any $B \in [0.4, 0.8]$, $\alpha \in [0.01, 0.05]$ and $\alpha^f \geq 22$. \square

A.3. Proofs of the Global Model through the KS algorithm

This section proceeds as follows: we begin with the definition of the KS algorithm in Algorithm 1. The KS algorithm iteratively prunes nodes in the graph and proceeds in two phases: the first phase ends when no nodes of degree 1 remain in the graph, and the second phase ends when all edges are removed from the graph. We construct a quantity $\mu^{\text{KS}}(b_l, b_r)$ based on analyses of the KS algorithm. Under Condition 1, Theorem 9 shows that this quantity is equal to $\mu(b_l, b_r)$. Thereafter, we verify Condition 1 for a subset of instances, which leads to Theorem 8 that states the equivalence of $\mu(b_l, b_r)$ and $\mu^{\text{KS}}(b_l, b_r)$ for a range of parameters. The quantity $\mu^{\text{KS}}(b_l, b_r)$ relies on solutions to a system of equations, which we can approximate with arbitrary precision. This allows us to compute $\mu^{\text{KS}}(b_l, b_r)$, and consequently $\mu(b_l, b_r)$, at a provable level of precision.

The KS-based analyses facilitate two of the results presented in Section 3. Firstly, it allows us to analytically compare the one-sided and the balanced allocations in the parameter regimes from Theorem 3 (ii). Secondly, it lets us investigate $\mu^{\text{KS}}(b_l, b_r)$ as a proxy measure of interest and establish its structural properties at $\mathbf{b} = (1/2, 1/2)$ in Theorem 7.

A.3.1. KS Derivations. Throughout the section we fix an arbitrary (b_l, b_r) and use G as the shorthand notation for $G_n^{\text{glb}}(b_l, b_r)$. In G , the *degree* of a node v is the number of edges that are incident to v , and we denote this number by $\deg(v)$. We now define the KS algorithm in Algorithm 1.

Based on Algorithm 1, the edges in G' form a matching; our goal will be to characterize the size of this matching. When all edges incident to a node v are deleted from G and yet v has degree 0 in G' , we know that v will not be part of the resulting matching and call it an *isolated* node. The key to finding the size of a matching based on the KS algorithm is to count the number of nodes that either become matched or isolated as edges are deleted from the graph. We denote the iterations before the first occurrence where no nodes have a degree of 1 in G as *Phase 1* of the KS algorithm. The subsequent iterations are referred to as *Phase 2* of the KS algorithm. A key property of the KS algorithm is that it is optimal in its handling of degree-1 vertices: given an edge e that is incident to a degree-1 vertex, there is always a maximum matching that contains e (Bohman and Frieze 2011, Balister and Gerke 2015). This result implies that the KS algorithm is optimal until the end of phase 1. Let M_1^l, M_1^r, M_2^l and M_2^r respectively denote the set of nodes in V_l and V_r that enter the matching (i.e., incident to edges in G') during phase 1 and 2. By symmetry, we know that

²⁵The computer-aided proof can be found at <https://bit.ly/3uQwGEI>.

Algorithm 1 Karp-Sipser's (KS) Algorithm

```

1: Input: Graph  $G$ 
2: Initialize graph  $G'$  as an empty graph on the same set of nodes as  $G$ 
3: while  $G$  has edges do
4:   if there exists a node of degree 1 in  $G$  then
5:     Choose an edge  $e$  that is incident to a node of degree 1 uniformly at random
6:   else
7:     Choose an edge  $e$  from all remaining edges uniformly at random
8:   Add edge  $e$  to graph  $G'$ 
9:   Delete edge  $e$  and all edges incident to  $e$  from graph  $G$ 
10: Output: The number of edges in  $G'$ 

```

$m_1 := |M_1^l| = |M_1^r|$ and $m_2 := |M_2^l| = |M_2^r|$. Similarly, let $\Psi_1^l, \Psi_1^r, \Psi_2^l$ and Ψ_2^r respectively represent the set of nodes that become isolated in V_l and V_r during phase 1 and 2, where Ψ_1^l and Ψ_1^r also include the nodes that are already isolated initially in graph G . We define $\psi_1 := \max\{|\Psi_1^l|, |\Psi_1^r|\}$ and

$$\psi_2 := n - m_1 - m_2 - \psi_1 = \min \left\{ n - |M_1^l| - |M_2^l| - |\Psi_1^l|, n - |M_1^r| - |M_2^r| - |\Psi_1^r| \right\} = \min\{|\Psi_2^l|, |\Psi_2^r|\}.$$

Intuitively, ψ_2 represents the number of nodes that become isolated in Phase 2 of the KS algorithm (excluding those already accounted for in Phase 1). It has been demonstrated that, for different types of sparse random graph settings, that the expected number of nodes becoming isolated in Phase 2 of the KS algorithm is $o(n)$, i.e., $\mathbb{E}[\psi_2] \in o(n)$. We state this as Condition 1, which we later verify for a subset of instances in our model.

Condition 1 *When the KS algorithm is applied to a random graph G of the global model, $\mathbb{E}[\psi_2] \in o(n)$.*

As the KS algorithm is optimal in Phase 1, Condition 1 guarantees that it is asymptotically optimal. Specifically, in Phase 2, the expected fraction of nodes that become isolated, and thus unmatched, is vanishingly small, i.e., it involves $o(n)$ nodes. Thus, to identify the number of unmatched nodes in both phases, it suffices to evaluate ψ_1 , for which we evaluate the probability of a node becoming isolated in Phase 1 of the KS algorithm. For $\mathbf{b} = (b_l, b_r)$, we will show that this probability is determined by the following set of equations:

$$\begin{aligned}
w_L^f(\mathbf{b}) &= e^{-2b_r \alpha^f (1 - \hat{w}_H^f(\mathbf{b})) - (1 - b_r) \cdot (\alpha^f + \alpha) (1 - \hat{w}_H^{nf}(\mathbf{b}))}, \\
w_L^{nf}(\mathbf{b}) &= e^{-b_r \cdot (\alpha^f + \alpha) (1 - \hat{w}_H^f(\mathbf{b})) - 2(1 - b_r) \alpha (1 - \hat{w}_H^{nf}(\mathbf{b}))}, \\
w_H^f(\mathbf{b}) &= 1 - e^{-2b_r \alpha^f \hat{w}_L^f(\mathbf{b}) - (1 - b_r) (\alpha^f + \alpha) \hat{w}_L^{nf}(\mathbf{b})}, \\
w_H^{nf}(\mathbf{b}) &= 1 - e^{-b_r (\alpha^f + \alpha) \hat{w}_L^f(\mathbf{b}) - 2(1 - b_r) \alpha \hat{w}_L^{nf}(\mathbf{b})}, \\
\hat{w}_L^f(\mathbf{b}) &= e^{-2b_l \alpha^f (1 - w_H^f(\mathbf{b})) - (1 - b_l) (\alpha^f + \alpha) (1 - w_H^{nf}(\mathbf{b}))}, \\
\hat{w}_L^{nf}(\mathbf{b}) &= e^{-b_l (\alpha^f + \alpha) (1 - w_H^f(\mathbf{b})) - 2(1 - b_l) \alpha (1 - w_H^{nf}(\mathbf{b}))}, \\
\hat{w}_H^f(\mathbf{b}) &= 1 - e^{-2b_l \alpha^f w_L^f(\mathbf{b}) - (1 - b_l) (\alpha^f + \alpha) w_L^{nf}(\mathbf{b})}, \\
\hat{w}_H^{nf}(\mathbf{b}) &= 1 - e^{-b_l (\alpha^f + \alpha) w_L^f(\mathbf{b}) - 2(1 - b_l) \alpha w_L^{nf}(\mathbf{b})}.
\end{aligned} \tag{11}$$

We denote the smallest set of solutions²⁶

$$\mathbf{w} = (w_L^f(\mathbf{b}), w_L^{nf}(\mathbf{b}), w_H^f(\mathbf{b}), w_H^{nf}(\mathbf{b}), \hat{w}_L^f(\mathbf{b}), \hat{w}_L^{nf}(\mathbf{b}), \hat{w}_H^f(\mathbf{b}), \hat{w}_H^{nf}(\mathbf{b}))$$

to (11) by $\mathbf{y} = (y_L^f(\mathbf{b}), y_L^{nf}(\mathbf{b}), y_H^f(\mathbf{b}), y_H^{nf}(\mathbf{b}), \hat{y}_L^f(\mathbf{b}), \hat{y}_L^{nf}(\mathbf{b}), \hat{y}_H^f(\mathbf{b}), \hat{y}_H^{nf}(\mathbf{b}))$.

THEOREM 9. *Let*

$$\begin{aligned}
\xi(b_l, b_r) &= 2 - b_l y_L^f(\mathbf{b}) - b_r (1 - \hat{y}_H^f(\mathbf{b})) \\
&\quad - b_r (1 - \hat{y}_H^f(\mathbf{b})) (2b_l \alpha^f y_L^f(\mathbf{b}) + (1 - b_l) (\alpha^f + \alpha) y_L^{nf}(\mathbf{b})) \\
&\quad - (1 - b_l) y_L^{nf}(\mathbf{b}) - (1 - b_r) (1 - \hat{y}_H^{nf}(\mathbf{b})) \\
&\quad - (1 - b_r) (1 - \hat{y}_H^{nf}(\mathbf{b})) (b_l (\alpha^f + \alpha) y_L^f(\mathbf{b}) + 2(1 - b_l) \alpha y_L^{nf}(\mathbf{b})),
\end{aligned} \tag{12}$$

$$\begin{aligned}
\hat{\xi}(b_l, b_r) &= 2 - b_r \hat{y}_L^f(\mathbf{b}) - b_l (1 - y_H^f(\mathbf{b})) \\
&\quad - b_l (1 - y_H^f(\mathbf{b})) (2b_r \alpha^f \hat{y}_L^f(\mathbf{b}) + (1 - b_r) (\alpha^f + \alpha) \hat{y}_L^{nf}(\mathbf{b})) \\
&\quad - (1 - b_r) \hat{y}_L^{nf}(\mathbf{b}) - (1 - b_l) (1 - y_H^{nf}(\mathbf{b})) \\
&\quad - (1 - b_l) (1 - y_H^{nf}(\mathbf{b})) (b_r (\alpha^f + \alpha) \hat{y}_L^f(\mathbf{b}) + 2(1 - b_r) \alpha \hat{y}_L^{nf}(\mathbf{b})).
\end{aligned} \tag{13}$$

Define $\mu^{KS}(b_l, b_r) = \min(\xi(b_l, b_r), \hat{\xi}(b_l, b_r))$. Then, under Condition 1, $\mu(b_l, b_r) = \mu^{KS}(b_l, b_r)$.

We now translate Condition 1 into a looser (i.e., sufficient but not necessary) condition that is much easier to verify.

LEMMA 4. *Condition 1 holds when the solution to (11) is unique.*

²⁶In line with terminology in Karp and Sipser (1981), the smallest set of solutions refers to the least fixed point of the system of equations in (11). Note that this is well defined since all variables in \mathbf{w} are increasing functions of each other.

Lemma 4 is instrumental for the proof of Theorem 8. The rest of this appendix is structured as follows:

- In Appendix A.3.2 we prove Theorem 9, Lemma 4, and Theorem 8. This requires us to first state the definitions and auxiliary results commonly associated with KS-style analyses, and we then prove each of these three results.
- In Appendix A.3.3 we provide our computer-aided proof of Theorem 3 (ii). Our proof partitions the region of interest into small cells and numerically derives lower bounds on $\mu(1, 0)$ and upper bounds on $\mu(1/2, 1/2)$ across each such cell. For each cell, we identify a particular point (α, α^f) at which we numerically solve (11) for both $\mathbf{b} = (1, 0)$ and $\mathbf{b} = (1/2, 1/2)$ within a given tolerance ϵ (see Claim 3). Crucially, that tolerance guarantees that the solution to (11) is within ϵ of the true solution; we analytically translate this bound into a bound on the gap between the numerically computed value and μ^{KS} . We also show that the smallest solution to (11) is continuous in α and α^f , which implies that the bound holds, with an additional error term, within a δ -neighborhood of (α, α^f) , which represents the cell that (α, α^f) is part of (Claim 4). We iterate over cells to verify for the entire region that our lower bounds on $\mu(1, 0)$ are greater than our upper bounds on $\mu(1/2, 1/2)$.
- In Appendix A.3.4 we provide the computer-aided proof of Theorem 7. We take directional second-order derivatives (SOD) of $\mu^{\text{KS}}(b_l, b_r)$ and evaluate them at $\mathbf{b} = (1/2, 1/2)$ to prove concavity and convexity results in the respective directions. In particular, the SODs depend only on α, α^f , and solutions to (11). Then, similar to the approach in Appendix A.3.2, we lower and upper bound the solution to (11) within every small cell and iterate over cells to verify the signs of the directional SODs.
- In Appendix A.3.5 we provide the proof of the auxiliary results in Appendix A.3.2.
- In Appendix A.3.6 we explain the setup of the computational results in Section 6 based on $\mu^{\text{KS}}(b_l, b_r)$, as well as the range of parameters that we experiment with.

A.3.2. Phase 1 of the KS Algorithm In this section, we analyze phase 1 of the KS algorithm for $G_n^{glb}(b_l, b_r)$, hereafter referred to as G for notational simplicity. The set of edges in G is denoted by E , and the set of nodes is denoted by $V := V_l \cup V_r$. Our analysis extends the results for sparse random graphs presented in Karp and Sipser (1981) to random bipartite graphs. Similar to Balister and Gerke (2015), we analyze bipartite graphs in which the degree distributions for nodes are heterogeneous; however, the “configuration model” considered in their paper does not capture our setting with flexible and regular nodes, and we require different probabilistic computations to handle the heterogeneous edge probabilities between nodes of different flexibility types (i.e., 2α between two regular nodes, $\alpha^f + \alpha$ between a flexible and a regular node, and $2\alpha^f$ between two flexible nodes). We next present all auxiliary results needed for Theorem 9, Lemma 4 and Theorem 8, the three main technical results based on KS-style analyses.

We begin by introducing the concept of a *derivation*, which is essential for computing the asymptotic size of a maximum matching. We shall show that nodes that appear in a derivation become either matched

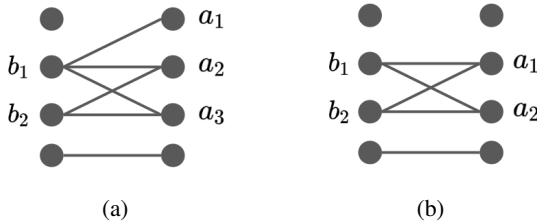


Figure 18 In Fig. 18 (a), the sequence a_1, b_1, a_2, b_2, a_3 is a derivation. Notice that all nodes in this derivation are either matched or isolated in phase 1 of the KS algorithm: the edge (a_1, b_1) is added to graph G' as a_1 is the only node of degree 1 within the connected component; we then delete all edges incident to a_1 and b_1 , leaving (a_2, b_2) and (b_2, a_3) as the only remaining edges in the graph; next, by adding (a_2, b_2) into G' (the case of (b_2, a_3) is symmetric as the sequence a_1, b_1, a_3, b_2, a_2 is also a derivation), a_1, b_1, a_2 and b_2 become matched while a_3 becomes isolated. In contrast, there is no derivation in Fig. 18 (b) that involves the connected component $\{a_1, b_1, a_2, b_2\}$ and none of these nodes become matched or isolated during phase 1 of the KS algorithm.

or isolated in Phase 1 of the KS algorithm. Moreover, depending on their positions in the derivation, nodes can be classified as either a *target* or a *loser*, which determines the number of nodes that become matched or isolated in Phase 1.

DEFINITION 3. A *derivation* is a sequence $a_1, b_1, a_2, b_2, \dots$, of distinct nodes such that, for $i = 1, 2, \dots$:

- (1) $\{a_i, b_i\} \in E$;
 (2) $\{a_i, b\} \in E$ implies $b \in \{b_1, b_2, \dots, b_i\}$.

For example, the sequence a_1, b_1, a_2, b_2, a_3 in Fig. 18 (a) is a derivation: node a_1 fulfills condition (1) because $\{a_1, b_1\} \in E$, and fulfills condition (2) because it is connected to no other node. Next, we verify that a_2 fulfills condition (1) because $\{a_2, b_2\} \in E$, and fulfills condition (2) because it is only connected to b_1 and b_2 . The sequence ends with node a_3 , which is again only connected to b_1 and b_2 . On the other hand, in Fig. 18 (b) there is no derivation involving the nodes $\{a_1, a_2, b_1, b_2\}$: for a_1 and a_2 there exists no ordering of b_1 and b_2 such that $\{a_i, b\} \in E$ uniquely identifies b .

In the upcoming proofs we will demonstrate that by following the KS algorithm one can optimally match nodes that appear in a derivation by starting with nodes of degree 1 and then iteratively resolving the remaining nodes.

Within a derivation, we categorize nodes into *target* and *loser* based on the following definition:

DEFINITION 4. We define the following relation $\otimes \subseteq V \times V$: $v \otimes u$ if there exists a derivation $a_1, b_1, a_2, b_2, \dots$ and an index i such that $v = a_i$ and $u = b_i$. We call u a *target* if for some v , $v \otimes u$, and we call u a *loser* if (1) for some v , $u \otimes v$ or (2) u is the last element of an odd length derivation.

Based on Definition 4, all members of derivations are targets or losers or both. For instance, in the derivation a_1, b_1, a_2, b_2, a_3 in Fig. 18 (a), a_1, a_2 and a_3 are losers while b_1 and b_2 are targets. The next result

characterizes the nodes that are *processed*, i.e., that become either matched or isolated in phase 1 of the KS algorithm. The result is an immediate application of Theorem 8 in Karp and Sipser (1981) to bipartite graphs. We defer the proofs of Proposition 1 and all auxiliary results in this section to Appendix A.3.5.

PROPOSITION 1 (Theorem 8 in Karp and Sipser (1981)). *Consider any execution of the KS algorithm on G . Denote by M_1 the set of edges (v, u) that are added to G' in Phase 1. Then:*

- (i) *a node v is processed in phase 1 iff v occurs in some derivation;*
- (ii) *if u is a target then M_1 contains exactly one edge (v, u) such that $v \otimes u$;*
- (iii) *if edge $(v, u) \in M_1$ then $v \otimes u$ or $u \otimes v$;*
- (iv) *if $v \otimes u$ and $u \otimes v$ then edge $(v, u) \in M_1$;*
- (v) $\psi_1 = \max \left(\left| \{v \in V_l \mid v \text{ is a loser}\} \right| - \left| \{v \in V_r \mid v \text{ is a target}\} \right|, \left| \{v \in V_r \mid v \text{ is a loser}\} \right| - \left| \{v \in V_l \mid v \text{ is a target}\} \right| \right).$

Thus, the key to finding $\mathbb{E}[\psi_1]$ and the asymptotic matching probability lies in determining the probability of a node v being a target and/or a loser. We provide asymptotic answers to these questions by (1) conducting a probabilistic analysis of derivations in random trees and (2) demonstrating that a random tree is a good approximation to the structure obtained by selecting a node v in G and conducting a breadth-first search from v .

We now construct a random tree $\bar{G}_n(b_l, b_r)$ to approximate the structure obtained from a breadth-first search from a node v in G . As illustrated in Fig. 19, we construct the layers of the tree sequentially, mimicking a breadth-first search from the root node. The flexibility types of all nodes in a given layer are sampled according to the same distribution, and the distribution for each layer alternates between Bernoulli(b_l) or Bernoulli(b_r). This mimics the alternation between nodes in V_l and V_r in the bipartite graph G . Specifically, the construction of $\bar{G}_n(b_l, b_r)$ follows a branching process: assume for simplicity that the flexibility type of the root node v is drawn from the Bernoulli(b_l) distribution, so that v is a flexible node (i.e., $F_v = 1$) with probability b_l and a regular node with probability $1 - b_l$. Then, v has n potential children, each being a flexible node (i.e., $F_u = 1$) with probability b_r and a regular node with probability $1 - b_r$. A potential child becomes a realized child of v with probability $2p_n + (F_v + F_u) \cdot (p_n^f - p_n)$. Each realized child u then has n potential children, with flexible and regular probabilities of b_l and $1 - b_l$, respectively. This branching process continues until no further child exists for a tree layer, a process that can be either finite or infinite. We omit the dependency on n and \mathbf{b} in $\bar{G}_n(b_l, b_r)$ whenever it is clear from the context.

To analyze the structure of \bar{G} and connect it to G , we define two subsets of nodes, L and H , through the procedure outlined in Algorithm 2. The set L_d contains all nodes added into set L in the first d repetitions of line 3 of Algorithm 2; similarly, we denote by H_d the nodes added into set H in the first d repetitions of line 3 of Algorithm 2. Since L contain all leaves of \bar{G} and all other nodes in \bar{G} have at least one child, every node in \bar{G} is added into either H or L . The classification of nodes into sets L and H is crucial for our study because it determines whether a node v is a target, a loser, or both, as stated in Lemma 5.

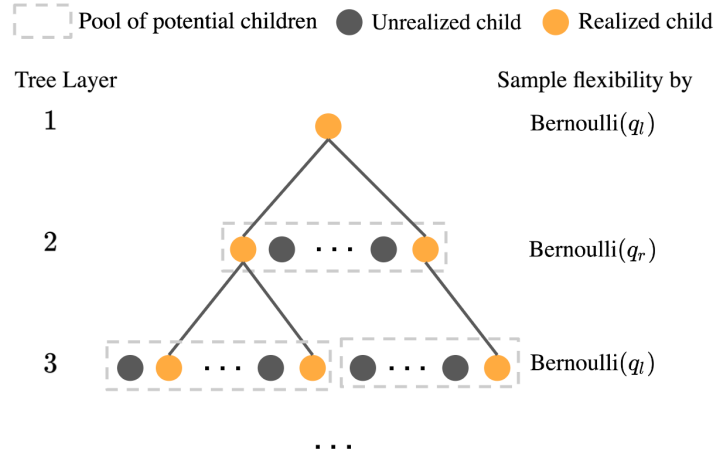


Figure 19 Illustration of the branching process for \bar{G}

Algorithm 2 Classification of Nodes in \bar{G}

- 1: **Input:** A random tree \bar{G} rooted at v .
 - 2: **Initialize:** $L = \{\text{Nodes in } \bar{G} \text{ with no children in } \bar{G}\}$, $H = \emptyset$
 - 3: **repeat**
 - 4: Add to H those nodes that have at least one child in L .
 - 5: Add to L those nodes that have only children in H .
 - 6: **until** No new nodes are added to either set
-

LEMMA 5 (Lemma 3 in Karp and Sipser (1981)). Let \bar{G} be a random tree rooted at v .

- (i) v is a target iff v is in H ;
- (ii) v is a loser iff either v is in L or v has exactly 1 child which is not in H .

Given that the nodes across different tree layers exhibit heterogeneity, we define two sets of nodes: the set S_l contains all nodes sampled from layers with $\text{Bernoulli}(b_l)$ and the set S_r contains all nodes from layers with $\text{Bernoulli}(b_r)$. For a flexible node in S_l , we denote the probabilities of it being in L and H as $y_L^f(\mathbf{b})$ and $y_H^f(\mathbf{b})$, respectively. Similarly, for a regular node in S_l , we denote the probabilities as $y_L^{nf}(\mathbf{b})$ and $y_H^{nf}(\mathbf{b})$. We use an additional hat symbol to denote the counterparts of these probabilities in S_r , a notation consistently applied throughout this paper to differentiate quantities associated with S_r from those associated with S_l . In Lemma 6, we state that the vector

$$\mathbf{y} = \left(y_L^f(\mathbf{b}), y_L^{nf}(\mathbf{b}), y_H^f(\mathbf{b}), y_H^{nf}(\mathbf{b}), \hat{y}_L^f(\mathbf{b}), \hat{y}_L^{nf}(\mathbf{b}), \hat{y}_H^f(\mathbf{b}), \hat{y}_H^{nf}(\mathbf{b}) \right)$$

can be computed as the smallest set of solutions to the equations in (11).

LEMMA 6. As $n \rightarrow \infty$ the probabilities encoded in \mathbf{y} converge to the smallest solution to (11).

Now, combining Lemma 5 with Lemma 6, we obtain the probability for nodes in \bar{G} to be a target or a loser.

LEMMA 7. *Let \bar{G} be a random tree rooted at v . Then, as $n \rightarrow \infty$,*

(i) *if v is a flexible node in S_l , v is a target with probability $y_H^f(\mathbf{b})$ and a loser with probability*

$$y_L^f(\mathbf{b}) + y_L^f(\mathbf{b}) \left((1+b_r)\alpha^f + (1-b_r)\alpha - b_r 2\alpha^f \hat{y}_H^f(\mathbf{b}) - (1-b_r)(\alpha^f + \alpha) \hat{y}_H^{nf}(\mathbf{b}) \right).$$

(ii) *if v is a regular node in S_l , v is a target with probability $y_H^{nf}(\mathbf{b})$ and a loser with probability*

$$y_L^{nf}(\mathbf{b}) + y_L^{nf}(\mathbf{b}) \left(b_r \alpha^f + (2-b_r)\alpha - b_r (\alpha^f + \alpha) \hat{y}_H^f(\mathbf{b}) - (1-b_r) 2\alpha \hat{y}_H^{nf}(\mathbf{b}) \right).$$

(iii) *if v is a flexible node in S_r , v is a target with probability $\hat{y}_L^f(\mathbf{b})$ and a loser with probability*

$$\hat{y}_L^f(\mathbf{b}) + \hat{y}_H^f(\mathbf{b}) \left((1+b_l)\alpha^f + (1-b_l)\alpha - b_l 2\alpha^f y_H^f(\mathbf{b}) - (1-b_l)(\alpha^f + \alpha) y_H^{nf}(\mathbf{b}) \right).$$

(iv) *if v is a regular node in S_r , v is a target with probability $\hat{y}_L^{nf}(\mathbf{b})$ and a loser with probability*

$$\hat{y}_H^{nf}(\mathbf{b}) + \hat{y}_L^{nf}(\mathbf{b}) \left(b_l \alpha^f + (2-b_l)\alpha - b_l (\alpha^f + \alpha) y_H^f(\mathbf{b}) - (1-b_l) 2\alpha y_H^{nf}(\mathbf{b}) \right).$$

Equipped with Lemma 7, we are ready to compute the probability that v appears in a derivation as $n \rightarrow \infty$.

PROPOSITION 2 (Extension of Theorem 9 (4) in Karp and Sipser (1981)). *Let v be a random node in G . Then, as $n \rightarrow \infty$:*

$$\begin{aligned} & \lim_{n \rightarrow \infty} \mathbb{P}[v \text{ in a derivation} \mid v \text{ is a flexible node in } V_l] \\ &= y_H^f(\mathbf{b}) + y_L^f(\mathbf{b}) + y_L^f(\mathbf{b}) \left[(1+b_r)\alpha^f + (1-b_r)\alpha \right] \cdot \\ & \quad \left[1 - \frac{b_r 2\alpha^f}{(1+b_r)\alpha^f + (1-b_r)\alpha} \left(\hat{y}_L^f(\mathbf{b}) + \hat{y}_H^f(\mathbf{b}) \right) - \frac{(1-b_r)(\alpha^f + \alpha)}{(1+b_r)\alpha^f + (1-b_r)\alpha} \left(\hat{y}_L^{nf}(\mathbf{b}) + \hat{y}_H^{nf}(\mathbf{b}) \right) \right], \\ & \lim_{n \rightarrow \infty} \mathbb{P}[v \text{ in a derivation} \mid v \text{ is a regular node in } V_l] \\ &= y_H^{nf}(\mathbf{b}) + y_L^{nf}(\mathbf{b}) + y_L^{nf}(\mathbf{b}) \left[b_r \alpha^f + (2-b_r)\alpha \right] \cdot \\ & \quad \left[1 - \frac{b_r (\alpha^f + \alpha)}{b_r \alpha^f + (2-b_r)\alpha} \left(\hat{y}_L^f(\mathbf{b}) + \hat{y}_H^f(\mathbf{b}) \right) - \frac{(1-b_r) 2\alpha}{b_r \alpha^f + (2-b_r)\alpha} \left(\hat{y}_L^{nf}(\mathbf{b}) + \hat{y}_H^{nf}(\mathbf{b}) \right) \right], \\ & \lim_{n \rightarrow \infty} \mathbb{P}[v \text{ in a derivation} \mid v \text{ is a flexible node in } V_r] \\ &= \hat{y}_H^f(\mathbf{b}) + \hat{y}_L^f(\mathbf{b}) + \hat{y}_L^f(\mathbf{b}) \left[(1+b_l)\alpha^f + (1-b_l)\alpha \right] \cdot \\ & \quad \left[1 - \frac{b_l 2\alpha^f}{(1+b_l)\alpha^f + (1-b_l)\alpha} \left(y_L^f(\mathbf{b}) + y_H^f(\mathbf{b}) \right) - \frac{(1-b_l)(\alpha^f + \alpha)}{(1+b_l)\alpha^f + (1-b_l)\alpha} \left(y_L^{nf}(\mathbf{b}) + y_H^{nf}(\mathbf{b}) \right) \right], \\ & \lim_{n \rightarrow \infty} \mathbb{P}[v \text{ in a derivation} \mid v \text{ is a regular node in } V_r] \\ &= \hat{y}_H^{nf}(\mathbf{b}) + \hat{y}_L^{nf}(\mathbf{b}) + \hat{y}_L^{nf}(\mathbf{b}) \left[b_l \alpha^f + (2-b_l)\alpha \right] \cdot \\ & \quad \left[1 - \frac{b_l (\alpha^f + \alpha)}{b_l \alpha^f + (2-b_l)\alpha} \left(y_L^f(\mathbf{b}) + y_H^f(\mathbf{b}) \right) - \frac{(1-b_l) 2\alpha}{b_l \alpha^f + (2-b_l)\alpha} \left(y_L^{nf}(\mathbf{b}) + y_H^{nf}(\mathbf{b}) \right) \right]. \end{aligned}$$

Now, equipped with the auxiliary results, we are ready to prove Theorem 9, Lemma 4 and Theorem 8.

Proof of Theorem 9 Recall that the KS algorithm is asymptotically optimal under Condition 1. Specifically, by Condition 1 we find

$$\begin{aligned}\mu(b_l, b_r) &= \lim_{n \rightarrow \infty} \frac{\mathbb{E}[\mathcal{M}_n(b_l, b_r)]}{n} = \lim_{n \rightarrow \infty} \frac{\mathbb{E}[|M_1^l| + |M_2^l|]}{n} = \lim_{n \rightarrow \infty} \frac{\mathbb{E}[n - \psi_1 - \psi_2]}{n} \\ &= 1 - \lim_{n \rightarrow \infty} \frac{\mathbb{E}[\psi_1]}{n} - \lim_{n \rightarrow \infty} \frac{\mathbb{E}[\psi_2]}{n} = 1 - \lim_{n \rightarrow \infty} \frac{\mathbb{E}[\psi_1]}{n}\end{aligned}$$

provided that these limits exist. From Proposition 1 (v), we know

$$\begin{aligned}\mu(b_l, b_r) &= 1 - \lim_{n \rightarrow \infty} \frac{\mathbb{E}[\psi_1]}{n} = 1 - \lim_{n \rightarrow \infty} \max \left\{ \mathbb{P}[v \in \Psi_1^l | v \in V_l], \mathbb{P}[v \in \Psi_1^r | v \in V_r] \right\} \\ &= 1 - \max \left\{ \lim_{n \rightarrow \infty} \mathbb{P}[v \text{ is a loser} | v \in V_l] - \lim_{n \rightarrow \infty} \mathbb{P}[v \text{ is a target} | v \in V_r], \right. \\ &\quad \left. \lim_{n \rightarrow \infty} \mathbb{P}[v \text{ is a loser} | v \in V_r] - \lim_{n \rightarrow \infty} \mathbb{P}[v \text{ is a target} | v \in V_l] \right\}\end{aligned}$$

provided that these limits exist. By the law of iterated expectations, we have

$$\begin{aligned}&\lim_{n \rightarrow \infty} \mathbb{P}[v \text{ is a loser} | v \in V_l] - \lim_{n \rightarrow \infty} \mathbb{P}[v \text{ is a target} | v \in V_r] \\ &= \lim_{n \rightarrow \infty} \mathbb{P}[v \text{ is a loser} | v \text{ is a flexible node in } V_l] \cdot \mathbb{P}[v \in v_l \text{ is a flexible node}] \\ &\quad + \lim_{n \rightarrow \infty} \mathbb{P}[v \text{ is a loser} | v \text{ is a regular node in } V_l] \cdot \mathbb{P}[v \in v_l \text{ is a regular node}] \\ &\quad - \lim_{n \rightarrow \infty} \mathbb{P}[v \text{ is a target} | v \text{ is a flexible node in } V_r] \cdot \mathbb{P}[v \in v_r \text{ is a flexible node}] \\ &\quad - \lim_{n \rightarrow \infty} \mathbb{P}[v \text{ is a target} | v \text{ is a regular node in } V_r] \cdot \mathbb{P}[v \in v_r \text{ is a regular node}]\end{aligned}$$

provided that these limits exist.

Now we can plug in probabilities derived in Lemma 7, which we have shown in Claim 6 to be equal to the corresponding probabilities in random graphs:

$$\begin{aligned}&\lim_{n \rightarrow \infty} \mathbb{P}[v \text{ is a loser} | v \in V_l] - \lim_{n \rightarrow \infty} \mathbb{P}[v \text{ is a target} | v \in V_r] \\ &= b_l \left(y_L^f(\mathbf{b}) + y_L^{nf}(\mathbf{b}) \left((1+b_r)\alpha^f + (1-b_r)\alpha - b_r 2\alpha^f \hat{y}_H^f(\mathbf{b}) - (1-b_r)(\alpha^f + \alpha) \hat{y}_H^{nf}(\mathbf{b}) \right) \right) - b_r \hat{y}_H^f(\mathbf{b}) \\ &\quad + (1-b_l) \left(y_L^{nf}(\mathbf{b}) + y_L^n(\mathbf{b}) \left(b_r \alpha^f + (2-b_r)\alpha - b_r (\alpha^f + \alpha) \hat{y}_H^f(\mathbf{b}) - (1-b_r) 2\alpha \hat{y}_H^{nf}(\mathbf{b}) \right) \right) - (1-b_r) \hat{y}_H^{nf}(\mathbf{b}) \\ &= b_l \left(y_L^f(\mathbf{b}) + y_L^{nf}(\mathbf{b}) \left(b_r 2\alpha^f (1 - \hat{y}_H^f(\mathbf{b})) + (1-b_r)(\alpha^f + \alpha) (1 - \hat{y}_H^{nf}(\mathbf{b})) \right) \right) - 1 + b_r (1 - \hat{y}_H^f(\mathbf{b})) \\ &\quad + (1-b_l) \left(y_L^{nf}(\mathbf{b}) + y_L^n(\mathbf{b}) \left(b_r (\alpha^f + \alpha) (1 - \hat{y}_H^f(\mathbf{b})) + (1-b_r) 2\alpha (1 - \hat{y}_H^{nf}(\mathbf{b})) \right) \right) + (1-b_r) (1 - \hat{y}_H^{nf}(\mathbf{b})) \\ &= b_l y_L^f(\mathbf{b}) + b_r (1 - \hat{y}_H^f(\mathbf{b})) (2b_l \alpha^f y_L^f(\mathbf{b}) + (1-b_l)(\alpha^f + \alpha) y_L^{nf}(\mathbf{b})) - 1 + b_r (1 - \hat{y}_H^f(\mathbf{b})) \\ &\quad + (1-b_l) y_L^{nf}(\mathbf{b}) + (1-b_r) (1 - \hat{y}_H^{nf}(\mathbf{b})) (b_l (\alpha^f + \alpha) y_L^f(\mathbf{b}) + 2(1-b_l)\alpha y_L^{nf}(\mathbf{b})) + (1-b_r) (1 - \hat{y}_H^{nf}(\mathbf{b})) \\ &=: 1 - \xi(b_l, b_r).\end{aligned}$$

Similarly, we find that

$$\begin{aligned}
 & \lim_{n \rightarrow \infty} \mathbb{P}[v \text{ is a loser} | v \in V_r] - \lim_{n \rightarrow \infty} \mathbb{P}[v \text{ is a target} | v \in V_l] \\
 &= b_r \hat{y}_L^f(\mathbf{b}) + b_l \left(1 - y_H^f(\mathbf{b})\right) \left(2b_r \alpha^f \hat{y}_L^f(\mathbf{b}) + (1 - b_r)(\alpha^f + \alpha) \hat{y}_L^{nf}(\mathbf{b})\right) - 1 + b_l \left(1 - y_H^f(\mathbf{b})\right) \\
 &\quad + (1 - b_r) \hat{y}_L^{nf}(\mathbf{b}) + (1 - b_l) \left(1 - y_H^{nf}(\mathbf{b})\right) \left(b_r (\alpha^f + \alpha) \hat{y}_L^f(\mathbf{b}) + 2(1 - b_r) \alpha \hat{y}_L^{nf}(\mathbf{b})\right) + (1 - b_l) \left(1 - y_H^{nf}(\mathbf{b})\right) \\
 &=: 1 - \hat{\xi}(b_l, b_r).
 \end{aligned}$$

Thus, under Condition 1

$$\begin{aligned}
 \mu(b_l, b_r) &= 1 - \max \left\{ \lim_{n \rightarrow \infty} \mathbb{P}[v \text{ is a loser} | v \in V_l] - \lim_{n \rightarrow \infty} \mathbb{P}[v \text{ is a target} | v \in V_r], \right. \\
 &\quad \left. \lim_{n \rightarrow \infty} \mathbb{P}[v \text{ is a loser} | v \in V_r] - \lim_{n \rightarrow \infty} \mathbb{P}[v \text{ is a target} | v \in V_l] \right\} \\
 &= 1 - \max \left(1 - \xi(b_l, b_r), 1 - \hat{\xi}(b_l, b_r)\right) = \min \left(\xi(b_l, b_r), \hat{\xi}(b_l, b_r)\right) := \mu^{\text{KS}}(b_l, b_r).
 \end{aligned}$$

□

Proof of Lemma 4 From Proposition 1 (i), it is known that

$$\lim_{n \rightarrow \infty} \frac{\mathbb{E}[m_1 + \psi_1]}{n} = \max \left\{ \lim_{n \rightarrow \infty} \mathbb{P}[v \text{ in a derivation} | v \in V_l], \lim_{n \rightarrow \infty} \mathbb{P}[v \text{ in a derivation} | v \in V_r] \right\}.$$

We next demonstrate that if the solution to (11) is unique, then

$$\lim_{n \rightarrow \infty} \mathbb{P}[v \text{ in a derivation} | v \in V_l] = \lim_{n \rightarrow \infty} \mathbb{P}[v \text{ in a derivation} | v \in V_r] = 1. \quad (14)$$

To establish (14), we leverage Proposition 2 and consider a random node v in G , which can be either flexible or regular and either in V_l or in V_r . If v is a flexible node in V_l , a regular node in V_l , a flexible node in V_r , or a regular node in V_r . We shall demonstrate that $\lim_{n \rightarrow \infty} \mathbb{P}[v \text{ in a derivation}] = 1$ when the solution to (11) is unique.

Note that for any solution vector \mathbf{w} to (11), it is always feasible to construct

$$\begin{aligned}
 x_L^f(b_l, b_r) &= w_L^f(\mathbf{b}), x_H^f(b_l, b_r) = 1 - w_L^f(\mathbf{b}), \\
 x_L^{nf}(b_l, b_r) &= w_L^{nf}(\mathbf{b}), x_H^{nf}(b_l, b_r) = 1 - w_L^{nf}(\mathbf{b}), \\
 \hat{x}_L^f(b_l, b_r) &= \hat{w}_L^f(\mathbf{b}), \hat{x}_H^f(b_l, b_r) = 1 - \hat{w}_L^f(\mathbf{b}), \\
 \hat{x}_L^{nf}(b_l, b_r) &= \hat{w}_L^{nf}(\mathbf{b}), \hat{x}_H^{nf}(b_l, b_r) = 1 - \hat{w}_L^{nf}(\mathbf{b}),
 \end{aligned} \quad (15)$$

so that \mathbf{x} is provably a solution to (11). Consequently, when (11) admits a unique solution, the smallest set of solutions \mathbf{y} must satisfy (15). We next substitute (15) into the expressions derived in Proposition 2 and simplify to find that

$$\lim_{n \rightarrow \infty} \mathbb{P}[v \text{ in a derivation} | v \text{ is a flexible node in } V_l]$$

$$\begin{aligned}
 &= y_H^f(\mathbf{b}) + y_L^f(\mathbf{b}) + y_L^f(\mathbf{b}) \left[(1+b_r)\alpha^f + (1-b_r)\alpha \right] \cdot \\
 &\quad \left[1 - \frac{b_r 2\alpha^f}{(1+b_r)\alpha^f + (1-b_r)\alpha} (\hat{y}_L^f(\mathbf{b}) + \hat{y}_H^f(\mathbf{b})) - \frac{(1-b_r)(\alpha^f + \alpha)}{(1+b_r)\alpha^f + (1-b_r)\alpha} (\hat{y}_L^{nf}(\mathbf{b}) + \hat{y}_H^{nf}(\mathbf{b})) \right] \\
 &= 1 + y_L^f(\mathbf{b}) \left[(1+b_r)\alpha^f + (1-b_r)\alpha \right] \cdot \left[1 - \frac{b_r 2\alpha^f}{(1+b_r)\alpha^f + (1-b_r)\alpha} - \frac{(1-b_r)(\alpha^f + \alpha)}{(1+b_r)\alpha^f + (1-b_r)\alpha} \right] \\
 &= 1 + y_L^f(\mathbf{b}) \left[(1+b_r)\alpha^f + (1-b_r)\alpha \right] \cdot 0 \\
 &= 1.
 \end{aligned}$$

One can show analogously that nodes in V_r or regular nodes in V_l have a probability of 1, asymptotically, to be in a derivation.

Consequently, we have

$$\begin{aligned}
 \lim_{n \rightarrow \infty} \frac{\mathbb{E}[\psi_2]}{n} &\leq 1 - \lim_{n \rightarrow \infty} \frac{\mathbb{E}[m_1 + \psi_1]}{n} \\
 &= 1 - \max \left\{ \lim_{n \rightarrow \infty} \mathbb{P}[v \text{ in a derivation} \mid v \in V_l], \lim_{n \rightarrow \infty} \mathbb{P}[v \text{ in a derivation} \mid v \in V_r] \right\} = 0,
 \end{aligned}$$

thereby verifying Condition 1. \square

Proof of Theorem 8 By Theorem 9 and Lemma 4, to establish Theorem 8 it is sufficient to demonstrate that when $10^{-4} < \alpha < \alpha^f$ and $\alpha^f + \alpha < e$ the solution to (11) is unique at the points $\mathbf{b} = (1, 0), (0, 1)$ and $(1/2, 1/2)$.

When $\mathbf{b} = (1, 0)$, all nodes in V_l are flexible nodes, while those in V_r are regular nodes. Thus, it suffices to analyze $w_L^f(\mathbf{b}), w_H^f(\mathbf{b}), \hat{w}_L^{nf}(\mathbf{b})$ and $\hat{w}_H^{nf}(\mathbf{b})$. Then, (11) reduces to

$$w_L^f(\mathbf{b}) = e^{-(\alpha^f + \alpha)(1 - \hat{w}_H^{nf}(\mathbf{b}))}, \hat{w}_H^{nf}(\mathbf{b}) = 1 - e^{-(\alpha^f + \alpha)w_L^f(\mathbf{b})}, \quad (16)$$

$$\hat{w}_L^{nf}(\mathbf{b}) = e^{-(\alpha^f + \alpha)(1 - w_H^f(\mathbf{b}))}, w_H^f(\mathbf{b}) = 1 - e^{-(\alpha^f + \alpha)\hat{w}_L^{nf}(\mathbf{b})}. \quad (17)$$

Since (16) and (17) are equivalent, it suffices to show that solution to the pair $(w_L^f(\mathbf{b}), \hat{w}_H^{nf}(\mathbf{b}))$ in (16) is unique. This is a direct application of the following result from Karp and Sipser (1981), by taking $L = w_L^f(\mathbf{b}), W = \hat{w}_H^{nf}(\mathbf{b})$ and $\lambda = \alpha^f + \alpha$:

CLAIM 1 (Lemma 1 in Karp and Sipser (1981)). Define $L = e^{-\lambda(1-W)}$, $W = 1 - e^{-\lambda L}$. Then, $L + W \leq 1$, with equality if and only if $\lambda \leq e$.

The case for $\mathbf{b} = (0, 1)$ is symmetric.

For the case of $\mathbf{b} = (1/2, 1/2)$, symmetry implies that

$$w_L^f(\mathbf{b}) = \hat{w}_L^f(\mathbf{b}), w_L^{nf}(\mathbf{b}) = \hat{w}_L^{nf}(\mathbf{b}), w_H^f(\mathbf{b}) = \hat{w}_H^f(\mathbf{b}), w_H^{nf}(\mathbf{b}) = \hat{w}_H^{nf}(\mathbf{b}).$$

Substituting $\mathbf{b} = (1/2, 1/2)$ into (11), we obtain the following equations:

$$\begin{aligned} w_L^f(\mathbf{b}) &= e^{-\frac{1}{2}2\alpha^f(1-\hat{w}_H^f(\mathbf{b})) - \frac{1}{2}(\alpha^f+\alpha)(1-\hat{w}_H^{nf}(\mathbf{b}))}, \\ w_L^{nf}(\mathbf{b}) &= e^{-\frac{1}{2}(\alpha^f+\alpha)(1-\hat{w}_H^f(\mathbf{b})) - \frac{1}{2}2\alpha(1-\hat{w}_H^{nf}(\mathbf{b}))}, \\ \hat{w}_H^f(\mathbf{b}) &= 1 - e^{-\frac{1}{2}2\alpha^f w_L^f(\mathbf{b}) - \frac{1}{2}(\alpha^f+\alpha)w_L^{nf}(\mathbf{b})}, \\ \hat{w}_H^{nf}(\mathbf{b}) &= 1 - e^{-\frac{1}{2}(\alpha^f+\alpha)w_L^f(\mathbf{b}) - \frac{1}{2}2\alpha w_L^{nf}(\mathbf{b})}. \end{aligned} \quad (18)$$

We observe that values of $w_L^f(\mathbf{b}), w_L^{nf}(\mathbf{b}), \hat{w}_H^f(\mathbf{b})$ and $\hat{w}_H^{nf}(\mathbf{b})$ are trivially bounded between 0 and 1, and all of the variables are increasing in each other. Thus, we initialize the values of $(w_L^f(\mathbf{b}, 0), w_L^{nf}(\mathbf{b}, 0), \hat{w}_H^f(\mathbf{b}, 0), \hat{w}_H^{nf}(\mathbf{b}, 0)) = (0, 0, 0, 0)$ and define, for any $d \in \mathbb{Z}^+$,

$$\begin{aligned} w_L^f(\mathbf{b}, d) &= e^{-\frac{1}{2}2\alpha^f(1-\hat{w}_H^f(\mathbf{b}, d-1)) - \frac{1}{2}(\alpha^f+\alpha)(1-\hat{w}_H^{nf}(\mathbf{b}, d-1))}, \\ w_L^{nf}(\mathbf{b}, d) &= e^{-\frac{1}{2}(\alpha^f+\alpha)(1-\hat{w}_H^f(\mathbf{b}, d-1)) - \frac{1}{2}2\alpha(1-\hat{w}_H^{nf}(\mathbf{b}, d-1))}, \\ \hat{w}_H^f(\mathbf{b}, d) &= 1 - e^{-\frac{1}{2}2\alpha^f w_L^f(\mathbf{b}, d-1) - \frac{1}{2}(\alpha^f+\alpha)w_L^{nf}(\mathbf{b}, d-1)}, \\ \hat{w}_H^{nf}(\mathbf{b}, d) &= 1 - e^{-\frac{1}{2}(\alpha^f+\alpha)w_L^f(\mathbf{b}, d-1) - \frac{1}{2}2\alpha w_L^{nf}(\mathbf{b}, d-1)}. \end{aligned}$$

Then, the smallest set of solutions to (18) is given by $\lim_{d \rightarrow \infty} (w_L^f(\mathbf{b}, d), w_L^{nf}(\mathbf{b}, d), \hat{w}_H^f(\mathbf{b}, d), \hat{w}_H^{nf}(\mathbf{b}, d))$.

For any $\vec{\mathbf{x}} \in \mathbb{R}^2$, define

$$F(\vec{\mathbf{x}}) = \begin{pmatrix} e^{-\frac{1}{2}2\alpha^f x_1 - \frac{1}{2}(\alpha^f+\alpha)x_2} \\ e^{-\frac{1}{2}(\alpha^f+\alpha)x_1 - \frac{1}{2}2\alpha x_2} \end{pmatrix}$$

and define $F^t(\vec{\mathbf{x}})$ the t th application of the function F on $\vec{\mathbf{x}}$. That is, $F^0(\vec{\mathbf{x}}) = \vec{\mathbf{x}}, F^1(\vec{\mathbf{x}}) = F(\vec{\mathbf{x}})$ and $F^2(\vec{\mathbf{x}}) = F(F(\vec{\mathbf{x}}))$. Then, the smallest solutions to $\begin{pmatrix} w_L^f(\mathbf{b}) \\ w_L^{nf}(\mathbf{b}) \end{pmatrix}$ and $\vec{1} - \begin{pmatrix} \hat{w}_H^f(\mathbf{b}) \\ \hat{w}_H^{nf}(\mathbf{b}) \end{pmatrix}$ are respectively given by $\lim_{t \rightarrow \infty} F^{2t}(\vec{1})$ and $\lim_{t \rightarrow \infty} F^{2t+1}(\vec{1})$. In particular, $\begin{pmatrix} w_L^f(\mathbf{b}) \\ w_L^{nf}(\mathbf{b}) \end{pmatrix} = \vec{1} - \begin{pmatrix} \hat{w}_H^f(\mathbf{b}) \\ \hat{w}_H^{nf}(\mathbf{b}) \end{pmatrix}$ and the solution is unique if $F(\vec{\mathbf{x}})$ has a unique fixed point, i.e., there exists a unique $\vec{\mathbf{x}}^*$ such that $F(\vec{\mathbf{x}}^*) = \vec{\mathbf{x}}^*$. Notice that in $F(\vec{\mathbf{x}}) = \vec{\mathbf{x}}$ we have $x_1 = e^{-\alpha^f x_1 - \frac{1}{2}(\alpha^f+\alpha)x_2}$, so $x_2 = -2\frac{\log(x_1) + \alpha^f x_1}{\alpha^f + \alpha}$. Plugging this into $x_2 = e^{-\frac{1}{2}(\alpha^f+\alpha)x_1 - \frac{1}{2}2\alpha x_2}$, we find that

$$-2\frac{\log(x_1) + \alpha^f x_1}{\alpha^f + \alpha} = e^{-\frac{1}{2}(\alpha^f+\alpha)x_1 + 2\frac{\alpha}{\alpha^f+\alpha}(\log(x_1) + \alpha^f x_1)}, \quad (19)$$

so it suffices to show that (19) has a unique solution when $\alpha^f + \alpha < e$.

Let

$$f_1(x_1) := e^{-\frac{1}{2}(\alpha^f+\alpha)x_1 + 2\frac{\alpha}{\alpha^f+\alpha}(\log(x_1) + \alpha^f x_1)} + 2\frac{\log(x_1) + \alpha^f x_1}{\alpha^f + \alpha}. \quad (20)$$

The next result establishes a monotonicity property of this function:

CLAIM 2. When $10^{-4} < \alpha < \alpha^f$ and $\alpha^f + \alpha < e$, $f'_1(x_1) > 1$ for any $x_1 \in (0, 1]$.

Since $f_1(0) = -\infty$ and $f_1(1) \geq 0$, by continuity of $f_1(x_1)$ with respect to x_1 we know that $f_1(x_1) = 0$ has at least one solution in $(0, 1]$. Since we also know from Claim 2 that $f_1(x_1)$ is strictly monotonically increasing with respect to x_1 in $(0, 1]$ when $10^{-4} < \alpha < \alpha^f$ and $\alpha^f + \alpha < e$, such solution for x_1 is unique. This completes the proof of Theorem 8. \square

A.3.3. Proof of Theorem 3 (ii)

Proof. Recall from Theorem 8 that, in the stated parameter regimes, $\mu(b_l, b_r) = \mu^{\text{KS}}(b_l, b_r)$ at $\mathbf{b} = (1, 0)$ and $(1/2, 1/2)$. Since the solution to (11) is unique at these points, (15) is satisfied by the smallest set of solutions \mathbf{y} . Plugging

$$y_L^f(\mathbf{b}) = 1 - y_H^f(\mathbf{b}), y_L^{nf}(\mathbf{b}) = y_H^f(\mathbf{b})$$

into (12) and (13), we find that at these values of \mathbf{b}

$$\begin{aligned} \mu(b_l, b_r) &= \xi(b_l, b_r) = \hat{\xi}(b_l, b_r) \\ &= 2 - b_l y_L^f(\mathbf{b}) - b_r e^{-b_1(b_l, b_r)} (1 + b_1(b_l, b_r)) - (1 - b_l) y_L^{nf}(\mathbf{b}) - (1 - b_r) e^{-b_2(b_l, b_r)} (1 + b_2(b_l, b_r)), \end{aligned}$$

where

$$\begin{aligned} b_1(b_l, b_r) &= b_l 2\alpha^f y_L^f(\mathbf{b}) + (1 - b_l) (\alpha^f + \alpha) y_L^{nf}(\mathbf{b}), \\ b_2(b_l, b_r) &= b_l (\alpha^f + \alpha) y_L^f(\mathbf{b}) + (1 - b_l) 2\alpha y_L^{nf}(\mathbf{b}). \end{aligned}$$

When $\mathbf{b} = (1, 0)$, $\mu(b_l, b_r)$ depends only on $y_L^f(\mathbf{b})$, which can be solved as the unique solution x^* to

$$x = e^{-(\alpha^f + \alpha)} e^{-(\alpha^f + \alpha)x}. \quad (21)$$

When $\mathbf{b} = (1/2, 1/2)$, $\mu(b_l, b_r)$ depends only on $(y_L^f(\mathbf{b}), y_L^{nf}(\mathbf{b}))$, which can be solved as the unique set of solution (x_1^*, x_2^*) to

$$\begin{aligned} x_1 &= e^{-\frac{1}{2}2\alpha^f x_1 - \frac{1}{2}(\alpha^f + \alpha)x_2}, \\ x_2 &= e^{-\frac{1}{2}(\alpha^f + \alpha)x_1 - \frac{1}{2}2\alpha x_2}. \end{aligned} \quad (22)$$

Our objective is to show that $\mu(1, 0) > \mu(1/2, 1/2)$ for any α^f and α satisfying $10^{-4} < \alpha < \alpha^f$ and $\alpha^f + \alpha < e$. To do so, we divide the parameter regions into small cells and prove the inequality by deriving bounds within each cell. We fix a constant $\delta > 0$ and derive for any α, α^f , a lower bound for the expression $\mu(1, 0) - \mu(1/2, 1/2)$ for any $(\bar{\alpha}^f, \bar{\alpha}) \in \mathcal{I}(\alpha, \alpha^f, \delta) := \{(\bar{\alpha}, \bar{\alpha}^f) : \bar{\alpha} \in [\alpha, \alpha + \delta], \bar{\alpha}^f \in [\alpha^f, \alpha^f + \delta]\}$. We then employ a computer-aided proof to iterate over all cells in the claimed region and verify if this lower bound is positive for the respective cell. To do so, we need to bound $\bar{\alpha}^f, \bar{\alpha}$ and the resulting \bar{x}, \bar{x}_1 and \bar{x}_2 in each cell. In $\mathcal{I}(\alpha, \alpha^f, \delta)$, if we know the respective lower and upper bounds of \bar{x}, \bar{x}_1 and \bar{x}_2 , which we denote by $x^{lb}, x^{ub}, x_1^{lb}, x_1^{ub}, x_2^{lb}$ and x_2^{ub} , then we can lower bound

$$\begin{aligned} \mu(1, 0) &= 2 - \bar{x} - e^{-(\bar{\alpha}^f + \bar{\alpha})\bar{x}} \left[1 + (\bar{\alpha}^f + \bar{\alpha}) \bar{x} \right] \\ &\geq 2 - x^{ub} - e^{-(\alpha^f + \alpha)x^{lb}} \left[1 + (\alpha^f + \alpha + 2\delta) x^{ub} \right], \forall (\bar{\alpha}^f, \bar{\alpha}) \in \mathcal{I}(\alpha, \alpha^f, \delta). \end{aligned} \quad (23)$$

Similarly, we can upper bound

$$\begin{aligned}
 \mu(1/2, 1/2) &= 2 - \frac{1}{2}\bar{x}_1 - \frac{1}{2}\bar{x}_2 - \frac{1}{2}e^{-(\bar{\alpha}^f)\bar{x}_1 - \frac{1}{2}(\bar{\alpha}^f + \bar{\alpha})\bar{x}_2} \left[1 + \bar{\alpha}^f \bar{x}_1 + \frac{1}{2} (\bar{\alpha}^f + \bar{\alpha}) \bar{x}_2 \right] \\
 &\quad - \frac{1}{2}e^{-\frac{1}{2}(\bar{\alpha}^f + \bar{\alpha})\bar{x}_1 - (\bar{\alpha})\bar{x}_2} \left[1 + \frac{1}{2} (\bar{\alpha}^f + \bar{\alpha}) \bar{x}_1 + \bar{\alpha} \bar{x}_2 \right] \\
 &\leq 2 - \frac{1}{2}x_1^{lb} - \frac{1}{2}x_2^{lb} \\
 &\quad - \frac{1}{2}e^{-(\alpha^f + \delta)x_1^{ub} - \frac{1}{2}(\alpha^f + \alpha + 2\delta)x_2^{ub}} \left[1 + \alpha^f x_1^{lb} + \frac{1}{2} (\alpha^f + \alpha) x_2^{lb} \right] \\
 &\quad - \frac{1}{2}e^{-\frac{1}{2}(\alpha^f + \alpha + 2\delta)x_1^{ub} - (\alpha + \delta)x_2^{ub}} \left[1 + \frac{1}{2} (\alpha^f + \alpha) x_1^{lb} + \alpha x_2^{lb} \right], \forall (\bar{\alpha}^f, \bar{\alpha}) \in \mathcal{I}(\alpha, \alpha^f, \delta).
 \end{aligned} \tag{24}$$

Thus, it suffices to find $x^{lb}, x^{ub}, x_1^{lb}, x_1^{ub}, x_2^{lb}$ and x_2^{ub} in the corresponding cell. To do this, we start by showing that, for given α^f and α , the solution returned by `nlsolve` package in Julia programming language is provably close to the true solution x^*, x_1^* and x_2^* , and then provide a continuity argument to bound the solution \bar{x}, \bar{x}_1 and \bar{x}_2 for any $(\bar{\alpha}^f, \bar{\alpha}) \in \mathcal{I}(\alpha, \alpha^f, \delta)$.

We start by bounding the value of x^*, x_1^* , and x_2^* based on the numerical solutions returned by Julia `nlsolve`. We parameterize the tolerance level $ftol$ in `nlsolve` by ϵ , which guarantees that, when solving the equation $g(x) = 0$ for any function $g : \mathbb{R} \mapsto \mathbb{R}$, `nlsolve` returns a solution x such that $|g(x)| < \epsilon$. We let $f(x) := x - e^{-(\alpha^f + \alpha)x}$ and recall from (20) that $f_1(x_1) = e^{-\frac{1}{2}(\alpha^f + \alpha)x_1 + 2\frac{\alpha}{\alpha^f + \alpha}(\log(x_1) + \alpha^f x_1)} + 2\frac{\log(x_1) + \alpha^f x_1}{\alpha^f + \alpha}$. Then, we leverage monotonicity properties of $f(x)$ and $f_1(x_1)$ to derive the following bounds on x^*, x_1^* and x_2^* :

CLAIM 3. Let x^{sol} and x_1^{sol} respectively denote the solutions returned by `nlsolve` for solving $f(x) = 0$ and $f_1(x_1) = 0$ with $ftol = \epsilon$. When $10^{-4} < \alpha < \alpha^f$ and $\alpha^f + \alpha < e$, we have:

$$\begin{aligned}
 x^* &\in [x^{sol} - \epsilon, x^{sol} + \epsilon], x_1^* \in [x_1^{sol} - \epsilon, x_1^{sol} + \epsilon], \text{ and} \\
 x_2^* &\in \left[-2\frac{\log(x_1^{sol} - \epsilon) + \alpha^f(x_1^{sol} - \epsilon)}{\alpha^f + \alpha}, -2\frac{\log(x_1^{sol} + \epsilon) + \alpha^f(x_1^{sol} + \epsilon)}{\alpha^f + \alpha} \right].
 \end{aligned}$$

Having established bounds on x^*, x_1^* and x_2^* for fixed α and α^f , we continue to bound \bar{x}, \bar{x}_1 and \bar{x}_2 for $(\bar{\alpha}^f, \bar{\alpha}) \in \mathcal{I}(\alpha, \alpha^f, \delta)$. Specifically, we leverage the following result on the continuity of x^*, x_1^* and x_2^* with respect to α^f and α .

CLAIM 4. Let x^*, x_1^* and x_2^* be the solution to (21) and (22) given α^f and α . Moreover, let \bar{x}, \bar{x}_1 and \bar{x}_2 be the solution to (21) and (22) given $\bar{\alpha}^f$ and $\bar{\alpha}$. Then, given any $\delta \in (0, 1/2)$, we know that for any $(\bar{\alpha}^f, \bar{\alpha}) \in \mathcal{I}(\alpha, \alpha^f, \delta)$ such that $10^{-4} < \bar{\alpha} < \bar{\alpha}^f$ and $\bar{\alpha}^f + \bar{\alpha} < e$:

- (i) $\bar{x} \in [x^*(1 - \delta), x^*]$;
- (ii) $\bar{x}_1 \in [x_1^*(1 - 2\delta), x_1^*]$ and $\bar{x}_2 \in [x_2^*(1 - 2\delta), x_2^*]$.

Combining Claim 3 and Claim 4, we can lower and upper bound the solution of \bar{x}, \bar{x}_1 and \bar{x}_2 for $(\bar{\alpha}^f, \bar{\alpha}) \in \mathcal{I}(\alpha, \alpha^f, \delta)$ where $\bar{\alpha}^f + \bar{\alpha} < e$. In particular, for given $\delta > 0$, we take

$$\begin{aligned} x^{lb} &= (x^{sol} - \epsilon)(1 - \delta), x^{ub} = (x^{sol} + \epsilon), \\ x_1^{lb} &= (x_1^{sol} - \epsilon)(1 - 2\delta), x_1^{ub} = (x_1^{sol} + \epsilon), \\ x_2^{lb} &= -2 \frac{\log(x_1^{sol} - \epsilon) + \alpha^f (x_1^{sol} - \epsilon)}{\alpha^f + \alpha} (1 - 2\delta), \\ x_2^{ub} &= -2 \frac{\log(x_1^{sol} + \epsilon) + \alpha^f (x_1^{sol} + \epsilon)}{\alpha^f + \alpha}. \end{aligned} \quad (25)$$

Plugging these values into (23) - (24), we obtain a lower bound of $\mu(1, 0) - \mu(1/2, 1/2)$ in each cell $\mathcal{I}(\alpha, \alpha^f, \delta)$. Whenever this lower bound exceeds 0, our reasoning implies that $\mu(1, 0) > \mu(1/2, 1/2)$ for any $(\bar{\alpha}^f, \bar{\alpha})$ within this cell. In `Theorem3.ipynb`,²⁷ we fix $\epsilon = 10^{-8}$ and compute the value of this lower bound for $\alpha^f, \alpha = \delta, 2\delta, \dots, e$ where $\alpha^f + \alpha < e$. We find that by taking $\delta = 0.01, 0.005, 0.0025$ and 0.001 we are able to verify $\mu(1, 0) > \mu(1/2, 1/2)$ in the respective red regions in Fig. 20.

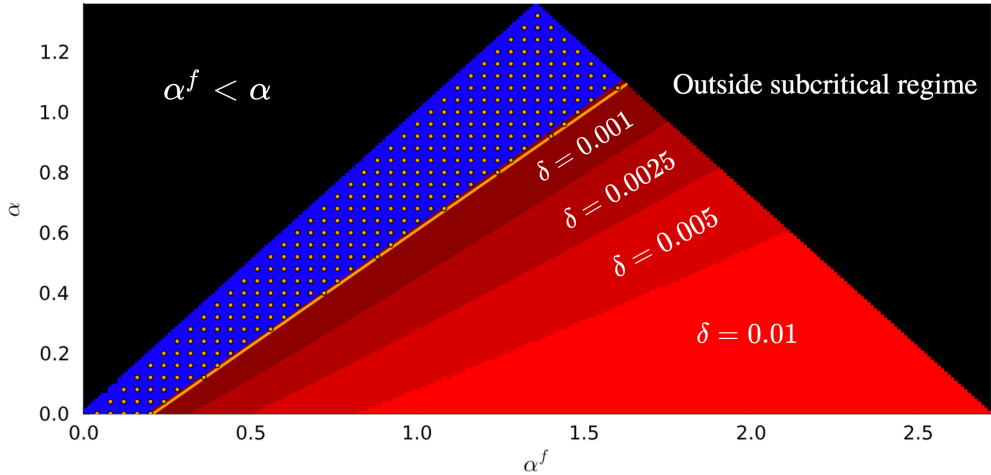


Figure 20 In the figure we denote the boundary where $\alpha = 0.77\alpha^f - 0.16$ by the orange line, and the area of subcritical regime where one-sided allocation dominates the balanced allocation is displayed in varying shades of red to the right of this boundary. This growth in the validation area with respect to δ is depicted through different red gradients. The black zone denotes parameters outside the feasible or subcritical regime. Although the inequality cannot be confirmed in the blue region when $\delta = 0.001$, by taking $\delta = 0$ we verify the inequality for a wide range of (α^f, α) values highlighted as orange dots.

□

²⁷The computer-aided proof can be found at <https://bit.ly/3UUVFRX>.

Proof of Claim 3 For $f(x) = x - e^{-(\alpha^f + \alpha)x}$, we find that $f'(x) > 1 \forall x$. When solving $f(x) = 0$, `nlsolve` is guaranteed to return a solution x^{sol} with $|f(x^{sol})| < \epsilon$. Since $f'(x) > 1 \forall x$, if $x^* > x^{sol} + \epsilon$ then

$$f(x^*) > f(x^{sol} + \epsilon) > f(x^{sol}) + \epsilon > 0,$$

which contradicts the fact that $f(x^*) = 0$. Similarly, we must have $x^* > x^{sol} - \epsilon$ and thus $x^* \in [x^{sol} - \epsilon, x^{sol} + \epsilon]$.

Since we know from Claim 2 that $f'_1(x_1) > 1$ in the specified parameter regime of α and α^f , through the same argument on $f_1(x_1)$ we find that $x_1^* \in [x_1^{sol} - \epsilon, x_1^{sol} + \epsilon]$. From (22) we know that $x_2^* = -2\frac{\log(x_1^*) + \alpha^f x_1^*}{\alpha^f + \alpha}$, which allows us to lower bound x_2^* by $-2\frac{\log(x_1^{sol} - \epsilon) + \alpha^f(x_1^{sol} - \epsilon)}{\alpha^f + \alpha}$ and upper bound x_2 by $-2\frac{\log(x_1^{sol} + \epsilon) + \alpha^f(x_1^{sol} + \epsilon)}{\alpha^f + \alpha}$. \square

Proof of Claim 4 We start by proving Claim 4 (i). We have shown in the proof of Theorem 8 that the solution to (21) is unique in the stated parameter regimes. Thus, we know that $x^* = e^{-(\alpha^f + \alpha)x^*}$ because this construction trivially satisfies (21). Similarly, $\bar{x} = e^{-(\bar{\alpha}^f + \bar{\alpha})\bar{x}}$. Now, given that $e^{-(\bar{\alpha}^f + \bar{\alpha})x^*} \leq e^{-(\alpha^f + \alpha)x^*} = x^*$ for any $(\bar{\alpha}^f, \bar{\alpha}) \in \mathcal{I}(\alpha, \alpha^f, \delta)$, we know that $\bar{x} \leq x^*$. Moreover, from the uniqueness of solution we know that it suffices to show that

$$x^*(1 - \delta) \leq e^{-(\alpha^f + \alpha + 2\delta)x^*(1 - \delta)} \leq e^{-(\bar{\alpha}^f + \bar{\alpha})x^*(1 - \delta)}$$

so then the unique solution $\bar{x} \geq x^*(1 - \delta)$. To do so, we observe that

$$e^{-(\alpha^f + \alpha)x^* - \delta x^*(1 - \delta)} \leq e^{-(\alpha^f + \alpha + 2\delta)x^*(1 - \delta)},$$

so it suffices to show that

$$x^*(1 - \delta) \leq e^{-(\alpha^f + \alpha)x^* - \delta x^*(1 - \delta)} = x^* e^{-\delta x^*(1 - \delta)}. \quad (26)$$

Since we trivially have $x^* \in (0, 1]$, we can cancel out x^* and take logarithm on both sides. We find that (26) is equivalent to $-\log(1 - \delta) \geq x^* \delta(1 - \delta)$. Since $x^* \in (0, 1]$, it is then sufficient to show that $\frac{-\log(1 - \delta)}{\delta(1 - \delta)} \geq 1$, which holds for all $\delta \in (0, 1)$.

We next prove Claim 4 (ii). Given that in the claimed region

$$\begin{aligned} x_1^* &= e^{-\frac{1}{2}2\alpha^f x_1^* - \frac{1}{2}(\alpha^f + \alpha)x_2^*} \geq e^{-\frac{1}{2}2\bar{\alpha}^f x_1^* - \frac{1}{2}(\bar{\alpha}^f + \bar{\alpha})x_2^*}, \\ x_2^* &= e^{-\frac{1}{2}(\alpha^f + \alpha)x_1^* - \frac{1}{2}2\alpha x_2^*} \geq e^{-\frac{1}{2}(\bar{\alpha}^f + \bar{\alpha})x_1^* - \frac{1}{2}2\bar{\alpha} x_2^*} \end{aligned}$$

for any $(\bar{\alpha}^f, \bar{\alpha}) \in \mathcal{I}(\alpha, \alpha^f, \delta)$, we know that $\bar{x}_1 \leq x_1^*$ and $\bar{x}_2 \leq x_2^*$.

To prove the claimed lower bound on \bar{x}_1 and \bar{x}_2 , we show that

$$\begin{aligned} x_1^*(1 - 2\delta) &\leq e^{-\frac{1}{2}2\bar{\alpha}^f x_1^*(1 - 2\delta) - \frac{1}{2}(\bar{\alpha}^f + \bar{\alpha})x_2^*(1 - 2\delta)}, \\ x_2^*(1 - 2\delta) &\leq e^{-\frac{1}{2}(\bar{\alpha}^f + \bar{\alpha})x_1^*(1 - 2\delta) - \frac{1}{2}2\bar{\alpha} x_2^*(1 - 2\delta)}. \end{aligned} \quad (27)$$

In particular, (27) is implied by

$$x_1^*(1-2\delta) \leq e^{-\frac{1}{2}2\alpha^f x_1^* - \delta x_1^*(1-2\delta) - \frac{1}{2}(\alpha^f + \alpha)x_2^* - \delta x_2^*(1-2\delta)} = x_1^* \cdot e^{-\delta x_1^*(1-2\delta) - \delta x_2^*(1-2\delta)}.$$

Since we trivially have $x_1^* \in (0, 1]$, we can cancel out x_1^* and take logarithm on both sides. We find that (27) is equivalent to $-\log(1-2\delta) \geq (x_1^* + x_2^*)\delta(1-2\delta)$. Since $x_1^* + x_2^* \in [0, 2]$, it is then sufficient to show that $\frac{-\log(1-2\delta)}{2\delta(1-2\delta)} \geq 1$, which holds for all $\delta \in (0, 1/2)$. The proof of $\bar{x}_2 \geq x_2^*(1-2\delta)$ is symmetric. \square

A.3.4. Proof of Theorem 7

Proof. We start by proving the convexity result in Theorem 7 (ii). Recall from (12) that

$$\begin{aligned} \xi(b_l, b_r) &= 2 - b_l y_L^f(\mathbf{b}) - b_r \left(1 - \hat{y}_H^f(\mathbf{b})\right) \\ &\quad - b_r \left(1 - \hat{y}_H^f(\mathbf{b})\right) \left(2b_l \alpha^f y_L^f(\mathbf{b}) + (1-b_l)(\alpha^f + \alpha)y_L^{nf}(\mathbf{b})\right) \\ &\quad - (1-b_l)y_L^{nf}(\mathbf{b}) - (1-b_r) \left(1 - \hat{y}_H^{nf}(\mathbf{b})\right) \\ &\quad - (1-b_r) \left(1 - \hat{y}_H^{nf}(\mathbf{b})\right) \left(b_l(\alpha^f + \alpha)y_L^f(\mathbf{b}) + 2(1-b_l)\alpha y_L^{nf}(\mathbf{b})\right), \end{aligned}$$

Since we are interested in the direction $(1, -1)$, for ease of notation we denote the sum of flexibility by B and replace b_r with $B - b_l$. Then, we can re-write $\xi(b_l, b_r) = \xi(b_l, B - b_l)$ as

$$\begin{aligned} &2 - b_l y_L^f(\mathbf{b}) - (B - b_l) \left(1 - \hat{y}_H^f(\mathbf{b})\right) \\ &- (B - b_l) \left(1 - \hat{y}_H^f(\mathbf{b})\right) \left(2b_l \alpha^f y_L^f(\mathbf{b}) + (1-b_l)(\alpha^f + \alpha)y_L^{nf}(\mathbf{b})\right) \\ &- (1-b_l)y_L^{nf}(\mathbf{b}) - (1-B+b_l) \left(1 - \hat{y}_H^{nf}(\mathbf{b})\right) \\ &- (1-B+b_l) \left(1 - \hat{y}_H^{nf}(\mathbf{b})\right) \left(b_l(\alpha^f + \alpha)y_L^f(\mathbf{b}) + 2(1-b_l)\alpha y_L^{nf}(\mathbf{b})\right). \end{aligned} \tag{28}$$

Then, the second-order derivative of $\xi(b_l, b_r)$ in the direction $(1, -1)$ is equal to $\frac{\partial^2 \xi(b_l, B - b_l)}{\partial b_l^2}$. We observe that

$$\xi(b_l, B - b_l) = 2 - b_l y_L^f(\mathbf{b}) - (B - b_l)e^{-b_1(b_l)}(1 + b_1(b_l)) - (1 - b_l)y_L^{nf}(\mathbf{b}) - (1 - B + b_l)e^{-b_2(b_l)}(1 + b_2(b_l)),$$

where

$$\begin{aligned} b_1(b_l) &= b_l \cdot 2\alpha^f \cdot y_L^f(\mathbf{b}) + (1 - b_l)(\alpha^f + \alpha)y_L^{nf}(\mathbf{b}), \\ b_2(b_l) &= b_l(\alpha^f + \alpha)y_L^f(\mathbf{b}) + (1 - b_l) \cdot 2\alpha \cdot y_L^{nf}(\mathbf{b}). \end{aligned}$$

Let

$$x_1(b_l, b_r) = e^{-b_l 2\alpha^f y_L^f(\mathbf{b}) - (1-b_l)(\alpha^f + \alpha)y_L^{nf}(\mathbf{b})} \text{ and } x_2(b_l, b_r) = e^{-b_l (\alpha^f + \alpha)y_L^f(\mathbf{b}) - (1-b_l) 2\alpha y_L^{nf}(\mathbf{b})} \tag{29}$$

For ease of notation we drop the dependency of x_1 and x_2 on \mathbf{b} . Then we simplify $\xi(b_l, B - b_l)$ into

$$\begin{aligned} \xi(b_l, B - b_l) &= 2 - b_l e^{-(B-b_l)2\alpha^f x_1 - (1-B+b_l)(\alpha^f + \alpha)x_2} - (B - b_l)x_1(1 - \log(x_1)) \\ &\quad - (1 - b_l)e^{-(B-b_l)(\alpha^f + \alpha)x_1 - (1-B+b_l)2\alpha x_2} - (1 - B + b_l)x_2(1 - \log(x_2)). \end{aligned}$$

By construction of x_1, x_2 and the definition of $y_L^f(q), y_L^{nf}(q)$, we have

$$x_1 = e^{-b_l 2\alpha^f e^{-(B-b_l)2\alpha^f} x_1 - (1-B+b_l)(\alpha^f + \alpha)x_2 - (1-b_l)(\alpha^f + \alpha)} e^{-(B-b_l)(\alpha^f + \alpha)x_1 - (1-B+b_l)2\alpha x_2}$$

$$x_2 = e^{-b_l(\alpha^f + \alpha)} e^{-(B-b_l)2\alpha^f x_1 - (1-B+b_l)(\alpha^f + \alpha)x_2 - (1-b_l)2\alpha} e^{-(B-b_l)(\alpha^f + \alpha)x_1 - (1-B+b_l)2\alpha x_2}.$$

For convenience we write

$$y_1 := e^{-(B-b_l)2\alpha^f x_1 - (1-B+b_l)(\alpha^f + \alpha)x_2} \text{ and } y_2 := e^{-(B-b_l)(\alpha^f + \alpha)x_1 - (1-B+b_l)2\alpha x_2}, \quad (30)$$

so that

$$x_1 = e^{-b_l 2\alpha^f y_1 - (1-b_l)(\alpha^f + \alpha)y_2}, x_2 = e^{-b_l(\alpha^f + \alpha)y_1 - (1-b_l)2\alpha y_2}.$$

Now, taking second order derivative of $\xi(b_l, B - b_l)$ with respect to b_l , we obtain

$$\begin{aligned} \frac{\partial^2 \xi(b_l, B - b_l)}{\partial b_l^2} = & -b_l \left(-2\alpha^f x_1 + (\alpha^f + \alpha)x_2 + (B - b_l)2\alpha^f \frac{\partial x_1}{\partial b_l} + (1 - B + b_l)(\alpha^f + \alpha) \frac{\partial x_2}{\partial b_l} \right)^2 y_1 \\ & - (1 - b_l) \left(-(\alpha^f + \alpha)x_1 + 2\alpha x_2 + (B - b_l)(\alpha^f + \alpha) \frac{\partial x_1}{\partial b_l} + (1 - B + b_l)2\alpha \frac{\partial x_2}{\partial b_l} \right)^2 y_2 \\ & + 2 \left(-2\alpha^f y_1 + (\alpha^f + \alpha)y_2 \right) x_1 + 2 \left((\alpha^f + \alpha)y_1 - 2\alpha y_2 \right) x_2 \\ & + (B - b_l)2 \left(2\alpha^f y_1 - (\alpha^f + \alpha)y_2 \right) \left(\frac{\partial x_1}{\partial b_l} \right) + (1 - B + b_l)2 \left((\alpha^f + \alpha)y_1 - 2\alpha y_2 \right) \left(\frac{\partial x_2}{\partial b_l} \right) \\ & + (B - b_l) \left(\frac{\partial x_1}{\partial b_l} \right)^2 / x_1 + (1 - B + b_l) \left(\frac{\partial x_2}{\partial b_l} \right)^2 / x_2. \end{aligned} \quad (31)$$

Moreover, by taking derivative of x_1 and x_2 with respect to b_l , we find that

$$\begin{aligned} \frac{\frac{\partial x_1}{\partial b_l}}{x_1} = & y_1 2\alpha^f b_l 2\alpha^f (B - b_l) \frac{\partial x_1}{\partial b_l} + y_2 (1 - b_l) (\alpha^f + \alpha) (B - b_l) (\alpha^f + \alpha) \frac{\partial x_1}{\partial b_l} + \\ & y_1 2\alpha^f b_l (\alpha^f + \alpha) (1 - B + b_l) \frac{\partial x_2}{\partial b_l} + y_2 (1 - b_l) (\alpha^f + \alpha) (1 - B + b_l) 2\alpha \frac{\partial x_2}{\partial b_l} + \\ & y_1 2\alpha^f b_l \left[(\alpha^f + \alpha)x_2 - 2\alpha^f x_1 \right] + y_2 (\alpha^f + \alpha) (1 - b_l) \left[2\alpha x_2 - (\alpha^f + \alpha)x_1 \right] - \\ & y_1 2\alpha^f + y_2 (\alpha^f + \alpha), \end{aligned} \quad (32)$$

and

$$\begin{aligned} \frac{\frac{\partial x_2}{\partial b_l}}{x_2} = & y_1 (\alpha^f + \alpha) b_l 2\alpha^f (B - b_l) \frac{\partial x_1}{\partial b_l} + y_2 (1 - b_l) 2\alpha (B - b_l) (\alpha^f + \alpha) \frac{\partial x_1}{\partial b_l} + \\ & y_1 (\alpha^f + \alpha) b_l (\alpha^f + \alpha) (1 - B + b_l) \frac{\partial x_2}{\partial b_l} + y_2 (1 - b_l) 2\alpha (1 - B + b_l) 2\alpha \frac{\partial x_2}{\partial b_l} + \\ & y_1 (\alpha^f + \alpha) b_l \left[(\alpha^f + \alpha)x_2 - 2\alpha^f x_1 \right] + y_2 2\alpha (1 - b_l) \left[2\alpha x_2 - (\alpha^f + \alpha)x_1 \right] - \\ & y_1 (\alpha^f + \alpha) + y_2 2\alpha. \end{aligned} \quad (33)$$

When $\mathbf{b} = (1/2, 1/2)$, $B = 1$ and $b_l = 1/2$. We find that $x_1 = y_1, x_2 = y_2$, which allows us to simplify (32) and (33) as:

$$\frac{\partial x_1}{\partial b_l} = \frac{2x_1 \left(\alpha^2 x_1 x_2 - 2\alpha^f \alpha x_1 x_2 - 2\alpha x_2 + (\alpha^f)^2 x_1 x_2 + 4\alpha^f x_1 - 2\alpha^f x_2 \right)}{\alpha^2 x_1 x_2 - 2\alpha \alpha^f x_1 x_2 + 4\alpha x_2 + (\alpha^f)^2 x_1 x_2 + 4\alpha^f x_1 - 4}, \quad (34)$$

$$\frac{\partial x_2}{\partial b_l} = -\frac{2x_2 \left(\alpha^2 x_1 x_2 - 2\alpha^f \alpha x_1 x_2 - 2\alpha x_1 + (\alpha^f)^2 x_1 x_2 + 4\alpha x_2 - 2\alpha^f x_1 \right)}{\alpha^2 x_1 x_2 - 2\alpha \alpha^f x_1 x_2 + 4\alpha x_2 + (\alpha^f)^2 x_1 x_2 + 4\alpha^f x_1 - 4}. \quad (35)$$

Then, plugging $x_1 = y_1, x_2 = y_2, B = 1$ and $b_l = 1/2$ into (31), we obtain

$$\begin{aligned} \frac{\partial^2 \xi(b_l, B - b_l)}{\partial b_l^2} \Bigg|_{B=1, b_l=\frac{1}{2}} &= -\frac{1}{2} \left(-2\alpha^f x_1 + (\alpha^f + \alpha) x_2 + \frac{1}{2} 2\alpha^f \frac{\partial x_1}{\partial b_l} + \frac{1}{2} (\alpha^f + \alpha) \frac{\partial x_2}{\partial b_l} \right)^2 x_1 \\ &\quad - \frac{1}{2} \left(-(\alpha^f + \alpha) x_1 + 2\alpha x_2 + \frac{1}{2} (\alpha^f + \alpha) \frac{\partial x_1}{\partial b_l} + \frac{1}{2} 2\alpha \frac{\partial x_2}{\partial b_l} \right)^2 x_2 \\ &\quad + 2 \left(-2\alpha^f x_1 + (\alpha^f + \alpha) x_2 \right) x_1 + 2 \left((\alpha^f + \alpha) x_1 - 2\alpha x_2 \right) x_2 \\ &\quad + \left(2\alpha^f x_1 - (\alpha^f + \alpha) x_2 \right) \left(\frac{\partial x_1}{\partial b_l} \right) + \left((\alpha^f + \alpha) x_1 - 2\alpha x_2 \right) \left(\frac{\partial x_2}{\partial b_l} \right) \\ &\quad + \frac{1}{2} \left(\frac{\partial x_1}{\partial b_l} \right)^2 / x_1 + \frac{1}{2} \left(\frac{\partial x_2}{\partial b_l} \right)^2 / x_2. \end{aligned}$$

By plugging the values of $\frac{\partial x_1}{\partial b_l}$ and $\frac{\partial x_2}{\partial b_l}$ from (34) and (35) into the above, we find that

$$\begin{aligned} \frac{\partial^2 \xi(b_l, B - b_l)}{\partial b_l^2} \Bigg|_{B=1, b_l=\frac{1}{2}} &= \frac{1}{\alpha^2 x_1 x_2 - 2\alpha \alpha^f x_1 x_2 + 4\alpha x_2 + (\alpha^f)^2 x_1 x_2 + 4\alpha^f x_1 - 4} \\ &\quad (4\alpha^2 x_1^2 x_2 + 4\alpha^2 x_1 x_2^2 - 8\alpha \alpha^f x_1^2 x_2 - 8\alpha \alpha^f x_1 x_2^2 - 16\alpha x_1 x_2 \\ &\quad + 16\alpha x_2^2 + 4(\alpha^f)^2 x_1^2 x_2 + 4(\alpha^f)^2 x_1 x_2^2 + 16\alpha^f x_1^2 - 16\alpha^f x_1 x_2) \\ &= \frac{(\alpha^f - \alpha)^2 4x_1 x_2 (x_1 + x_2) - 16(x_2 - x_1)(\alpha^f x_1 - \alpha x_2)}{(\alpha^f - \alpha)^2 x_1 x_2 + 4(\alpha x_2 + \alpha^f x_1 - 1)}. \end{aligned} \quad (36)$$

Recall that we have

$$x_1 = e^{-\alpha^f x_1 - 1/2(\alpha^f + \alpha) x_2}, x_2 = e^{-1/2(\alpha^f + \alpha) x_1 - \alpha x_2} \quad (37)$$

when $B = 1, b_l = 1/2$. This allows us to solve x_1 and x_2 and determine the size of convexity numerically. In particular, we know from (25) that we can provide bounds $x_1^{lb}, x_1^{ub}, x_2^{lb}, x_2^{ub}$ for any $(\bar{\alpha}^f, \bar{\alpha}) \in \mathcal{I}(\alpha, \alpha^f, \delta)$ where $10^{-4} < \bar{\alpha} < \bar{\alpha}^f$ and $\bar{\alpha}^f + \bar{\alpha} < e$. Thus, we can lower bound (36) for any $(\bar{\alpha}^f, \bar{\alpha}) \in \mathcal{I}(\alpha, \alpha^f, \delta)$ as:

$$\begin{aligned} &\frac{(\bar{\alpha}^f - \bar{\alpha})^2 4\bar{x}_1 \bar{x}_2 (\bar{x}_1 + \bar{x}_2) - 16(\bar{x}_2 - \bar{x}_1)(\bar{\alpha}^f \bar{x}_1 - \bar{\alpha} \bar{x}_2)}{(\bar{\alpha}^f - \bar{\alpha})^2 \bar{x}_1 \bar{x}_2 + 4(\bar{\alpha} \bar{x}_2 + \bar{\alpha}^f \bar{x}_1 - 1)} \\ &\geq \frac{-(\alpha^f - \alpha + \delta)^2 4x_1^{ub} x_2^{ub} (x_1^{ub} + x_2^{ub}) + 16 \max(0, x_2^{lb} - x_1^{ub}) \alpha^f x_1^{lb} - 16(x_2^{ub} - x_1^{lb})(\alpha + \delta)x_2^{ub}}{-\left(\max(\alpha^f - \alpha - \delta, 0)\right)^2 x_1^{lb} x_2^{lb} + 4[1 - \alpha x_2^{lb} - \alpha^f x_1^{lb}]} \end{aligned} \quad (38)$$

If this lower bound exceeds 0, we know that $\xi(b_l, b_r)$ is strictly convex in the direction $(1, -1)$ at $\mathbf{b} = (1/2, 1/2)$ for any $(\bar{\alpha}^f, \bar{\alpha}) \in \mathcal{I}(\alpha, \alpha^f, \delta)$. At $\mathbf{b} = (1/2, 1/2)$, we find by symmetry that $\xi(b_l, b_r) = \hat{\xi}(b_l, b_r)$,

$$\frac{\partial \xi(b_l, B - b_l)}{\partial b_l} \Big|_{B=1, b_l=\frac{1}{2}} = \frac{\partial \hat{\xi}(b_l, B - b_l)}{\partial b_l} \Big|_{B=1, b_l=\frac{1}{2}} = 0 \text{ and } \frac{\partial^2 \xi(b_l, B - b_l)}{\partial b_l^2} \Big|_{B=1, b_l=\frac{1}{2}} = \frac{\partial^2 \hat{\xi}(b_l, B - b_l)}{\partial b_l^2} \Big|_{B=1, b_l=\frac{1}{2}}.$$

Thus, at $\mathbf{b} = (1/2, 1/2)$, by Claim 5 below we know that to show $\nabla_{(1,-1)}^2 \mu^{\text{KS}}(b_l, b_r) > 0$ it suffices to verify strict local convexity for $\xi(b_l, b_r)$ in the direction $(1, -1)$. That is, we verify $\frac{\partial^2 \xi(b_l, B - b_l)}{\partial b_l^2} \Big|_{B=1, b_l=\frac{1}{2}} > 0$.

CLAIM 5. *If for some $\mathbf{b}' \in (0, 1)^2$ and direction $v \in \mathbb{R}^2$, $\hat{\xi}(\mathbf{b}') = \hat{\xi}(\mathbf{b}')$, $\nabla_v \hat{\xi}(\mathbf{b}') = \nabla_v \hat{\xi}(\mathbf{b}')$ and $\nabla_v^2 \hat{\xi}(\mathbf{b}') = \nabla_v^2 \hat{\xi}(\mathbf{b}')$, then $\nabla_v^2 \mu^{\text{KS}}(\mathbf{b}') = \nabla_v^2 \hat{\xi}(\mathbf{b}') = \nabla_v^2 \hat{\xi}(\mathbf{b}')$.*

In Theorem7.ipynb,²⁸ we compute the lower bound of $\frac{\partial^2 \xi(b_l, B - b_l)}{\partial b_l^2} \Big|_{B=1, b_l=\frac{1}{2}}$ in (38) for $\alpha^f, \alpha = \delta, 2\delta, \dots, e$ where $\alpha^f + \alpha < e$. We find that by taking $\delta = 0.01, 0.005, 0.0025$ and 0.001 we are able to verify strict local convexity of $\mu^{\text{KS}}(1/2, 1/2)$ in the direction $(1, -1)$ in the respective red regions in Fig. 21.

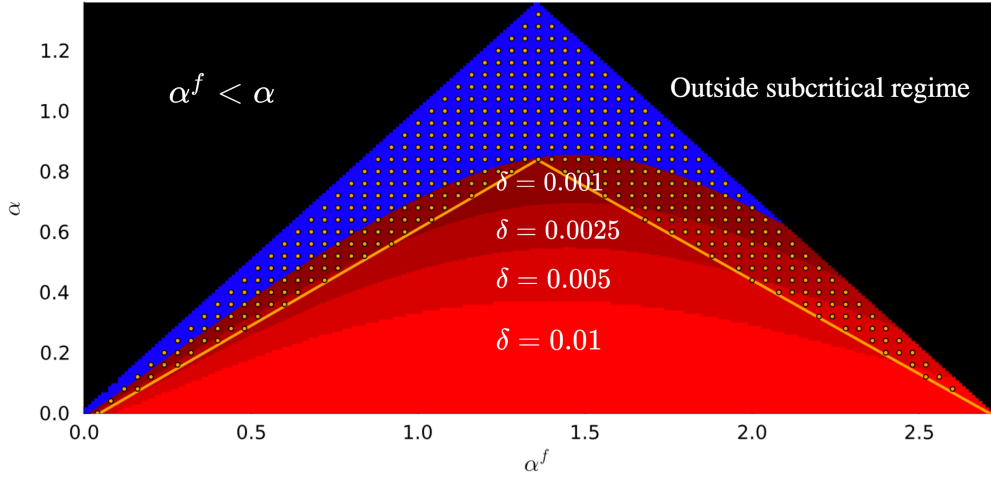


Figure 21 In the figure we denote the boundary where $10^{-4} < \alpha < 0.64\alpha^f - 0.03$ and $0.62\alpha^f + \alpha < 1.68$ by the orange lines, and the area of subcritical regime where convexity and concavity properties are verified is displayed in varying shades of red below this boundary. The growth in the validation area with respect to δ is depicted through different red gradients. The black zone denotes parameters outside the feasible or subcritical regime. Although the convexity and concavity properties cannot be confirmed in the blue region when $\delta = 0.001$, by taking $\delta = 0$ we verify the properties for a wide range of (α^f, α) values highlighted as orange dots.

We next prove the concavity result in Theorem 7 (i). We again focus on $\xi(b_l, b_r)$, and the second-order derivative of $\xi(b_l, b_r)$ in the direction $(0, 1)$ is equal to $\frac{\partial^2 \xi(b_l, B - b_l)}{\partial B^2}$.

²⁸The computer-aided proof can be found at <https://bit.ly/3P1f6oi>.

Based on x_1, x_2, y_1, y_2 constructed in (29) and (30), we obtain

$$\begin{aligned} \frac{\partial^2 \xi(b_l, B - b_l)}{\partial B^2} = & -b_l \left(2\alpha^f x_1 - (\alpha^f + \alpha)x_2 + (B - b_l)2\alpha^f \frac{\partial x_1}{\partial B} + (1 - B + b_l)(\alpha^f + \alpha) \frac{\partial x_2}{\partial B} \right)^2 y_1 \\ & - (1 - b_l) \left((\alpha^f + \alpha)x_1 - 2\alpha x_2 + (B - b_l)(\alpha^f + \alpha) \frac{\partial x_1}{\partial B} + (1 - B + b_l)2\alpha \frac{\partial x_2}{\partial B} \right)^2 y_2 \\ & + (B - b_l) \left(\frac{\partial x_1}{\partial B} \right)^2 / x_1 + (1 - B + b_l) \left(\frac{\partial x_2}{\partial B} \right)^2 / x_2. \end{aligned} \quad (39)$$

Moreover, by taking derivative of x_1 and x_2 with respect to B , we find that

$$\begin{aligned} \frac{\frac{\partial x_1}{\partial B}}{x_1} = & y_1 2\alpha^f b_l 2\alpha^f (B - b_l) \frac{\partial x_1}{\partial B} + y_2 (1 - b_l) (\alpha^f + \alpha) (B - b_l) (\alpha^f + \alpha) \frac{\partial x_1}{\partial B} + \\ & y_1 2\alpha^f b_l (\alpha^f + \alpha) (1 - B + b_l) \frac{\partial x_2}{\partial B} + y_2 (1 - b_l) (\alpha^f + \alpha) (1 - B + b_l) 2\alpha \frac{\partial x_2}{\partial B} - \\ & y_1 2\alpha^f b_l \left[(\alpha^f + \alpha)x_2 - 2\alpha^f x_1 \right] - y_2 (\alpha^f + \alpha) (1 - b_l) \left[2\alpha x_2 - (\alpha^f + \alpha)x_1 \right], \end{aligned}$$

and

$$\begin{aligned} \frac{\frac{\partial x_2}{\partial B}}{x_2} = & y_1 (\alpha^f + \alpha) b_l 2\alpha^f (B - b_l) \frac{\partial x_1}{\partial B} + y_2 (1 - b_l) 2\alpha (B - b_l) (\alpha^f + \alpha) \frac{\partial x_1}{\partial B} + \\ & y_1 (\alpha^f + \alpha) b_l (\alpha^f + \alpha) (1 - B + b_l) \frac{\partial x_2}{\partial B} + y_2 (1 - b_l) 2\alpha (1 - B + b_l) 2\alpha \frac{\partial x_2}{\partial B} - \\ & y_1 (\alpha^f + \alpha) b_l \left[(\alpha^f + \alpha)x_2 - 2\alpha^f x_1 \right] - y_2 2\alpha (1 - b_l) \left[2\alpha x_2 - (\alpha^f + \alpha)x_1 \right]. \end{aligned}$$

When $B = 1$ and $b_l = 1/2$, we have $x_1 = y_1, x_2 = y_2$. Applying these observations to simplify (39), we obtain

$$\begin{aligned} \left. \frac{\partial^2 \xi(b_l, B - b_l)}{\partial B^2} \right|_{a=1, q=\frac{1}{2}} = & \frac{1}{-\left(x_1 x_2 (\alpha^f - \alpha)^2\right)^2 + 8x_1 x_2 (\alpha^f + \alpha)^2 + 16\left(\alpha^2 x_2^2 + (\alpha^f)^2 x_1^2 - 1\right)} \cdot \\ & (-2(x_1 + x_2) \left(x_1 x_2 (\alpha^f - \alpha)^2\right)^2 - 16(x_1 + x_2) x_1 x_2 \alpha^f \alpha \\ & + 8\left(\alpha^f\right)^2 x_1 (x_2^2 - 3x_1 x_2 + 4x_1^2) + 8\alpha^2 x_2 (x_1^2 - 3x_1 x_2 + 4x_2^2)). \end{aligned} \quad (40)$$

Again, we know from (25) that we can provide bounds $x_1^{lb}, x_1^{ub}, x_2^{lb}, x_2^{ub}$ for any $(\bar{\alpha}^f, \bar{\alpha}) \in \mathcal{I}(\alpha, \alpha^f, \delta)$ where $\bar{\alpha}^f + \bar{\alpha} < e$. Thus, we can upper bound (40) for any $(\bar{\alpha}^f, \bar{\alpha}) \in \mathcal{I}(\alpha, \alpha^f, \delta)$ as:

$$\begin{aligned} & \frac{1}{-\left[x_1^{ub}x_2^{ub}(\alpha^f - \alpha + \delta)^2\right]^2 + 8(\alpha^f + \alpha)^2x_1^{lb}x_2^{lb} + 16\alpha^2(x_2^{lb})^2 + 16(\alpha^f)^2(x_1^{lb})^2 - 16} \\ & \cdot \left(-2\left(x_1^{lb} + x_2^{lb}\right)\left[x_1^{lb}x_2^{lb}\left(\max(0, \alpha^f - \alpha - \delta)\right)^2\right]^2 - 16(x_1^{lb} + x_2^{lb})x_1^{lb}x_2^{lb}\alpha^f\alpha \right. \\ & + 8(\alpha^f + \delta)^2\left(x_1^{ub}\left(x_2^{ub}\right)^2 + 4\left(x_1^{ub}\right)^3\right) + 8(\alpha + \delta)^2\left(x_2^{ub}\left(x_1^{ub}\right)^2 + 4\left(x_2^{ub}\right)^3\right) \\ & \left. - 24\left(\alpha^f\right)^2\left(x_1^{lb}\right)^2x_2^{lb} - 24\alpha^2\left(x_2^{lb}\right)^2x_1^{lb} \right). \end{aligned} \quad (41)$$

If this upper bound is strictly below 0, we know that $\xi(b_l, b_r)$ is strictly concave in the direction $(0, 1)$ at $\mathbf{b} = (1/2, 1/2)$ for any $(\bar{\alpha}^f, \bar{\alpha}) \in \mathcal{I}(\alpha, \alpha^f, \delta)$. By symmetry at $\mathbf{b} = (1/2, 1/2)$ we find that $\xi(b_l, b_r) = \hat{\xi}(b_l, b_r)$,

$$\frac{\partial \xi(b_l, B - b_l)}{\partial B} \Big|_{B=1, b_l=\frac{1}{2}} = \frac{\partial \hat{\xi}(b_l, B - b_l)}{\partial B} \Big|_{B=1, b_l=\frac{1}{2}} \text{ and } \frac{\partial^2 \xi(b_l, B - b_l)}{\partial B^2} \Big|_{B=1, b_l=\frac{1}{2}} = \frac{\partial^2 \hat{\xi}(b_l, B - b_l)}{\partial B^2} \Big|_{B=1, b_l=\frac{1}{2}}.$$

Thus, at $\mathbf{b} = (1/2, 1/2)$, by Claim 5 we know it suffices to verify strict local concavity for $\xi(b_l, b_r)$ in the direction $(0, 1)$. That is, we verify $\frac{\partial^2 \xi(b_l, B - b_l)}{\partial B^2} \Big|_{B=1, b_l=\frac{1}{2}} < 0$.

In Theorem7.ipynb,²⁹ we compute the upper bound of $\frac{\partial^2 \xi(b_l, B - b_l)}{\partial B^2} \Big|_{a=1, q=\frac{1}{2}}$ in (41) for $\alpha^f, \alpha = 10^{-4}, \delta, 2\delta, \dots, e$ where $\alpha^f + \alpha < e$. We find that taking $\delta = 0.01$ is sufficient for verifying (41) < 0 for all α^f and α such that $10^{-4} < \alpha < \alpha^f$ and $\alpha^f + \alpha < e$. The concavity in the direction $(1, 0)$ is exactly symmetric.

□

Proof of Claim 5 By definition, we need to show that

$$\nabla_{\mathbf{v}}^2 \mu^{\text{KS}}(\mathbf{b}') = \lim_{h \rightarrow 0} \frac{\mu^{\text{KS}}(\mathbf{b}' + \mathbf{v}h) - 2\mu^{\text{KS}}(\mathbf{b}') + \mu^{\text{KS}}(\mathbf{b}' - \mathbf{v}h)}{h^2}$$

exists and is equal to the claimed value. By Taylor series expansion, we know that for $h \in \mathbb{R}$,

$$\begin{aligned} \xi(\mathbf{b}' + \mathbf{v}h) &= \xi(\mathbf{b}') + h \cdot \nabla_{\mathbf{v}}\xi(\mathbf{b}') + h^2 \cdot \nabla_{\mathbf{v}}^2\xi(\mathbf{b}') + o(h^2), \\ \hat{\xi}(\mathbf{b}' + \mathbf{v}h) &= \hat{\xi}(\mathbf{b}') + h \cdot \nabla_{\mathbf{v}}\hat{\xi}(\mathbf{b}') + h^2 \cdot \nabla_{\mathbf{v}}^2\hat{\xi}(\mathbf{b}') + o(h^2), \\ \xi(\mathbf{b}' - \mathbf{v}h) &= \xi(\mathbf{b}') - h \cdot \nabla_{\mathbf{v}}\xi(\mathbf{b}') - h^2 \cdot \nabla_{\mathbf{v}}^2\xi(\mathbf{b}') - o(h^2), \\ \hat{\xi}(\mathbf{b}' - \mathbf{v}h) &= \hat{\xi}(\mathbf{b}') - h \cdot \nabla_{\mathbf{v}}\hat{\xi}(\mathbf{b}') - h^2 \cdot \nabla_{\mathbf{v}}^2\hat{\xi}(\mathbf{b}') - o(h^2). \end{aligned}$$

²⁹The computer-aided proof can be found at <https://bit.ly/3P1f6oi>.

In particular, since $\hat{\xi}(\mathbf{b}') = \hat{\xi}(\mathbf{b}')$, $\nabla_v \hat{\xi}(\mathbf{b}') = \nabla_v \hat{\xi}(\mathbf{b}')$ and $\nabla_v^2 \hat{\xi}(\mathbf{b}') = \nabla_v^2 \hat{\xi}(\mathbf{b}')$, from the above we know that

$$\xi(\mathbf{b}' + \mathbf{v}h) - \hat{\xi}(\mathbf{b}' + \mathbf{v}h) = o(h^2) \text{ and } \xi(\mathbf{b}' - \mathbf{v}h) - \hat{\xi}(\mathbf{b}' - \mathbf{v}h) = o(h^2).$$

Thus,

$$\begin{aligned} \nabla_{\mathbf{v}}^2 \mu^{\text{KS}}(\mathbf{b}') &= \lim_{h \rightarrow 0} \frac{\mu^{\text{KS}}(\mathbf{b}' + \mathbf{v}h) - 2\mu^{\text{KS}}(\mathbf{b}') + \mu^{\text{KS}}(\mathbf{b}' - \mathbf{v}h)}{h^2} \\ &= \lim_{h \rightarrow 0} \frac{\min(\xi(\mathbf{b}' + \mathbf{v}h), \hat{\xi}(\mathbf{b}' + \mathbf{v}h)) - 2\min(\xi(\mathbf{b}'), \hat{\xi}(\mathbf{b}')) + \min(\xi(\mathbf{b}' - \mathbf{v}h), \hat{\xi}(\mathbf{b}' - \mathbf{v}h))}{h^2} \\ &= \lim_{h \rightarrow 0} \frac{\xi(\mathbf{b}' + \mathbf{v}h) - 2\xi(\mathbf{b}') + \xi(\mathbf{b}' - \mathbf{v}h) + o(h^2)}{h^2} \\ &= \nabla_{\mathbf{v}}^2 \xi(\mathbf{b}') = \nabla_{\mathbf{v}}^2 \hat{\xi}(\mathbf{b}'). \end{aligned}$$

□

A.3.5. Proofs of the Auxiliary Results in Appendix A.3.2

Proof of Proposition 1 Theorem 8 in Karp and Sipser (1981) (1) - (4) establishes the validity of the statements in Proposition 1 (i) - (iv) for a general graph $G = (V, E)$. Since bipartite graphs are a subset of such general graphs, these results immediately extend.

For Proposition 1 (v), to determine $|\Psi_1^l|$ and $|\Psi_1^r|$, we start by finding m_1 . By (iii), every edge in M_1 is connected to at least one target. By (ii), if an edge in M_1 is connected to two targets u and v , then $v \otimes u$ and $u \otimes v$. Hence,

$$m_1 = |M_1| \leq \left| \{v \in V_l \mid v \text{ is a target}\} \right| + \left| \{v \in V_r \mid v \text{ is a target}\} \right| - \left| \{(v, u) \mid v \otimes u \text{ and } u \otimes v\} \right|.$$

The equality follows from (ii) because every target is connected to an edge in M_1 .

By Theorem 9 (4) in Karp and Sipser (1981), a node v appears in a derivation if and only if it is a target or a loser or both. Furthermore, v is both a target and a loser if and only if there exists a unique u such that $v \otimes u$ and $u \otimes v$. Hence, the number of nodes in V_l that appear in a derivation is given by

$$\left| \{v \in V_l \mid v \text{ is a target}\} \right| + \left| \{v \in V_l \mid v \text{ is a loser}\} \right| - \left| \{(v, u) \mid v \otimes u \text{ and } u \otimes v\} \right|.$$

Then, we can find Ψ_1^l as the set of nodes in V_l that appear in a derivation but do not belong to M_1^l . Specifically,

$$\begin{aligned} |\Psi_1^l| &= \left| \{v \in V_l \mid v \text{ is a target}\} \right| + \left| \{v \in V_l \mid v \text{ is a loser}\} \right| - \left| \{(v, u) \mid v \otimes u \text{ and } u \otimes v\} \right| \\ &\quad - \left(\left| \{v \in V_l \mid v \text{ is a target}\} \right| + \left| \{v \in V_r \mid v \text{ is a target}\} \right| - \left| \{(v, u) \mid v \otimes u \text{ and } u \otimes v\} \right| \right) \\ &= \left| \{v \in V_l \mid v \text{ is a loser}\} \right| - \left| \{v \in V_r \mid v \text{ is a target}\} \right|. \end{aligned}$$

The computation of $|\Psi_1^r|$ is symmetric. Since $\psi_1 = \max \{|\Psi_1^l|, |\Psi_1^r|\}$ by definition, we obtain Proposition 1 (v). □

Proof of Lemma 6 We start from the leaf of a random tree, i.e., $d = 1$, and iteratively trace back to the root of the tree as d scales large. For a flexible node $u \in S_l$, the number of its children follows a Binomial distribution $\text{Binom}(n, (1 + b_r)p_n^f + (1 - b_r)p_n)$. Thus, the probability for it to have k children is given by

$$z_k^f(\mathbf{b}) := \binom{n}{k} \left((1 + b_r)p_n^f + (1 - b_r)p_n \right)^k \left(1 - (1 + b_r)p_n^f - (1 - b_r)p_n \right)^{n-k} \forall k.$$

Moreover, since the probability that u connects with a flexible node is $2p_n^f$ and the probability that it connects with a regular node is $p_n^f + p_n$, by Bayes' Theorem we have

$$\begin{aligned} \mathbb{P}[u' \text{ is flexible} | u \text{ is flexible}, u' \text{ is a child of } u] &= \frac{b_r \cdot 2p_n^f}{b_r \cdot 2p_n^f + (1 - b_r) \cdot (p_n^f + p_n)} \\ &= \frac{b_r \cdot 2p_n^f}{(1 + b_r)p_n^f + (1 - b_r)p_n} \end{aligned}$$

and similarly

$$\mathbb{P}[u' \text{ is regular} | u \text{ is flexible}, u' \text{ is a child of } u] = \frac{(1 - b_r) \cdot (p_n^f + p_n)}{(1 + b_r)p_n^f + (1 - b_r)p_n}.$$

By definition, u is in L if all of its children are in H , including when it has no children. Thus,

$$\begin{aligned} y_L^f(\mathbf{b}, d) &= \sum_{k=0}^n z_k^f(\mathbf{b}) \cdot \left(\frac{2b_r p_n^f}{(1 + b_r)p_n^f + (1 - b_r)p_n} \hat{y}_H^f(\mathbf{b}, d-1) + \frac{(1 - b_r) \cdot (p_n^f + p_n)}{(1 + b_r)p_n^f + (1 - b_r)p_n} \hat{y}_H^{nf}(\mathbf{b}, d-1) \right)^k \\ &= \sum_{k=0}^n \binom{n}{k} \left((1 + b_r)p_n^f + (1 - b_r)p_n \right)^k \left(1 - (1 + b_r)p_n^f - (1 - b_r)p_n \right)^{n-k} \\ &\quad \cdot \left(\frac{2b_r p_n^f}{(1 + b_r)p_n^f + (1 - b_r)p_n} \hat{y}_H^f(\mathbf{b}, d-1) + \frac{(1 - b_r) \cdot (p_n^f + p_n)}{(1 + b_r)p_n^f + (1 - b_r)p_n} \hat{y}_H^{nf}(\mathbf{b}, d-1) \right)^k \\ &= \sum_{k=1}^n \binom{n}{k} \left(1 - (1 + b_r)p_n^f - (1 - b_r)p_n \right)^{n-k} \cdot \left(2b_r p_n^f \hat{y}_H^f(\mathbf{b}, d-1) + (1 - b_r) \cdot (p_n^f + p_n) \hat{y}_H^{nf}(\mathbf{b}, d-1) \right)^k \\ &= \left[2b_r p_n^f \hat{y}_H^f(\mathbf{b}, d-1) + (1 - b_r) \cdot (p_n^f + p_n) \hat{y}_H^{nf}(\mathbf{b}, d-1) + 1 - (1 + b_r)p_n^f - (1 - b_r)p_n \right]^n \\ &= \left[1 - 2b_r p_n^f \left(1 - \hat{y}_H^f(\mathbf{b}, d-1) \right) - (1 - b_r) \cdot (p_n^f + p_n) \left(1 - \hat{y}_H^{nf}(\mathbf{b}, d-1) \right) \right]^n \\ &= \left[1 - \frac{2b_r \alpha^f \left(1 - \hat{y}_H^f(\mathbf{b}, d-1) \right) - (1 - b_r) \cdot (\alpha^f + \alpha) \left(1 - \hat{y}_H^{nf}(\mathbf{b}, d-1) \right)}{n} \right]^n \\ &= e^{-2b_r \alpha^f \left(1 - \hat{y}_H^f(\mathbf{b}, d-1) \right) - (1 - b_r) \cdot (\alpha^f + \alpha) \left(1 - \hat{y}_H^{nf}(\mathbf{b}, d-1) \right)} \text{ as } n \rightarrow \infty. \end{aligned}$$

Notice that the fourth equality is an application of the Binomial Theorem, and the last equality follows from

$$\lim_{n \rightarrow \infty} \left(1 - \frac{x}{n} \right)^n = e^{-x}, \forall x.$$

The expressions for $y_L^{nf}(\mathbf{b}, d)$, $\hat{y}_L^f(\mathbf{b}, d)$ and $\hat{y}_L^{nf}(\mathbf{b}, d)$ can be derived in a similar fashion.

Next, by definition, u is in H if it has at least one child in L . Thus,

$$\begin{aligned}
y_H^f(\mathbf{b}, d) &= 1 - \sum_{k=0}^n z_k^f(\mathbf{b}) \cdot \left(\frac{2b_r p_n^f}{(1+b_r)p_n^f + (1-b_r)p_n} (1 - \hat{y}_L^f(\mathbf{b}, d-1)) + \frac{(1-b_r) \cdot (p_n^f + p_n)}{(1+b_r)p_n^f + (1-b_r)p_n} (1 - \hat{y}_L^{nf}(\mathbf{b}, d-1)) \right. \\
&= 1 - \sum_{k=0}^n \binom{n}{k} \left((1+b_r)p_n^f + (1-b_r)p_n \right)^k \left(1 - (1+b_r)p_n^f - (1-b_r)p_n \right)^{n-k} \\
&\quad \cdot \left(\frac{2b_r p_n^f}{(1+b_r)p_n^f + (1-b_r)p_n} (1 - \hat{y}_L^f(\mathbf{b}, d-1)) + \frac{(1-b_r) \cdot (p_n^f + p_n)}{(1+b_r)p_n^f + (1-b_r)p_n} (1 - \hat{y}_L^{nf}(\mathbf{b}, d-1)) \right)^k \\
&= 1 - \sum_{k=1}^n \binom{n}{k} \left(1 - (1+b_r)p_n^f - (1-b_r)p_n \right)^{n-k} \\
&\quad \cdot \left(2b_r p_n^f (1 - \hat{y}_L^f(\mathbf{b}, d-1)) + (1-b_r) \cdot (p_n^f + p_n) (1 - \hat{y}_L^{nf}(\mathbf{b}, d-1)) \right)^k \\
&= 1 - \left[2b_r p_n^f (1 - \hat{y}_L^f(\mathbf{b}, d-1)) + (1-b_r) \cdot (p_n^f + p_n) (1 - \hat{y}_L^{nf}(\mathbf{b}, d-1)) + 1 - (1+b_r)p_n^f - (1-b_r)p_n \right]^n \\
&= 1 - \left[1 - 2b_r p_n^f \hat{y}_L^f(\mathbf{b}, d-1) - (1-b_r) \cdot (p_n^f + p_n) \hat{y}_L^{nf}(\mathbf{b}, d-1) \right]^n \\
&= 1 - \left[1 - \frac{2b_r \alpha^f \hat{y}_L^f(\mathbf{b}, d-1) - (1-b_r) \cdot (\alpha^f + \alpha) \hat{y}_L^{nf}(\mathbf{b}, d-1)}{n} \right]^n \\
&= 1 - e^{-2b_r \alpha^f \hat{y}_L^f(\mathbf{b}, d-1) - (1-b_r) \cdot (\alpha^f + \alpha) \hat{y}_L^{nf}(\mathbf{b}, d-1)} \text{ as } n \rightarrow \infty.
\end{aligned}$$

The expressions for $y_H^{nf}(\mathbf{b}, d)$, $\hat{y}_H^f(\mathbf{b}, d)$ and $\hat{y}_H^{nf}(\mathbf{b}, d)$ can be derived in a similar fashion. Since all leaf nodes are in L , we have

$$y_H^f(\mathbf{b}, 1) = y_H^{nf}(\mathbf{b}, 1) = \hat{y}_H^f(\mathbf{b}, 1) = \hat{y}_H^{nf}(\mathbf{b}, 1) = 0.$$

Moreover, since $y_L^f(\mathbf{b}, d)$, $y_L^{nf}(\mathbf{b}, d)$, $\hat{y}_L^f(\mathbf{b}, d)$, $\hat{y}_L^{nf}(\mathbf{b}, d)$, $y_H^f(\mathbf{b}, d)$, $y_H^{nf}(\mathbf{b}, d)$, $\hat{y}_H^f(\mathbf{b}, d)$, $\hat{y}_H^{nf}(\mathbf{b}, d)$ are all bounded increasing sequences with respect to d , these sequences converge as $d \rightarrow \infty$ and \mathbf{y} is given by the smallest solution to (11). \square

Proof of Lemma 5 Lemma 3.1 and 3.2 in Karp and Sipser (1981) respectively establish the statements in Lemma 5(i) and (ii) for a general tree rooted at vertex v . As \bar{G} under consideration is also rooted at vertex v , these results immediately extend. \square

Proof of Lemma 7 By Lemma 5 (i), we have

$$\mathbb{P}[v \text{ is a target} | v \text{ is a flexible node in } S_l] = \mathbb{P}[v \in H | v \text{ is a flexible node in } S_l] = y_H^f(\mathbf{b}).$$

To find the probability for a flexible node v in S_l to be a loser, we need to sum the probability that v is in L and that v has exactly 1 child which is not in H . The former is simply given by $y_L^f(\mathbf{b})$, while the latter can be computed as

$$\mathbb{P}[v \text{ has exactly 1 child that is in } H | v \text{ is a flexible node in } S_l]$$

$$\begin{aligned}
&= \sum_{k=0}^n z_k^f(\mathbf{b}) \cdot k \cdot \left(\frac{2b_r p_n^f}{(1+b_r)p_n^f + (1-b_r)p_n} \hat{y}_H^f(\mathbf{b}) + \frac{(1-b_r) \cdot (p_n^f + p_n)}{(1+b_r)p_n^f + (1-b_r)p_n} \hat{y}_H^{nf}(\mathbf{b}) \right)^{k-1} \\
&\quad \cdot \left(1 - \frac{2b_r p_n^f}{(1+b_r)p_n^f + (1-b_r)p_n} \hat{y}_H^f(\mathbf{b}) - \frac{(1-b_r) \cdot (p_n^f + p_n)}{(1+b_r)p_n^f + (1-b_r)p_n} \hat{y}_H^{nf}(\mathbf{b}) \right) \\
&= \sum_{k=0}^n \binom{n}{k} \left((1+b_r)p_n^f + (1-b_r)p_n \right)^k \left(1 - (1+b_r)p_n^f - (1-b_r)p_n \right)^{n-k} \\
&\quad \cdot k \cdot \left(\frac{2b_r p_n^f}{(1+b_r)p_n^f + (1-b_r)p_n} \hat{y}_H^f(\mathbf{b}) + \frac{(1-b_r) \cdot (p_n^f + p_n)}{(1+b_r)p_n^f + (1-b_r)p_n} \hat{y}_H^{nf}(\mathbf{b}) \right)^{k-1} \\
&\quad \cdot \left(1 - \frac{2b_r p_n^f}{(1+b_r)p_n^f + (1-b_r)p_n} \hat{y}_H^f(\mathbf{b}) - \frac{(1-b_r) \cdot (p_n^f + p_n)}{(1+b_r)p_n^f + (1-b_r)p_n} \hat{y}_H^{nf}(\mathbf{b}) \right) \\
&= \sum_{k=1}^n n \binom{n-1}{k-1} \left((1+b_r)p_n^f + (1-b_r)p_n \right)^{k-1} \left(1 - (1+b_r)p_n^f - (1-b_r)p_n \right)^{n-k} \\
&\quad \cdot \left(\frac{2b_r p_n^f}{(1+b_r)p_n^f + (1-b_r)p_n} \hat{y}_H^f(\mathbf{b}) + \frac{(1-b_r) \cdot (p_n^f + p_n)}{(1+b_r)p_n^f + (1-b_r)p_n} \cdot \hat{y}_H^{nf}(\mathbf{b}) \right)^{k-1} \\
&\quad \cdot \left((1+b_r)p_n^f + (1-b_r)p_n - 2b_r p_n^f \hat{y}_H^f(\mathbf{b}) - (1-b_r) \cdot (p_n^f + p_n) \hat{y}_H^{nf}(\mathbf{b}) \right) \\
&= \sum_{k=0}^n \binom{n-1}{k} \left((1+b_r)p_n^f + (1-b_r)p_n \right)^k \left(1 - (1+b_r)p_n^f - (1-b_r)p_n \right)^{n-1-k} \\
&\quad \cdot \left(\frac{2b_r p_n^f}{(1+b_r)p_n^f + (1-b_r)p_n} \hat{y}_H^f(\mathbf{b}) + \frac{(1-b_r) \cdot (p_n^f + p_n)}{(1+b_r)p_n^f + (1-b_r)p_n} \cdot \hat{y}_H^{nf}(\mathbf{b}) \right)^k \\
&\quad \cdot n \cdot \left((1+b_r)p_n^f + (1-b_r)p_n - 2b_r p_n^f \hat{y}_H^f(\mathbf{b}) - (1-b_r) \cdot (p_n^f + p_n) \hat{y}_H^{nf}(\mathbf{b}) \right) \\
&= \sum_{k=0}^n \binom{n-1}{k} \left(1 - (1+b_r)p_n^f - (1-b_r)p_n \right)^{n-1-k} \cdot \left(2b_r p_n^f \hat{y}_H^f(\mathbf{b}) + (1-b_r) \cdot (p_n^f + p_n) \hat{y}_H^{nf}(\mathbf{b}) \right)^k \\
&\quad \cdot \left((1+b_r)\alpha^f + (1-b_r)\alpha - 2b_r \alpha^f \hat{y}_H^f(\mathbf{b}) - (1-b_r) \cdot (\alpha^f + \alpha) \hat{y}_H^{nf}(\mathbf{b}) \right) \\
&= \left(1 - (1+b_r)p_n^f - (1-b_r)p_n + 2b_r p_n^f \hat{y}_H^f(\mathbf{b}) + (1-b_r) \cdot (p_n^f + p_n) \hat{y}_H^{nf}(\mathbf{b}) \right)^{n-1} \\
&\quad \cdot \left((1+b_r)\alpha^f + (1-b_r)\alpha - 2b_r \alpha^f \hat{y}_H^f(\mathbf{b}) - (1-b_r) \cdot (\alpha^f + \alpha) \hat{y}_H^{nf}(\mathbf{b}) \right) \\
&= \left[1 - \frac{2b_r \alpha^f \left(1 - \hat{y}_H^f(\mathbf{b}) \right) - (1-b_r) \cdot (\alpha^f + \alpha) \left(1 - \hat{y}_H^{nf}(\mathbf{b}) \right)}{n} \right]^{n-1} \\
&\quad \cdot \left((1+b_r)\alpha^f + (1-b_r)\alpha - 2b_r \alpha^f \hat{y}_H^f(\mathbf{b}) - (1-b_r) \cdot (\alpha^f + \alpha) \hat{y}_H^{nf}(\mathbf{b}) \right) \\
&= e^{-2b_r \alpha^f \left(1 - \hat{y}_H^f(\mathbf{b}) \right) - (1-b_r) \cdot (\alpha^f + \alpha) \left(1 - \hat{y}_H^{nf}(\mathbf{b}) \right)} \\
&\quad \cdot \left((1+b_r)\alpha^f + (1-b_r)\alpha - 2b_r \alpha^f \hat{y}_H^f(\mathbf{b}) - (1-b_r) \cdot (\alpha^f + \alpha) \hat{y}_H^{nf}(\mathbf{b}) \right) \text{ as } n \rightarrow \infty \\
&= y_L^f(\mathbf{b}) \left((1+b_r)\alpha^f + (1-b_r)\alpha - b_r 2\alpha^f \hat{y}_H^f(\mathbf{b}) - (1-b_r) \left(\alpha^f + \alpha \right) \hat{y}_H^{nf}(\mathbf{b}) \right) \text{ as } n \rightarrow \infty.
\end{aligned}$$

Notice that the third equality above follows from $k(n)_k = n(n-1)_{k-1}$, the fourth equality substitutes k with $k-1$ everywhere and starts summation from $k=0$, and the sixth equality is an application of the Binomial Theorem.

Thus, $\mathbb{P}[v \text{ is a target} | v \text{ is a flexible node in } S_l]$ is given by

$$y_L^f(\mathbf{b}) + y_L^f(\mathbf{b}) \left((1+b_r)\alpha^f + (1-b_r)\alpha - b_r 2\alpha^f \hat{y}_H^f(\mathbf{b}) - (1-b_r)(\alpha^f + \alpha) \hat{y}_H^{nf}(\mathbf{b}) \right).$$

The probabilities conditional on v being a regular node or being from S_r can be derived analogously.

□

Proof of Proposition 2 Following closely the proof of Theorem 9 in Karp and Sipser (1981), we start by showing that a random tree is a good approximation to the structure obtained by conducting a breadth-first search from v . Denote the sub-graph of G induced by vertices at most distance d from v as the d -neighborhood of v . A vertex v is referred to as a d -target if there exists a derivation proving v to be a target within the d -neighborhood of v . Note that if d -neighborhood proves that v is a target then v is a target in any other graph that yields the same d -neighborhood.

Let

$$Y_n := \mathbb{P}[v \text{ is a target in } G_n | v \text{ is a flexible node in } V_l],$$

$$Y_n^d := \mathbb{P}[v \text{ is a } d\text{-target in } G_n | v \text{ is a flexible node in } V_l],$$

$$Y^d := \mathbb{P}[v \text{ is a } d\text{-target root in } \bar{G} | v \text{ is a flexible node in } S_l].$$

Claim 6 shows that, for large n , the probability that a d -neighborhood occurs in a random graph approaches the probability of that d -neighborhood occurring in a random tree.

CLAIM 6.

$$\lim_{n \rightarrow \infty} Y_n = \lim_{n \rightarrow \infty} \lim_{d \rightarrow \infty} Y_n^d = \lim_{d \rightarrow \infty} \lim_{n \rightarrow \infty} Y_n^d = \lim_{d \rightarrow \infty} Y^d = y_H^f(\mathbf{b}).$$

That is, $\mathbb{P}[v \text{ is a target} | v \text{ is a flexible node in } V_l] = y_H^f(\mathbf{b})$ as $n \rightarrow \infty$. Similarly, the probabilities for v to be a target or a loser, when $v \in V_l$ or V_r , and when v is a flexible or regular node, follow those derived for random trees in Lemma 7.

Since all members of derivations are targets or losers or both, we next find the probability for a random edge (v, u) in G to satisfy both $v \otimes u$ and $u \otimes v$ i.e., v is both a target and a loser. By Theorem 9 (3) in Karp and Sipser (1981), in \bar{G} this occurs if and only if both u and v are in L . We compute this probability conditional on the types of root nodes v , and the extension from \bar{G} to G follows from Claim 6.

$$\lim_{n \rightarrow \infty} \mathbb{P}[v \otimes u \text{ and } u \otimes v | v \text{ is a flexible node in } V_l]$$

$$\begin{aligned}
 &= \mathbb{P}[v, u \text{ are both in } L \mid v \text{ is a flexible node in } V_l] \\
 &= y_L^f(\mathbf{b}) \mathbb{P}[u \text{ is a flexible node} \mid (v, u) \in E] \hat{y}_L^f(\mathbf{b}) + y_L^f(\mathbf{b}) \mathbb{P}[u \text{ is a regular node} \mid (v, u) \in E] \hat{y}_L^{nf}(\mathbf{b}) \\
 &= y_L^f(\mathbf{b}) \frac{b_r 2\alpha^f}{(1+b_r)\alpha^f + (1-b_r)\alpha} \hat{y}_L^f(\mathbf{b}) + y_L^f(\mathbf{b}) \frac{(1-b_r)(\alpha^f + \alpha)}{(1+b_r)\alpha^f + (1-b_r)\alpha} \hat{y}_L^{nf}(\mathbf{b}).
 \end{aligned}$$

Similarly, we find

$$\begin{aligned}
 &\lim_{n \rightarrow \infty} \mathbb{P}\left[v \bigotimes u \text{ and } u \bigotimes v \mid v \text{ is a regular node in } V_l\right] \\
 &= y_L^{nf}(\mathbf{b}) \frac{b_r(\alpha^f + \alpha)}{b_r\alpha^f + (2-b_r)\alpha} \hat{y}_L^f(\mathbf{b}) + y_L^{nf}(\mathbf{b}) \frac{(1-b_r)2\alpha}{b_r\alpha^f + (2-b_r)\alpha} \hat{y}_L^{nf}(\mathbf{b}), \\
 &\lim_{n \rightarrow \infty} \mathbb{P}\left[v \bigotimes u \text{ and } u \bigotimes v \mid v \text{ is a flexible node in } V_r\right] \\
 &= \hat{y}_L^f(\mathbf{b}) \frac{b_l 2\alpha^f}{(1+b_l)\alpha^f + (1-b_l)\alpha} y_L^f(\mathbf{b}) + \hat{y}_L^f(\mathbf{b}) \frac{(1-b_l)(\alpha^f + \alpha)}{(1+b_l)\alpha^f + (1-b_l)\alpha} y_L^{nf}(\mathbf{b}), \\
 &\lim_{n \rightarrow \infty} \mathbb{P}\left[v \bigotimes u \text{ and } u \bigotimes v \mid v \text{ is a regular node in } V_r\right] \\
 &= \hat{y}_L^{nf}(\mathbf{b}) \frac{b_l(\alpha^f + \alpha)}{b_l\alpha^f + (2-b_l)\alpha} y_L^f(\mathbf{b}) + \hat{y}_L^{nf}(\mathbf{b}) \frac{(1-b_l)2\alpha}{b_l\alpha^f + (2-b_l)\alpha} y_L^{nf}(\mathbf{b}).
 \end{aligned}$$

Thus,

$$\begin{aligned}
 &\lim_{n \rightarrow \infty} \mathbb{P}[v \text{ in a derivation} \mid v \text{ is a flexible node in } V_l] \\
 &= \lim_{n \rightarrow \infty} \mathbb{P}[v \text{ is a target} \mid v \text{ is a flexible node in } V_l] + \lim_{n \rightarrow \infty} \mathbb{P}[v \text{ is a loser} \mid v \text{ is a flexible node in } V_l] \\
 &\quad - \lim_{n \rightarrow \infty} \mathbb{P}\left[v \bigotimes u \text{ and } u \bigotimes v \mid v \text{ is a regular node in } V_l\right] \cdot \mathbb{E}\left[\left|u \text{ s.t. } (v, u) \in E\right| \middle| v \text{ is a regular node in } V_l\right] \\
 &= y_H^f(\mathbf{b}) + y_L^f(\mathbf{b}) + y_L^f(\mathbf{b}) \left((1+b_r)\alpha^f + (1-b_r)\alpha - b_r 2\alpha^f \hat{y}_H^f(\mathbf{b}) - (1-b_r)(\alpha^f + \alpha) \hat{y}_H^{nf}(\mathbf{b}) \right) \\
 &\quad - \left[y_L^f(\mathbf{b}) \frac{b_r 2\alpha^f}{(1+b_r)\alpha^f + (1-b_r)\alpha} \hat{y}_L^f(\mathbf{b}) + y_L^f(\mathbf{b}) \frac{(1-b_r)(\alpha^f + \alpha)}{(1+b_r)\alpha^f + (1-b_r)\alpha} \hat{y}_L^{nf}(\mathbf{b}) \right] \cdot \left((1+b_r)\alpha^f + (1-b_r)\alpha \right) \\
 &= y_H^f(\mathbf{b}) + y_L^f(\mathbf{b}) + y_L^f(\mathbf{b}) \left[(1+b_r)\alpha^f + (1-b_r)\alpha \right] \cdot \\
 &\quad \left[1 - \frac{b_r 2\alpha^f}{(1+b_r)\alpha^f + (1-b_r)\alpha} (\hat{y}_L^f(\mathbf{b}) + \hat{y}_H^f(\mathbf{b})) - \frac{(1-b_r)(\alpha^f + \alpha)}{(1+b_r)\alpha^f + (1-b_r)\alpha} (\hat{y}_L^{nf}(\mathbf{b}) + \hat{y}_H^{nf}(\mathbf{b})) \right].
 \end{aligned}$$

The probabilities conditional on other types of nodes are computed similarly. \square

Proof of Claim 6 The first and last equalities in the claim arise directly from our definitions and Lemma 7. We now prove the third and the second equality. By the Poisson Limit Theorem, for any flexible node $v \in V_l$, the distribution of its degrees follows Poisson $(b_r 2\alpha^f + (1-b_r)(\alpha^f + \alpha))$ as $n \rightarrow \infty$. Thus, for any $\epsilon > 0$ there is a constant k such that $\lim_{n \rightarrow \infty} \mathbb{P}[\text{there is a node of degree } > k \text{ in the } d\text{-neighborhood of } v] < \epsilon$. The rest of the analyses exactly follow the proof of Theorem 9 (1) in Karp and Sipser (1981), which shows $\lim_{n \rightarrow \infty} Y_n^d = Y^d$ because (i)

there are finitely many d -neighborhoods that lack a vertex of degree $> k$, and (ii) the probability of encountering each such d -neighborhood around a node v in G_n is close to that around a root v in \bar{G} as $n \rightarrow \infty$. This proves the third equality.

Finally, we justify the limit exchange in the second equality. We leverage the result from Theorem 9 (1) in Karp and Sipser (1981) that, for every positive ϵ , there exists a d such that for all sufficiently large n , $\mathbb{P}[v \text{ is a target but not a } d\text{-target}] < \epsilon$.³⁰ This implies that for all sufficiently large $n, n'd, d', Y_n^d$ is close to $Y_{n'}^{d'}$ and thus we may exchange limit. \square

Proof of Claim 2 Firstly, we calculate the derivative of $f_1(x_1)$:

$$\begin{aligned} f'_1(x_1) &= \frac{\partial e^{-\frac{1}{2}(\alpha^f+\alpha)x_1+2\frac{\alpha}{\alpha^f+\alpha}(\log(x_1)+\alpha^fx_1)}{\partial x_1} + 2\frac{\log(x_1)+\alpha^fx_1}{\alpha^f+\alpha} \\ &= e^{-\frac{1}{2}(\alpha^f+\alpha)x_1+2\frac{\alpha}{\alpha^f+\alpha}(\log(x_1)+\alpha^fx_1)} \left(-\frac{1}{2}(\alpha^f+\alpha) + 2\frac{\alpha}{\alpha^f+\alpha}(\alpha^f+1/x_1) \right) + \frac{2}{\alpha^f+\alpha}(\alpha^f+1/x_1). \end{aligned}$$

We next employ a computer-aided proof to verify that $f'_1(x_1) > 1$ for any $x_1 \in (0, 1]$ when $10^{-4} < \alpha < \alpha^f$ and $\alpha^f + \alpha < e$. Fixing $\delta_1, \delta_2 > 0$, we establish a lower bound on the value of $f'_1(x_1)$ for any $(\bar{\alpha}^f, \bar{\alpha}, \bar{x}_1)$ in the set $[\alpha^f, \alpha^f + \delta_1] \times [\alpha, \alpha + \delta_1] \times [x_1, x_1 + \delta_2]$, where $10^{-4} < \alpha < \alpha^f$ and $\alpha^f + \alpha < e$. We find that:

$$\begin{aligned} f'_1(x_1) &\geq e^{-\frac{1}{2}(\alpha^f+\alpha)x_1+2\frac{2(\alpha^f+\delta_1)(\alpha+\delta_1)(x_1+\delta_2)}{\alpha^f+\alpha}+\frac{2\alpha\log(x_1+\delta_2)}{\alpha^f+\alpha+2\delta_1}} \left(-\frac{1}{2}(\alpha^f+\alpha+2\delta_1) \right) \\ &\quad + e^{-\frac{1}{2}(\alpha^f+\alpha+2\delta_1)(x_1+\delta_2)+2\frac{2\alpha^f\alpha x_1}{\alpha^f+\alpha+2\delta_1}+\frac{2(\alpha+\delta_1)\log(x_1)}{\alpha^f+\alpha}} \left(\frac{2\alpha\left(\alpha^f+\frac{1}{x_1+\delta_2}\right)}{\alpha^f+\alpha+2\delta_1} \right) \\ &\quad + \frac{2\left(\alpha^f+\frac{1}{x_1+\delta_2}\right)}{\alpha^f+\alpha+2\delta_1} \text{ when } x_1 > 0, \\ f'_1(x_1) &\geq e^{-\frac{1}{2}(\alpha^f+\alpha)x_1+2\frac{2(\alpha^f+\delta_1)(\alpha+\delta_1)(x_1+\delta_2)}{\alpha^f+\alpha}+\frac{2\alpha\log(x_1+\delta_2)}{\alpha^f+\alpha+2\delta_1}} \left(-\frac{1}{2}(\alpha^f+\alpha+2\delta_1) \right) \\ &\quad + \frac{2\left(\alpha^f+\frac{1}{x_1+\delta_2}\right)}{\alpha^f+\alpha+2\delta_1} \text{ when } x_1 = 0. \end{aligned} \tag{42}$$

For given $\delta_1, \delta_2 > 0$, if the lower bound in (42) is greater than 1, then $f'_1(x_1) > 1$ for any $(\bar{\alpha}^f, \bar{\alpha}, \bar{x}_1)$ in the corresponding set $[\alpha^f, \alpha^f + \delta_1] \times [\alpha, \alpha + \delta_1] \times [x_1, x_1 + \delta_2]$. In the computational notebook titled `Claim3.ipynb`,³¹ we compute the value of (42) for $x_1 = 0, \delta_2, 2\delta_2, \dots, 1$ and $\alpha^f, \alpha = 10^{-4}, \delta_1, 2\delta_1, \dots, e$, under the constraint $\alpha^f + \alpha < e$. Through this computation, we find that taking $\delta_1 = \delta_2 = 0.01$ is sufficient for verifying (42) > 1 for all $x_1 \in (0, 1], 10^{-4} < \alpha < \alpha^f$ and $\alpha^f + \alpha < e$.

\square

³⁰This result relies on probabilistic bounds on the length of a shortest derivation that proves v to be a target.

³¹The computer-aided proof can be found at <https://bit.ly/3VhfumL>.

A.3.6. Computational results based on $\mu^{\text{KS}}(b_l, b_r)$. To compute $\mu^{\text{KS}}(b_l, b_r)$, we resort to the `NLsolve` package available in the Julia Programming Language to solve (11) at a tolerance level $ftol = 10^{-8}$. Specifically, `NLsolve` iteratively refines candidate solutions using the Trust Region Method until the infinite norm of the residuals of the current solution falls below the threshold $ftol = 10^{-8}$ (NLsolve 2017). When $10^{-4} < \alpha < \alpha^f$ and $\alpha^f + \alpha < e$, at $\mathbf{b} = (1/2, 1/2), (1, 0)$ and $(0, 1)$ we find that (11) reduces to a single non-linear equation that exhibits strict monotonicity on both sides and can be solved to provable precision using this method (see the proof of Theorem 3 (ii) for details). In other cases where there are no theoretical guarantees for the closeness of $\mu^{\text{KS}}(b_l, b_r)$ to $\mu(b_l, b_r)$, numerical studies indicate that $\mu_n^{\text{EMP}}(b_l, b_r)$ still tends to converge to $\mu^{\text{KS}}(b_l, b_r)$ as n scales large. We thus employ $\mu^{\text{KS}}(b_l, b_r)$ to compare the one-sided and the balanced allocations for a wide range of parameters. Specifically, the findings presented in Section 6 are based on values of $(B, b_l, \alpha^f, \alpha)$ in a set S that contains all $B \in \{0.1, 0.2, \dots, 1\}, b_l \in \{0, 0.01, \dots, 1\}, \alpha^f \in \{0.05, 0.10, \dots, 7.45, 7.50\}$ and $\alpha \in \{0, 0.05, 0.10, \dots, 2.95, 3.00\}$ such that $B \geq b_l$ and $\alpha^f > \alpha$.

Appendix B: Proofs of the 2×2 Model

In the 2×2 model, we show below that the function $\mu(b_l, b_r)$ can be expressed as an eighth-order polynomial with respect to b_l , b_r , p^f , and p ; we derive a closed-form solution of $\mu(b_l, b_r)$ by complete enumeration of the possible vertex-flexibility and subsequent edge realizations. This facilitates the comparison between one-sided and balanced allocation and enables the convexity and concavity analyses of $\mu(b_l, b_r)$.

B.1. Proof of Theorem 1

Proof. We start by deriving the expected fraction of nodes involved in a maximum matching in the 2×2 model. We denote by $k_l \in \{0, 1, 2\}$ and $k_r \in \{0, 1, 2\}$, respectively, the number of flexible nodes in V_l and V_r and analyze the expected maximum matching size for each possible realization of k_l and k_r . Throughout, we use the shorthand *w.p.* to denote “with probability.”

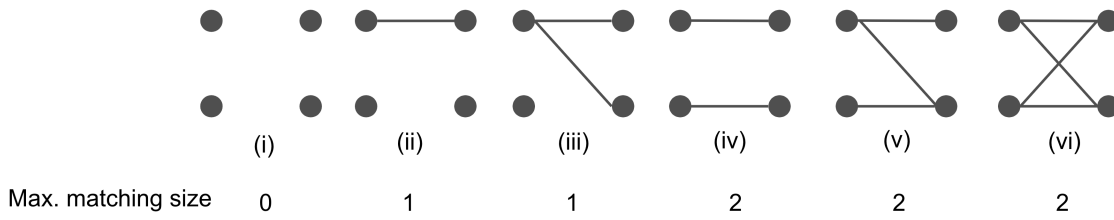


Figure 22 Illustrations of the realized edges and the resulting maximum matching sizes.

$k_l = 0, k_r = 0$: This scenario occurs *w.p.* $(1 - b_l)^2(1 - b_r)^2$. Under such a realization of nodes, we have the following probabilities for scenarios (i)-(vi) in Fig. 22 to realize (up to isomorphism):

- (i) $(1 - 2p)^4$;
- (ii) $4(1 - 2p)^32p$;
- (iii) $4(1 - 2p)^2(2p)^2$;

- (iv) $2(1 - 2p)^2(2p)^2$;
- (v) $4(1 - 2p)(2p)^3$;
- (vi) $(2p)^4$.

Combining these probabilities with the corresponding maximum matching size, we compute the expected number of matches, conditioned on $k_l = 0, k_r = 0$, as

$$4(1 - 2p)^3 2p + 4(1 - 2p)^2 (2p)^2 + 2 [2(1 - 2p)^2 (2p)^2 + 4(1 - 2p)(2p)^3 + (2p)^4]. \quad (43)$$

$k_l = 1, k_r = 0$ or $k_l = 0, k_r = 1$: This scenario occurs w.p. $2b_l(1 - b_l)(1 - b_r)^2 + 2b_r(1 - b_r)(1 - b_l)^2$. By substituting the edge probability for two of the four potential edges by $p^f + p$ rather than $2p$, we similarly compute the probabilities of having 0, 1, or 2 matches under such a realization of nodes and find an expected matching size of

$$\begin{aligned} & 2(p^f + p)(1 - p^f - p)(1 - p)^2 + 2(1 - p^f - p)^2 2p(1 - 2p) + ((p^f + p)(1 - 2p) + (1 - p^f - p)2p)^2 \\ & + 2 \cdot [2(p^f + p)2p(1 - p^f - p)(1 - 2p) + 2(p^f + p)^2 2p(1 - 2p) + 2(p^f + p)(1 - p^f - p)(2p)^2 + (p^f + p)^2 (2p)^2]. \end{aligned} \quad (44)$$

$k_l = 1, k_r = 1$: This scenario occurs w.p. $4b_l(1 - b_l)b_r(1 - b_r)$. Given such a realization of nodes, the edge probabilities for the four edges become $2p^f, p^f + p, p^f + p$, and $2p$, respectively, which yields an expected matching size of

$$\begin{aligned} & (2p^f)(1 - p^f - p)^2(1 - 2p) + (1 - 2p^f)2p(1 - p^f - p)^2 + 2(p^f + p)(1 - p^f - p)(1 - 2p^f)(1 - 2p) \\ & + 2(2p^f)(p^f + p)(1 - p^f - p)(1 - 2p) + 2(2p)(p^f + p)(1 - p^f - p)(1 - 2p^f) \\ & + 2 \cdot \left((p^f + p)^2(1 - 2p^f)(1 - 2p) + (2p^f)(2p)(1 - p^f - p)^2 + 2(2p^f)(2p)(p^f + p)(1 - p^f - p) \right. \\ & \left. + (2p^f)(p^f + p)^2(1 - 2p) + (1 - 2p^f)(p^f + p)^2(2p) + (2p^f)(p^f + p)^2 2p \right). \end{aligned} \quad (45)$$

$k_l = 2, k_r = 0$ or $k_l = 0, k_r = 2$: This scenario occurs w.p. $b_l^2(1 - b_r)^2 + b_r^2(1 - b_l)^2$. Given such a realization of nodes, the edge probability is $p^f + p$ for all four edges, which yields an expected matching size of

$$\begin{aligned} & 4(1 - p^f - p)^3(p^f + p) + 4(1 - p^f - p)^2(p^f + p)^2 \\ & + 2 \cdot [2(1 - p^f - p)^2(p^f + p)^2 + 4(1 - p^f - p)(p^f + p)^3 + (p^f + p)^4]. \end{aligned} \quad (46)$$

$k_l = 2, k_r = 1$ or $k_l = 1, k_r = 2$: This scenario occurs w.p. $2b_l^2 b_r(1 - b_r) + 2b_r^2 b_l(1 - b_l)$. Given such a realization of nodes, the edge probability is equal to $2p^f$ for two of the edges and $p^f + p$ for the other two, which yields an expected matching size of

$$\begin{aligned} & 2(2p^f)(1 - p^f - p)^2(1 - 2p^f) + 2(1 - 2p^f)^2(p^f + p)(1 - p^f - p) + ((2p^f)(1 - p^f - p) + (1 - 2p^f)(p^f + p))^2 \\ & + 2 \cdot \left(2(2p^f)(p^f + p)(1 - p^f - p)(1 - 2p^f) + 2(2p^f)^2(p^f + p)(1 - p^f - p) \right. \\ & \left. + 2(2p^f)(1 - 2p^f)(p^f + p)^2 + (2p^f)^2(p^f + p)^2 \right). \end{aligned}$$

(47)

$k_l = 2, k_r = 2$: This scenario occurs w.p. $b_l^2 b_r^2$. Given such a realization of nodes, the edge probability is $2p^f$ for all four edges, which yields an expected matching size of

$$4(1 - 2p^f)^3 2p^f + 4(1 - 2p^f)^2 (2p^f)^2 + 2 \left[2(1 - 2p^f)^2 (2p^f)^2 + 4(1 - 2p^f)(2p^f)^3 + (2p^f)^4 \right]. \quad (48)$$

Multiplying equations (43)-(48) by their respective scenario probabilities, and then dividing by $n = 2$, we obtain:

$$\begin{aligned} \mu(b_l, b_r) = & -p^4 \left((4 - 3b_r)^2 + b_l^2 (9 - 10b_r + 2b_r^2) - 2b_l (12 - 16b_r + 5b_r^2) \right) \\ & - p^f \left(b_r \left(-2 + p^f + p^f b_r - 2(p^f)^2 b_r + (p^f)^3 b_r \right) \right. \\ & + b_l \left(-2 + p^f + 4p^f b_r + 6(p^f)^3 b_r^2 - 4(p^f)^2 b_r (1 + b_r) \right) \\ & \left. + p^f b_l^2 \left(1 - 2p^f (1 + 2b_r) + (p^f)^2 (1 + 6b_r + 2b_r^2) \right) \right) \\ & + 2p^3 \left((-4 + 3b_r) \left(-2 + b_r + 2p^f b_r \right) + b_l^2 \left(3 - 2b_r + 2p^f (3 - 6b_r + 2b_r^2) \right) \right. \\ & \left. - 2b_l \left(5 - 5b_r + b_r^2 + 2p^f (2 - 6b_r + 3b_r^2) \right) \right) \\ & + 2p \left(2 + \left(-1 - 3p^f + 2(p^f)^2 \right) b_r + \left(p^f + (p^f)^2 - 2(p^f)^3 \right) b_r^2 \right. \\ & + b_l \left(-1 + 4(p^f)^3 (-2 + b_r) b_r + p^f (-3 + 4b_r) + (p^f)^2 (2 + 6b_r - 6b_r^2) \right) \\ & \left. + p^f b_l^2 \left(1 + p^f - 6p^f b_r + (p^f)^2 (-2 + 4b_r + 4b_r^2) \right) \right) \\ & - p^2 \left(8 + \left(-7 - 16p^f + 8(p^f)^2 \right) b_r + \left(1 + 10p^f - 2(p^f)^2 \right) b_r^2 \right. \\ & + b_l \left(-7 + 4b_r + (p^f)^2 (8 - 12b_r^2) - 4p^f (4 - 9b_r + 3b_r^2) \right) \\ & \left. + b_l^2 \left(1 - 2p^f (-5 + 6b_r) + 2(p^f)^2 (-1 - 6b_r + 6b_r^2) \right) \right). \end{aligned} \quad (49)$$

Given the closed-form expression for $\mu(b_l, b_r)$ in (49), to prove Theorem 1 it suffices to compute $\mu(B, 0) - \mu(B/2, B/2)$ and verify that the difference is strictly positive. Using Wolfram Mathematica, as documented in `Theorem1.nb`,³² we verify that $\mu(B, 0) - \mu(B/2, B/2) > 0$ holds true for all $B \in (0, 1]$ and $0 \leq p < p^f \leq 1/2$.

□

³²The codes can be found at <https://bit.ly/3P1Ch1D>.

B.2. Proof of Theorem 5

Proof. For the proof of Theorem 5 (i), we calculate $\nabla_{(0,1)}^2 \mu(b_l, b_r)$, which is equivalently expressed as $\frac{\partial^2 \mu(b_l, b_r)}{\partial b_r^2}$. This calculation is verified in Theorem5.nb,³³ using Wolfram Mathematica, establishing that $\frac{\partial^2 \mu(b_l, b_r)}{\partial b_r^2} < 0$ for all $\mathbf{b} \in (0, 1)^2$ and $0 \leq p < p^f \leq 1/2$. The case for $\nabla_{(1,0)}^2 \mu(b_l, b_r)$ is symmetric. Furthermore, for $\nabla_{(1,1)}^2 \mu(b_l, b_r)$, we compute $\frac{\partial^2 \mu(b_l+h, b_r+h)}{\partial h^2} \Big|_{h=0}$ and verify that it is negative under the same conditions.

Next, to prove Theorem 5 (ii), we observe that $\nabla_{(1,-1)}^2 \mu(b_l, b_r)$ is equivalent to $\frac{\partial^2 \mu(b_l, B-b_l)}{\partial b_l^2}$. Verification in Wolfram Mathematica, as documented in Theorem5.nb, shows that $\frac{\partial^2 \mu(b_l, B-b_l)}{\partial b_l^2} > 0$ for all $b_l \in (0, 1)$, $B \in (b_l, b_l + 1)$ and $0 \leq p < p^f \leq 1/2$. This result implies that $\nabla_{(1,-1)}^2 \mu(b_l, b_r) > 0$ for all $\mathbf{b} \in (0, 1)^2$ and $0 \leq p < p^f \leq 1/2$.

□

Appendix C: Proofs of the Local Model

In this section, we prove the results for the local model. We derive a closed-form expression for $\mu(b_l, b_r)$ as a rational function, in which both the denominator and numerator are eighth-order polynomials in terms of b_l , b_r , p^f , and p . This expression facilitates the comparison between one-sided and balanced allocation, as well as the analysis of the convexity and concavity properties of $\mu(b_l, b_r)$ along specific diagonals where analyses of directional second-order derivatives are tractable.

C.1. Proof of Theorem 2

Proof. We begin by characterizing the asymptotic fraction of nodes matched in the local model. Let E denote the set of all edges. We propose Algorithm 3 to construct a matching M , and argue that it is at most 1 below the size of a maximum matching (thus, the matching probability under Algorithm 3 is the same, asymptotically, as that under a maximum matching).

Our analysis focuses on the nodes in V_r that are being matched through Algorithm 3, as opposed to the ones that could be matched in a maximum matching. Recall that each node v_i^l in V_l can only connect to its two neighbors in V_r . If $(v_i^l, v_i^r) \notin E$ and $(v_i^l, v_{i+1}^r) \in E$, then there exists a maximum matching that contains (v_i^l, v_{i+1}^r) . This is because node v_i^l cannot be matched otherwise, and not using (v_i^l, v_{i+1}^r) in the matching would at most save v_{i+1}^r for one additional match. Hence, this algorithm is provably optimal for all nodes in V_r except v_1^r , which is myopically matched to v_1^l if an edge exists. As we are interested in computing $\mu(b_l, b_r) = \lim_{n \rightarrow \infty} \mathbb{E} \left[\frac{\mathcal{M}_n(b_l, b_r)}{n} \right]$, the resulting error in $\mu(b_l, b_r)$ approaches 0 in the asymptotic setting where $n \rightarrow \infty$.

³³The codes can be found at <https://bit.ly/30XR4L2>.

Algorithm 3 Maximum Matching Construction in Local Model

```

1: Initialize the matching set  $M \leftarrow \emptyset$ 
2: if  $(v_1^l, v_1^r) \in E$  then
3:   Add  $(v_1^l, v_1^r)$  to  $M$ 
4: for each subsequent node  $v_i^r$  with  $i > 1$  do
5:   if  $(v_{i-1}^l, v_i^r) \in E$  and  $v_{i-1}^l$  is not already matched in  $M$  then
6:     Add  $(v_{i-1}^l, v_i^r)$  to  $M$ 
7:   else if  $(v_i^l, v_i^r) \in E$  then
8:     Add  $(v_i^l, v_i^r)$  to  $M$ 
9: return  $M$ 

```

Therefore, to compute $\mu(b_l, b_r)$ it is sufficient to calculate the asymptotic fraction of nodes matched through this algorithm. Observe that whether a node $v_i^r \in V_r$ is matched to $v_{i-1}^l \in V_l$ depends only on edges incident to v_{i-1}^l and is independent of v_i^l . For each v_i^r with $i \in \{2, \dots, n\}$, we define

$$x_i^f := \mathbb{P} \left[(v_{i-1}^l, v_i^r) \in M \mid v_i^r \text{ is flexible} \right] \text{ and } x_i^n := \mathbb{P} \left[(v_{i-1}^l, v_i^r) \in M \mid v_i^r \text{ is regular} \right].$$

We now establish a system of equations to compute (x_{i+1}^f, x_{i+1}^n) based on (x_i^f, x_i^n) , which hold for any $i \in \{2, \dots, n\}$. To compute x_{i+1}^f , we consider all possible scenarios in which v_{i+1}^r gets matched to v_i^l : (1) $(v_{i-1}^l, v_i^r) \in M$ and $(v_i^l, v_{i+1}^r) \in E$, or (2) $(v_{i-1}^l, v_i^r) \notin M$, $(v_i^l, v_i^r) \notin E$ and $(v_i^l, v_{i+1}^r) \in E$. Suppose v_i^l and v_i^r are both flexible nodes; if v_{i+1}^r is also flexible then (1) occurs w.p. $x_i^f 2p^f$ and (2) occurs w.p. $(1 - x_i^f)(1 - 2p^f)2p^f$. Thus, conditioned on v_i^l , v_i^r , and v_{i+1}^r all being flexible nodes, $(v_i^l, v_{i+1}^r) \in M$ with probability $x_i^f 2p^f + (1 - x_i^f)(1 - 2p^f)2p^f$.

For the cases where v_i^l or v_i^r are of other node types, we compute (conditioned on node types) the respective probabilities of the events

$$\left\{ \left\{ (v_{i-1}^l, v_i^r) \in M \right\} \cap \left\{ (v_i^l, v_{i+1}^r) \in E \right\} \right\} \text{ and } \left\{ \left\{ (v_{i-1}^l, v_i^r) \notin M \right\} \cap \left\{ (v_i^l, v_i^r) \notin E \right\} \cap \left\{ (v_i^l, v_{i+1}^r) \in E \right\} \right\}$$

accordingly and find that:

$$\begin{aligned} x_{i+1}^f = f_1(x_i^f, x_i^n) &:= b_l b_r \left[x_i^f 2p^f + (1 - x_i^f)(1 - 2p^f)2p^f \right] + (1 - b_l) b_r \left[x_i^f (p^f + p) + (1 - x_i^f)(1 - p^f - p)(p^f + p) \right] \\ &\quad + b_l (1 - b_r) \left[x_i^n 2p^f + (1 - x_i^n)(1 - p^f - p)2p^f \right] + (1 - b_l)(1 - b_r) \left[x_i^n (p^f + p) + (1 - x_i^n)(1 - 2p)(p^f + p) \right]. \end{aligned} \tag{50}$$

Similarly, for x_{i+1}^n we find that:

$$\begin{aligned} x_{i+1}^n = f_2(x_i^f, x_i^n) &:= b_l b_r \left[x_i^f (p^f + p) + (1 - x_i^f)(1 - 2p^f)(p^f + p) \right] + (1 - b_l) b_r \left[x_i^f 2p + (1 - x_i^f)(1 - p^f - p)2p \right] \\ &\quad + b_l (1 - b_r) \left[x_i^n (p^f + p) + (1 - x_i^n)(1 - p^f - p)(p^f + p) \right] + (1 - b_l)(1 - b_r) \left[x_i^n 2p + (1 - x_i^n)(1 - 2p)2p \right]. \end{aligned}$$

(51)

Since $f_1(x_i^f, x_i^n)$ and $f_2(x_i^f, x_i^n)$ are linear with respect to x_i^f and x_i^n , they are trivially continuous. Since $b_l, b_r \in [0, 1]$ and $0 \leq 2p < p + p^f < 2p^f \leq 1$, we also find that $\frac{\partial f_1(x_i^f, x_i^n)}{\partial x_i^f}, \frac{\partial f_1(x_i^f, x_i^n)}{\partial x_i^n}, \frac{\partial f_2(x_i^f, x_i^n)}{\partial x_i^f}, \frac{\partial f_2(x_i^f, x_i^n)}{\partial x_i^n} \in [0, 1]$. Thus, by applying the Banach fixed-point theorem, we know that as $i \rightarrow \infty$ the fixed-point iteration $(x_{i+1}^f, x_{i+1}^n) = (f_1(x_i^f, x_i^n), f_2(x_i^f, x_i^n))$ converges to the unique fixed point (x^f, x^n) such that $(x^f, x^n) = (f_1(x^f, x^n), f_2(x^f, x^n))$. This is a linear system of equations, the solutions of which provide the limiting values for x^f and x^n (see below in (53)).

We next compute $\mu(b_l, b_r)$ using x^f and x^n . The asymptotic fraction of matched nodes is equal to the asymptotic probability that a random node $v_i^r \in V_r$ is matched. If v_i^r is a flexible node, it is matched with v_{i-1}^l with probability x_i^f and matched with v_i^l with probability $(1 - x_i^f)[(1 + b_l)p^f + (1 - b_l)p]$. If it is a regular node, it is matched with v_{i-1}^l with probability x_i^n and matched with v_i^l with probability $(1 - x_i^n)[b_l p^f + (2 - b_l)p]$. Thus,

$$\begin{aligned}\mu(b_l, b_r) &= \lim_{i \rightarrow \infty} b_r x_i^f + b_r (1 - x_i^f) [(1 + b_l)p^f + (1 - b_l)p] + (1 - b_r)x_i^n + (1 - b_r)(1 - x_i^n) [b_l p^f + (2 - b_l)p] \\ &= b_r x^f + b_r (1 - x^f) [(1 + b_l)p^f + (1 - b_l)p] + (1 - b_r)x^n + (1 - b_r)(1 - x^n) [b_l p^f + (2 - b_l)p].\end{aligned}\quad (52)$$

Solving x^f and x^n from (50)-(51) and plugging into (52), we obtain

$$\begin{aligned}\mu(b_l, b_r) &= \left(2(b_l + b_r)^2 p^4 b_l^2 - 2(b_l + b_r)^2 p^4 b_l - 8(b_l + b_r)^2 p^3 p^f b_l^2 + 8(b_l + b_r)^2 p^3 p^f b_l + 12(b_l + b_r)^2 p^2 \left(p^f\right)^2 b_l^2 \right. \\ &\quad - 12(b_l + b_r)^2 p^2 \left(p^f\right)^2 b_l - (b_l + b_r)^2 p^2 - 8(b_l + b_r)^2 p \left(p^f\right)^3 b_l^2 + 8(b_l + b_r)^2 p \left(p^f\right)^3 b_l + 2(b_l + b_r)^2 p p^f b_l^2 \\ &\quad + 2(b_l + b_r)^2 \left(p^f\right)^4 b_l^2 - 2(b_l + b_r)^2 \left(p^f\right)^4 b_l - (b_l + b_r)^2 \left(p^f\right)^2 - 4(b_l + b_r)p^4 b_l^3 + 2(b_l + b_r)p^4 b_l^2 \\ &\quad + 2(b_l + b_r)p^4 b_l + 16(b_l + b_r)p^3 p^f b_l^3 - 8(b_l + b_r)p^3 p^f b_l^2 - 8(b_l + b_r)p^3 p^f b_l - 24(b_l + b_r)p^2 \left(p^f\right)^2 b_l^3 \\ &\quad + 12(b_l + b_r)p^2 \left(p^f\right)^2 b_l^2 + 12(b_l + b_r)p^2 \left(p^f\right)^2 b_l - 2(b_l + b_r)p^2 b_l + 7(b_l + b_r)p^2 + 16(b_l + b_r)p \left(p^f\right)^3 b_l^2 \\ &\quad - 8(b_l + b_r)p \left(p^f\right)^3 b_l^2 - 8(b_l + b_r)p \left(p^f\right)^3 b_l + 4(b_l + b_r)p p^f b_l - 6(b_l + b_r)p p^f - 2(b_l + b_r)p \\ &\quad - 4(b_l + b_r) \left(p^f\right)^4 b_l^3 + 2(b_l + b_r) \left(p^f\right)^4 b_l^2 + 2(b_l + b_r) \left(p^f\right)^4 b_l - 2(b_l + b_r) \left(p^f\right)^2 b_l - (b_l + b_r) \left(p^f\right)^2 b_l \\ &\quad + 2(b_l + b_r)p^f + 2p^4 b_l^4 - 2p^4 b_l^2 - 8p^3 p^f b_l^4 + 8p^3 p^f b_l^2 + 12p^2 \left(p^f\right)^2 b_l^4 - 12p^2 \left(p^f\right)^2 b_l^2 \\ &\quad + 2p^2 b_l^2 - 8p^2 - 8p \left(p^f\right)^3 b_l^4 + 8p \left(p^f\right)^3 b_l^2 - 4p p^f b_l^2 + 4p + 2 \left(p^f\right)^4 b_l^4 - 2 \left(p^f\right)^4 b_l^2 + 2 \left(p^f\right)^2 b_l^2 \Big) / \\ &\quad \left((b_l + b_r)^2 p^4 b_l^2 - (b_l + b_r)^2 p^4 b_l - 4(b_l + b_r)^2 p^3 p^f b_l^2 + 4(b_l + b_r)^2 p^3 p^f b_l + 6(b_l + b_r)^2 p^2 \left(p^f\right)^2 b_l^2 \right. \\ &\quad \left. - 6(b_l + b_r)^2 p^2 \left(p^f\right)^2 b_l - 4(b_l + b_r)^2 p \left(p^f\right)^3 b_l^2 + 4(b_l + b_r)^2 p \left(p^f\right)^3 b_l + (b_l + b_r)^2 \left(p^f\right)^4 b_l^2 \right)\end{aligned}$$

$$\begin{aligned}
 & - (b_l + b_r)^2 \left(p^f \right)^4 b_l - 2(b_l + b_r)p^4 b_l^3 + (b_l + b_r)p^4 b_l^2 + (b_l + b_r)p^4 b_l + 8(b_l + b_r)p^3 p^f b_l^3 - 4(b_l + b_r)p^3 p^f b_l^2 \\
 & - 4(b_l + b_r)p^3 p^f b_l - 12(b_l + b_r)p^2 \left(p^f \right)^2 b_l^3 + 6(b_l + b_r)p^2 \left(p^f \right)^2 b_l^2 + 6(b_l + b_r)p^2 \left(p^f \right)^2 b_l - 2(b_l + b_r)p^2 b_l \\
 & + 3(b_l + b_r)p^2 + 8(b_l + b_r)p \left(p^f \right)^3 b_l^3 - 4(b_l + b_r)p \left(p^f \right)^3 b_l^2 - 4(b_l + b_r)p \left(p^f \right)^3 b_l + 4(b_l + b_r)p p^f b_l \\
 & - 2(b_l + b_r)p p^f - 2(b_l + b_r) \left(p^f \right)^4 b_l^3 + (b_l + b_r) \left(p^f \right)^4 b_l^2 + (b_l + b_r) \left(p^f \right)^4 b_l - 2(b_l + b_r) \left(p^f \right)^2 b_l \\
 & - (b_l + b_r) \left(p^f \right)^2 + p^4 b_l^4 - p^4 b_l^2 - 4p^3 p^f b_l^4 + 4p^3 p^f b_l^2 + 6p^2 \left(p^f \right)^2 b_l^4 - 6p^2 \left(p^f \right)^2 b_l^2 + 2p^2 b_l^2 - 4p^2 \\
 & - 4p \left(p^f \right)^3 b_l^4 + 4p \left(p^f \right)^3 b_l^2 - 4p p^f b_l^2 + \left(p^f \right)^4 b_l^4 - \left(p^f \right)^4 b_l^2 + 2 \left(p^f \right)^2 b_l^2 + 1 \Big). \quad (53)
 \end{aligned}$$

Given the closed-form expression for $\mu(b_l, b_r)$ in (53), to prove Theorem 2 it suffices to compute $\mu(B, 0) - \mu(B/2, B/2)$ and verify that the difference is strictly positive. Using Wolfram Mathematica in Theorem2.nb,³⁴ we verify that $\mu(B, 0) - \mu(B/2, B/2) > 0$ for all $B \in (0, 1]$ and $0 \leq p < p^f \leq 1/2$. \square

C.2. Proof of Theorem 6

Proof. For the concavity result, we evaluate $\nabla_{(0,1)}^2 \mu(b_l, b_r)$ with $b_l = 1/2$, which is equivalent to $\frac{\partial^2 \mu(1/2, b_r)}{\partial b_r^2}$. In Theorem6.nb,³⁵ we again use Wolfram Mathematica to verify that $\frac{\partial^2 \mu(1/2, b_r)}{\partial b_r^2} < 0$ for all $b_r \in (0, 1)$ and $0 \leq p < p^f \leq 1/2$. The case for the direction $(1, 0)$ is symmetric. The proof for $\frac{\partial^2 \mu(0, b_r)}{\partial b_r^2} < 0$ for all $b_r \in (0, 1)$ and $0 \leq p < p^f \leq 1/2$ follows from the same analyses by taking $b_l = 0$.

The convexity result is easier to analyze by hands. We set $b_r = 1 - b_l$ to simplify (53) to

$$\mu(b_l, 1 - b_l) = 2 \frac{(p^f)^2 b_l^2 - (p^f)^2 b_l - 2p^f p b_l^2 + 2p^f p b_l + p^f + p^2 b_l^2 - p^2 b_l + p}{(p^f)^2 b_l^2 - (p^f)^2 b_l - 2p^f p b_l^2 + 2p^f p b_l + p^f + p^2 b_l^2 - p^2 b_l + p + 1}.$$

Taking the second-order derivative with respect to b_l , we obtain

$$\frac{\partial^2 \mu(b_l, 1 - b_l)}{\partial b_l^2} = \frac{4(p^f - p)^2 \underbrace{\left[- (p^f)^2 - 3b_l^2 (p^f - p)^2 + 3b_l (p^f - p)^2 + 2p^f p + p^f - p^2 + p + 1 \right]}_{(I)}}{\underbrace{\left(b_l^2 (p^f - p)^2 - b_l (p^f - p)^2 + p^f + p + 1 \right)}_{{(II)}}^3}.$$

We demonstrate that both (I) and (II) are strictly positive for all $b_l \in (0, 1)$ and $0 \leq p < p^f \leq 1/2$, ensuring $\frac{\partial^2 \mu(b_l, 1 - b_l)}{\partial b_l^2} > 0$.

For (I) we have

$$(I) = 3b_l(1 - b_l) (p^f - p)^2 - (p^f - p)^2 + p^f + p + 1$$

³⁴The codes can be found at <https://bit.ly/3uS7wW6>.

³⁵The codes can be found at <https://bit.ly/3uRh6bQ>.

$$\begin{aligned}
&= (3b_l - 3b_l^2 - 1) \left(p^f - p \right)^2 + p^f + p + 1 \\
&\geq - \left(p^f - p \right)^2 + p^f + p + 1 \geq -0.25 + p^f + p + 1 > 0,
\end{aligned}$$

where the first inequality comes from $b_l - b_l^2 \geq 0$ and the second from $(p^f - p)^2 \leq 0.25$.

For (II) we have

$$(II) = (b_l^2 - b_l) \left(p^f - p \right)^2 + p^f + p + 1 \geq -0.25 + p^f + p + 1 > 0,$$

where the first inequality comes from $b_l^2 - b_l \geq -1$ and $(p^f - p)^2 \leq 0.25$. (since $p^f \leq 1/2$). Since $\nabla_{(1,-1)}^2 \mu(b_l, b_r)$ with $b_l + b_r = 1$ is equivalent to $\frac{\partial^2 \mu(b_l, 1-b_l)}{\partial b_l^2} > 0$, we conclude the proof. \square

Appendix D: Implications of the Structural Properties

In this appendix, we interpret the convexity and concavity results from Section 3 in the context of a game between two players that set the flexibility on each side. This reflects two separate verticals or teams within an organization, that each control (independently) one lever of flexibility. Our characterizations in this section illustrate that balanced allocation may emerge as a sub-optimal (local) Nash Equilibrium (NE) in such a context. We start by providing, in Definition 5 - 6, the textbook definition of NE and local NE for a general payoff function $g(b_l, b_r)$; we also define saddle points in Definition 7. We then verify these conditions for $g^{2 \times 2}(b_l, b_r)$, $g^{loc}(b_l, b_r)$ and $g^{glb}(b_l, b_r)$. Notably, the suboptimal outcomes occur in our settings in spite of both teams sharing the same objective, i.e., there is no misalignment of incentives.

DEFINITION 5 (GAME Γ). A game Γ is defined by:

1. The set of players $\{1, 2\}$;
2. For each player $i \in \{1, 2\}$, $\mathcal{B}_i = [0, 1]$ is the set of strategies available to player i ;
3. $g : \mathcal{B}_l \times \mathcal{B}_r \rightarrow \mathbb{R}$ is the payoff function, with $g(b_l, b_r)$ representing the payoff to each player for the strategy profile $\mathbf{b} = (b_l, b_r) \in \mathcal{B}_1 \times \mathcal{B}_2 \subseteq \mathbb{R}^2$.

DEFINITION 6 (NASH EQUILIBRIUM). In a game Γ where the function $g(b_l, b_r)$ has its domain $\mathcal{B} = \mathcal{B}_1 \times \mathcal{B}_2 \subseteq \mathbb{R}^2$,

- (i) A point \mathbf{b}' is a *Nash Equilibrium (NE)* if

$$g(b'_l, b'_r) \geq g(b_l, b'_r), \forall b_l \in \mathcal{B}_1 \text{ and } g(b'_l, b'_r) \geq g(b'_l, b_r), \forall b_r \in \mathcal{B}_2.$$

- (ii) A point \mathbf{b}' is a *local Nash Equilibrium* if there exists some $\delta > 0$ such that

$$g(b'_l, b'_r) \geq g(b_l, b'_r), \forall b_l \in \mathcal{B}_1 \cap (b_l - \delta, b_l + \delta), \text{ and}$$

$$g(b'_l, b'_r) \geq g(b'_l, b_r), \forall b_r \in \mathcal{B}_2 \cap (b_r - \delta, b_r + \delta).$$

- (iii) A point \mathbf{b}' is a *sub-optimal (local) Nash Equilibrium* if \mathbf{b}' is an (local) NE but there exists another point \mathbf{b}^* for which $g(b_l^*, b_r^*) > g(b'_l, b'_r)$.

DEFINITION 7 (SADDLE POINT). For a function $g(b_l, b_r) : \mathcal{B} = \mathcal{B}_1 \times \mathcal{B}_2 \rightarrow \mathbb{R}$, assume that its first and second directional derivatives exist in all directions at $\mathbf{b}' \in \mathcal{B}$. Then, \mathbf{b}' is said to be a saddle point of g if the following conditions are satisfied:

- (i) The gradient $\nabla g(\mathbf{b}') = \mathbf{0}$;
- (ii) The second directional derivatives $\nabla_{\mathbf{v}}^2 g(\mathbf{b}') < 0$ and $\nabla_{\mathbf{u}}^2 g(\mathbf{b}') > 0$ in some directions \mathbf{v} and $\mathbf{u} \in \mathbb{R}^2$.

To identify sub-optimal (local) NE in the models we leverage the results that $g(b_l, b_r)$ is concave in the directions $(0, 1)$ and $(1, 0)$, and convex in the directions $(-1, 1)$ and $(1, -1)$. Because the directional derivative at an NE is zero along all directions, having both concavity and convexity effectively means that the NE is also a saddle point. We formalize these conditions in Lemma 8 and Lemma 9.

DEFINITION 8 (INTERIOR OF A SET). Let (\mathcal{B}, τ) be a topological space. Then

- (i) A point $\mathbf{b} \in \mathcal{B}$ is an *interior point* of the set \mathcal{B} if there exists an open set U with $\mathbf{b} \in U \subseteq \mathcal{B}$.
- (ii) The *interior* of \mathcal{B} , denoted by $\text{int}(\mathcal{B})$, consists of all its interior points.

LEMMA 8 (Sub-Optimal NE and Saddle Point). In a game Γ where the function $g(b_l, b_r)$ has its domain $\mathcal{B} \subseteq \mathbb{R}^2$, assume that its first and second directional derivatives exist in all directions for any $\mathbf{b} \in \text{int}(\mathcal{B})$. Suppose some NE $\mathbf{b}' \in \text{int}(\mathcal{B})$ satisfies the following conditions:

- (i) $g(b_l, b_r)$ is strictly concave in the direction $(0, 1)$ at any $\mathbf{b} \in \text{int}(\mathcal{B})$ such that $b_l = b'_l$;
- (ii) $g(b_l, b_r)$ is strictly concave in the direction $(1, 0)$ at any $\mathbf{b} \in \text{int}(\mathcal{B})$ such that $b_r = b'_r$;
- (iii) $g(b_l, b_r)$ is strictly convex in the direction $(1, -1)$ for any $\mathbf{b} \in \text{int}(\mathcal{B})$ such that $b_l + b_r = b'_l + b'_r$.

Then \mathbf{b}' is a sub-optimal NE and a saddle point.

LEMMA 9 (Sub-Optimal Local NE and Saddle Point). In a game Γ where the function $g(b_l, b_r)$ has its domain $\mathcal{B} \subseteq \mathbb{R}^2$, assume that its first and second directional derivatives exist in all directions at $\mathbf{b}' \in \text{int}(\mathcal{B})$. Suppose

- (i) $g(b_l, b_r)$ is strictly concave in the directions $(0, 1)$ and $(1, 0)$ at \mathbf{b}' ;
- (ii) $g(b_l, b_r)$ is strictly convex in the direction $(1, -1)$ at \mathbf{b}' ;
- (iii) The gradient of $g(b_l, b_r)$ is the zero vector at \mathbf{b}' .

Then \mathbf{b}' is a sub-optimal local NE and a saddle point.

We now demonstrate that the balanced allocation is indeed a sub-optimal NE and a saddle point for a range of graph models examined in this paper.

PROPOSITION 3. In the 2×2 model, for any $c \in \left(\frac{\partial \mu(B/2, B/2)}{\partial B} \Big|_{B=2}, \frac{\partial \mu(B/2, B/2)}{\partial B} \Big|_{B=0} \right)$, there exists a $B' \in (0, 2)$ such that $\mathbf{b}' = (B'/2, B'/2)$ is a sub-optimal NE and a saddle point for $g(b_l, b_r)$.

PROPOSITION 4. *In the local model, there exists $c > 0$ such that $\mathbf{b}' = (1/2, 1/2)$ is a sub-optimal NE and a saddle point for $g(b_l, b_r)$.*

PROPOSITION 5. *In the global model, assume that $10^{-4} < \alpha < 0.64\alpha^f - 0.03$ and $0.62\alpha^f + \alpha < 1.68$. Then, there exists $c > 0$ such that $\mathbf{b}' = (1/2, 1/2)$ is a sub-optimal local NE and a saddle point for $\bar{g}(b_l, b_r) := \mu^{KS}(b_l, b_r) - \Gamma(b_l, b_r)$.*

D.1. Proofs for Nash Equilibrium and Saddle Point

Proof of Lemma 8 Let \mathbf{b}' be a Nash Equilibrium (NE) in $\text{int}(\mathcal{B})$ for the function $g(b_l, b_r)$ with domain $\mathcal{B} \subseteq \mathbb{R}^2$. We start by showing that $g(b_l, b_r)$ has a gradient of $\mathbf{0}$ at \mathbf{b}' . If $\nabla_{(0,1)}g(\mathbf{b}') > 0$, then there exists $\epsilon > 0$ such that $g(b'_l, b'_r + \epsilon) > g(b'_l, b'_r)$, contradicting the definition of NE. Similarly, if $\nabla_{(0,1)}g(\mathbf{b}') < 0$, then there exists $\epsilon > 0$ such that $g(b'_l, b'_r - \epsilon) > g(b'_l, b'_r)$, again contradicting the definition of NE. Thus, $\nabla_{(0,1)}g(\mathbf{b}') = 0$. Applying a similar argument to the direction of $(1, 0)$ we find that $\nabla_{(1,0)}g(\mathbf{b}') = 0$. Since $g(b_l, b_r)$ has a directional derivative of 0 in two orthogonal directions at \mathbf{b}' , it has a gradient of $\mathbf{0}$ at \mathbf{b}' . Since we also know that $\nabla_{(0,1)}^2g(\mathbf{b}') < 0$ and $\nabla_{(1,-1)}^2g(\mathbf{b}') > 0$, \mathbf{b}' is a saddle point.

We then show that \mathbf{b}' is a sub-optimal NE. Since $g(b_l, b_r)$ is strictly convex in the direction of $(1, -1)$ at any \mathbf{b} such that $b_l + b_r = b'_l + b'_r$ and $g(b_l, b_r)$ has a gradient of $\mathbf{0}$ at \mathbf{b}' , \mathbf{b}' is a global minimum in the direction of $(1, -1)$. That is, there exists $\epsilon > 0$ such that $g(b'_l + \epsilon, b'_r - \epsilon) > g(b'_l, b'_r)$. Thus, $g(b_l, b_r)$ is a sub-optimal NE. \square

Proof of Lemma 9 Since $g(b_l, b_r)$ is strictly concave in the direction of $(0, 1)$ and $(1, 0)$ but also strictly convex in the direction of $(1, -1)$ at \mathbf{b}' , \mathbf{b}' is neither a local maximum nor a local minimum. Combined with the condition that $g(b_l, b_r)$ has a gradient of $\mathbf{0}$ at \mathbf{b}' , we conclude that \mathbf{b}' is a saddle point.

Now, since $\nabla_{(0,1)}g(\mathbf{b}') = 0$ and $\nabla_{(0,1)}^2g(b_l, b_r) < 0$, we know that \mathbf{b}' is a local maximum in the direction of $(0, 1)$ and we can find $\epsilon_1 > 0$ such that

$$g(b'_l, b'_r) \geq g(b'_l, b_r), \forall b_r \in b_r \cap (b_r - \epsilon_1, b_r + \epsilon_1).$$

Similarly, from $\nabla_{(1,0)}g(\mathbf{b}') = 0$ and $\nabla_{(1,0)}^2g(b_l, b_r) < 0$ we find $\epsilon_2 > 0$ such that

$$g(b'_l, b'_r) \geq g(b_l, b'_r), \forall b_l \in b_l \cap (b_l - \epsilon_2, b_l + \epsilon_2).$$

Taking $\delta = \min(\epsilon_1, \epsilon_2)$, we find that \mathbf{b}' is a local NE.

We then show that \mathbf{b}' is a sub-optimal local NE. Since $\nabla_{(1,-1)}g(\mathbf{b}') = 0$ and $\nabla_{(1,-1)}^2g(b_l, b_r) > 0$, \mathbf{b}' is a local minimum in the direction of $(1, -1)$. That is, there exists $\epsilon > 0$ such that $g(b'_l + \epsilon, b'_r - \epsilon) > g(b'_l, b'_r)$. Thus, $g(b_l, b_r)$ is a sub-optimal local NE. \square

Proof of Proposition 3 In Theorem 5, we have verified the local convexity of $\mu(b_l, b_r)$ in the direction $(1, -1)$ and local concavity in the directions $(0, 1)$ and $(1, 0)$ for any $\mathbf{b} \in (0, 1)^2$. Consequently, $g(b_l, b_r)$ exhibits the same local convexity and concavity properties. Given that both conditions in Lemma 8 are satisfied, it suffices to demonstrate that for any $c \in \left(\frac{\partial \mu(B/2, B/2)}{\partial B} \Big|_{B=2}, \frac{\partial \mu(B/2, B/2)}{\partial B} \Big|_{B=0} \right)$, there exists a $B' \in (0, 2)$ such that $\mathbf{b}' = (B'/2, B'/2)$ is an NE.

By concavity of $\mu(b_l, b_r)$ in the direction $(1, 1)$ we know that $\frac{\partial \mu(B/2, B/2)}{\partial B}$ is monotonically decreasing with respect to B and the interval $\left(\frac{\partial \mu(B/2, B/2)}{\partial B} \Big|_{B=2}, \frac{\partial \mu(B/2, B/2)}{\partial B} \Big|_{B=0} \right)$ is non-empty. Thus, for any c in the interval, by continuity of the directional derivative we know that $c = \frac{\partial \mu(B/2, B/2)}{\partial B} \Big|_{B=B'} = \nabla_{(1/2, 1/2)} \mu(b_l, b_r) \Big|_{\mathbf{b}=(B'/2, B'/2)}$ at some $B' \in (0, 2)$. Thus, we have

$$\nabla_{(1/2, 1/2)} g(b_l, b_r) \Big|_{\mathbf{b}=(B'/2, B'/2)} = \nabla_{(1/2, 1/2)} \mu(b_l, b_r) \Big|_{\mathbf{b}=(B'/2, B'/2)} - c = 0.$$

Given that $\nabla_{(1, -1)}^2 g(b_l, b_r) \Big|_{\mathbf{b}=(B'/2, B'/2)} > 0$ and by the symmetry $g(b_l, b_r) = \bar{g}(b_r, b_l), \forall (b_l, b_r) \in (0, 1)^2$, $\nabla_{(1, -1)} g(b_l, b_r)$ is well-defined at $(B'/2, B'/2)$. If the directional derivative is strictly positive, there exists $\epsilon > 0$ such that $g(B'/2 + \epsilon, B'/2 - \epsilon) > g(B'/2 - \epsilon, B'/2 + \epsilon)$, which contradicts the symmetry condition. By the same argument the directional derivative cannot be strictly negative, leading to $\nabla_{(1, -1)} g(b_l, b_r) = 0$ at $(B'/2, B'/2)$. Since at $\mathbf{b}' = (B'/2, B'/2)$ the derivative of $g(b_l, b_r)$ is equal to 0 in two independent directions, the gradient of $g(b_l, b_r)$ is $\mathbf{0}$ at $\mathbf{b}' = (B'/2, B'/2)$.

Combined with the result that $g(b_l, b_r)$ is strictly concave in the direction $(1, 0)$ when $b_r = B'/2$, we conclude that the point $\mathbf{b}' = (B'/2, B'/2)$ is a global maximum in this direction. That is,

$$g(B'/2, B'/2) \geq g(b_l, B'/2), \forall b_l \in (0, 1).$$

By symmetry, the same result holds in the direction $(0, 1)$. Thus, by Definition 6 (i), we establish that for the given c , the point $\mathbf{b}' = (B'/2, B'/2)$ is an NE. This completes the proof. \square

Proof of Proposition 4 As established in Theorem 6, we have verified the local convexity of $\mu(b_l, b_r)$ in the direction $(1, -1)$ and local concavity in the directions $(0, 1)$ and $(1, 0)$ along diagonals that intersect at $\mathbf{b}' = (1/2, 1/2)$. Consequently, the function $g(b_l, b_r)$ exhibits the same local convexity and concavity properties. According to Lemma 8, to demonstrate the existence of a constant $c > 0$ such that $\mathbf{b}' = (1/2, 1/2)$ is a sub-optimal Nash Equilibrium (NE) for $\bar{g}(b_l, b_r)$, it is sufficient to show that $(1/2, 1/2)$ is indeed an NE.

We construct $c = \nabla_{(1, 0)} \mu(b_l, b_r) = \frac{\partial \mu(b_l, 1/2)}{\partial b_l} \Big|_{b_l=1/2}$. Then, we have

$$\nabla_{(1, 0)} g(b_l, b_r) = \nabla_{(1, 0)} \mu(b_l, b_r) - c = 0.$$

Since $g(b_l, b_r)$ is strictly concave in the direction of $(1, 0)$ when $b_r = 1/2$, $\mathbf{b}' = (1/2, 1/2)$ is a global maximum in the direction $(1, 0)$. That is,

$$g(1/2, 1/2) \geq g(b_l, 1/2), \forall b_l \in (0, 1).$$

By symmetry, the same result holds in the direction $(0, 1)$. Thus, according to Definition 6 (i), we conclude that the point $\mathbf{b}' = (1/2, 1/2)$ is indeed an NE for the selected constant c . This completes the proof. \square

Proof of Proposition 5 Given that Theorem 7 has established the local convexity of $\mu^{\text{KS}}(b_l, b_r)$ in the direction $(1, -1)$ and its local concavity in the directions $(0, 1)$ and $(1, 0)$ within the specified region of α^f and α , the same local convexity and concavity properties hold for $\bar{g}(b_l, b_r) := \mu^{\text{KS}}(b_l, b_r) - \Gamma(b_l, b_r)$. By Lemma 9, to show that there exists $c > 0$ such that $\mathbf{b}' = (1/2, 1/2)$ is a sub-optimal local NE for $\bar{g}(b_l, b_r)$, it suffices to show that there exists $c > 0$ such that the gradient of $\bar{g}(b_l, b_r)$ is the zero vector at $\mathbf{b} = (1/2, 1/2)$.

Since $\nabla_{(1,-1)}^2 \bar{g}(b_l, b_r) > 0$ at $(1/2, 1/2)$ and by symmetry we have $\bar{g}(b_l, b_r) = \bar{g}(b_r, b_l), \forall (b_l, b_r) \in (0, 1)^2$, $\nabla_{(1,-1)} \bar{g}(b_l, b_r)$ is well-defined at $(1/2, 1/2)$. Now, if the directional derivative is strictly positive, we know that there exists $\epsilon > 0$ such that $\bar{g}(1/2 + \epsilon, 1/2 - \epsilon) > \bar{g}(1/2 - \epsilon, 1/2 + \epsilon)$, which contradicts the symmetry condition. By the same argument the directional derivative cannot be strictly negative, so we find that $\nabla_{(1,-1)} \bar{g}(b_l, b_r) = 0$ at $(1/2, 1/2)$.

We then construct $c = \frac{\partial \mu^{\text{KS}}(b_l, 1/2)}{\partial b_l} \Big|_{b_l=1/2}$. Since $\nabla_{(1,0)}^2 \mu^{\text{KS}}(b_l, b_r) < 0$ at $(1/2, 1/2)$, $\nabla_{(1,0)} \mu^{\text{KS}}(b_l, b_r)$ is well-defined and equal to $\frac{\partial \mu^{\text{KS}}(b_l, 1/2)}{\partial b_l} \Big|_{b_l=1/2}$. Now, since $c = \frac{\partial \mu^{\text{KS}}(b_l, 1/2)}{\partial b_l} \Big|_{b_l=1/2}$, we have

$$\nabla_{(1,0)} \bar{g}(b_l, b_r) = \nabla_{(1,0)} \mu^{\text{KS}}(b_l, b_r) - c = 0.$$

Since the derivative of $\bar{g}(b_l, b_r)$ at $\mathbf{b}' = (1/2, 1/2)$ is zero in two independent directions, it implies that the gradient of $\bar{g}(b_l, b_r)$ is a zero vector at $\mathbf{b}' = (1/2, 1/2)$, thereby completing the proof. \square

Appendix E: Additional Simulation Results

In this section we consider an alternative model of an imbalanced market in which a flexibility allocation (b_l, b_r) means that drivers and riders are flexible with probability b_l and b_r , respectively. This modeling approach guarantees that the expected number of edges for flexibility allocations $(B, 0)$ and $(0, B)$ are the same, though they result in a different expected number of flexible nodes. Indeed, with this modeling approach the one-sided allocation $(B, 0)$ produces more flexible nodes in expectation than any other flexibility design with the same flexibility budget B , and this leads to a significant advantage for the one-sided allocation. Fig. 23 (a) and (b) show that the additional flexible nodes ensure that the one-sided allocation $(B, 0)$ outperforms the balanced allocation for any sufficiently large α and α^f , regardless of whether $B < 1$, overshadowing the flexibility abundance effect. Thus, the abundance effect disappears, while the cannibalization effect remains. At the same time, we still observe the balanced allocation outperforming the one-sided allocation in the regime with very small α, α^f , where the number of edges is much larger for the balanced allocation (see Section 7.1).

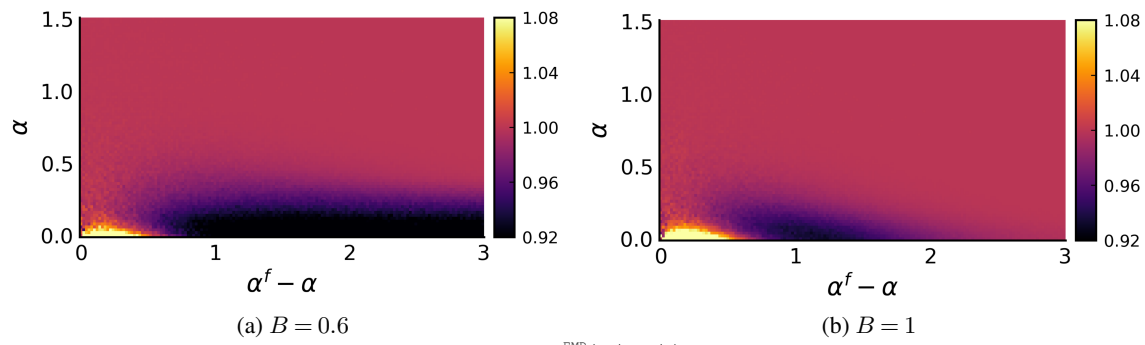


Figure 23 The plots present heat-map values of $\frac{\mu_{\text{EMP}}(B/2, B/2)}{\mu_{\text{EMP}}(B, 0)}$ across varying α and $\alpha^f - \alpha$ when $\lambda = 0.8$.